CNIC-01300
CNDC-0023
INDC(CPR)-047 / L

CNIC-01300
CNDC-0023
INDC(CPR)-047/L

CN9901201

COMMUNICATION OF NUCLEAR DATA PROGRESS

No.20 (1998)

China Nuclear Data Center

China Nuclear Information Centre

Atomic Energy Press

Beijing, December, 1998

EDITORIAL NOTE

This is the 20th issue of *Communication of Nuclear Data Progress* (CNDP), in which the achievements in nuclear data field for the last year in China are carried. It includes the measurement of cross sections for $^{92}Mo(n,p)^{92m}Nb$ reaction and deduction of low energy neutron; theoretical calculations of n+^{9}Be, ^{12}C, $^{85,87}Rb$, $^{88,89,90}Sr$, ^{89}Y, ^{113}Cd, ^{115}In, $^{121,123}Sb$ below 20 MeV and γ+^{51}V, $^{180,182,183,184,186}W$ below 30 MeV; evaluations of $^{63,65,Nat}Cu(n,\alpha)$, $(n,n'\alpha)$ and γ+^{51}V reactions and ^{238}U fission product yields; a method and program CABEI for adjusting consistancy between the cross section data of natural element and its isotopes; testing of the tritium production for ^{6}Li and ^{7}Li; and fragment angular anisotropies and inertia parameters.

The editors hope that our readers and colleagues will not spare their comments, in order to improve this publication.

Please write to Drs. Liu Tingjin and Zhuang Youxiang
Mailing Address: China Nuclear Data Center
China Institute of Atomic Energy
P.O.Box 275 (41), Beijing 102413
People's Republic of China
Telephone: 86-10-69357729 or 69357830
Telex: 222373 IAE CN
Facsimile: 86-10-6935 7008
E-mail: cndc @ mipsa.ciae.ac.cn

EDITORIAL BOARD

Editor-in-Chief

Liu Tingjin Zhuang Youxiang

Members

Cai Chonghai Li Manli Liu Jianfeng Liu Tingjin
Liu Tong Ma Gonggui Shen Qingbiao Song Qinglin
Tang Guoyou Tang Hongqing Wang Yansen
Liu Guisheng Zhang Jingshang Zhuang Youxiang

Editorial Department

Li Manli Xu Ling Li Shuzhen

CONTENTS

CN9901202

I EXPERIMENTAL MEASUREMENT

Measurement of Cross Section for $^{92}Mo(n,p)^{92m}Nb$ Reaction and Deduction of Low Energy Neutron

Zhao Wenrong Lu Hanlin Yu Weixiang Han Xiaogang Huang Xiaolong
(China Institute of Atomic Energy, Beijing, 102413)

Introduction

Molybdenum is an important component of structural material for fission and future fusion reactors. It consists of seven isotopes. Therefore, fast neutrons can lead to many nuclear reactions. One of them is $^{92}Mo(n,p)^{92m}Nb$ reaction. Several authors published their data for this reaction, while most of the cross section determinations were concentrated on about 14 MeV energy range. For the neutron energy below 12 MeV, there are only two sets of measured data, with a large discrepancy between them. The tendency of the cross sections of Liskien[1] is higher with the neutron energy increasing, in energy range above 18 MeV. And the same situation exists also for the reactions with low threshold, such as $^{58}Ni(n,p)^{58}Co$, $^{64}Zn(n,p)^{64}Cu$ and etc.

In present work the cross sections for the reaction were measured in the energy range from 5 to 19 MeV. And the influence of various kinds of low energy neutrons was considered very carefully. Especially in high energy range, "gas out" irradiation was performed to deduct the effect of D-d low energy neutrons, and a reasonable tendency of the cross sections was obtained.

1 Experimental Procedure

The cross sections were measured in neutron energy range from 5 to 19 MeV using the activation technique. Natural metal molybdenum plate was machined into the samples with 20 mm in diameter and 1mm in thickness. The samples were irradiated in

the 0° direction relative to incident particles. The irradiation time was 4 to 9 h and the distance between the samples and the neutron source was 2 to 4 cm. The neutron flux was determined via the monitor reactions.

In the energy range below 12 MeV, $D(d,n)^3He$ reaction was used to produce the neutrons by D_2 gas target at HI-13 tandem accelerator and solid D-Ti target at Van de Graaff accelerator and small tandem.

The activities of the Mo sample and monitors of $^{58}Ni(n,p)^{58}Co$ and $^{56}Fe(n,p)^{56}Mn$ reactions were corrected for the contributions from D-d low energy neutrons of self-building D target by gas in and gas out runs in the energy range of 5 to 7 MeV.

In 8 to 12 MeV range, a group of monitors was selected with different threshold, such as $^{58}Ni(n,p)^{58}Co$, $^{56}Fe(n,p)^{56}Mn$, $^{27}Al(n,\alpha)^{24}Na$, $^{197}Au(n,2n)^{196}Au$ and etc. and irradiated with Mo sample together. After that , a relationship between neutron flux and threshold was obtained. The neutron flux at the measured energy can be given through this relationship, according to the threshold of $^{92}Mo(n,p)^{92m}Nb$ reaction. In this way, the influence of low energy neutrons was well deducted, which include of the D-d low energy neutron from self building D target, breakup neutron, the neutron from A(d,xn)B reaction and the scattering, where A means the structure materials of target or sample.

The neutrons above 14 MeV were produced via $T(d,n)^4He$ reaction. The cross sections were measured relative to $^{56}Fe(n,p)^{56}Mn$ and $^{27}Al(n,\alpha)^{24}Na$ reactions at Cockroft Wetten accelerator. To reduce the effect of D-d low energy neutron, a new T-Ti target was used and the irradiation time was as short as possible for the measurement in about 14 MeV range.

In high energy range of 17.30 and 19.09 MeV the $^{27}Al(n,\alpha)^{24}Na$ reaction was used as monitor to determine the neutron flux. To correct the influence of D-d low energy neutrons, the "gas out" irradiation was performed, where the "gas out" means the target with free from tritium.

In all the measurements, the corrections were made for the fluctuation of the neutron flux during the irradiation.

Table 1 The decay parameters of products

reaction	half-live	E_γ / keV	I_γ / %
$^{27}Al(n,\alpha)^{24}Na$	15 h	1368.6	100
$^{56}Fe(n,p)^{56}Mn$	2.5785 h	846.8	98.9
$^{58}Ni(n,p)^{58}Co$	70.916 h	810.8	99.5
$^{92}Mo(n,p)^{92m}Nb$	10.15 d	934.5	99
$^{197}Au(n,2n)^{196}Au$	6.18 d	356	87.6

The activities of the products were determined by Ge(Li) gamma-ray spectroscopy. The decay parameters of the products are summarized in Table 1. The count rates were corrected for the gamma ray self-absorption in sample and the cascade effect.

2 Result and Discussion

The cross sections for ^{92}Mo(n,p)^{92m}Nb reaction are listed in Table 2. The principal sources of error include the error of the efficiency of gamma ray detector, the cross section of monitors, counting statistics, and some corrections for the gamma-ray self absorption in sample, for effect of low energy neutron and etc. Combing those errors in quadrature, the total error for each cross section was obtained.

Table 2 The measured cross sections of ^{92}Mo(n,p)^{92m}Nb reaction

E_n / MeV	σ / mb	E_n / MeV	σ / mb
5.03±0.16	42.6±2.3	11.40±0.35	118.0±6.4
6.00±0.17	69.1±3.9	14.00±0.05	70.3±2.1
6.57±0.26	73.7±3.5	14.70±0.15	61.0±1.8
7.07±0.19	82.8±4.4	14.83±0.15	56.4±1.5
8.37±0.58	85.8±4.6	17.30±0.20	36.5±3.6
9.37±0.46	95.0±5.1	19.09±0.22	29.8±1.5
10.40±0.33	104.7±5.5		

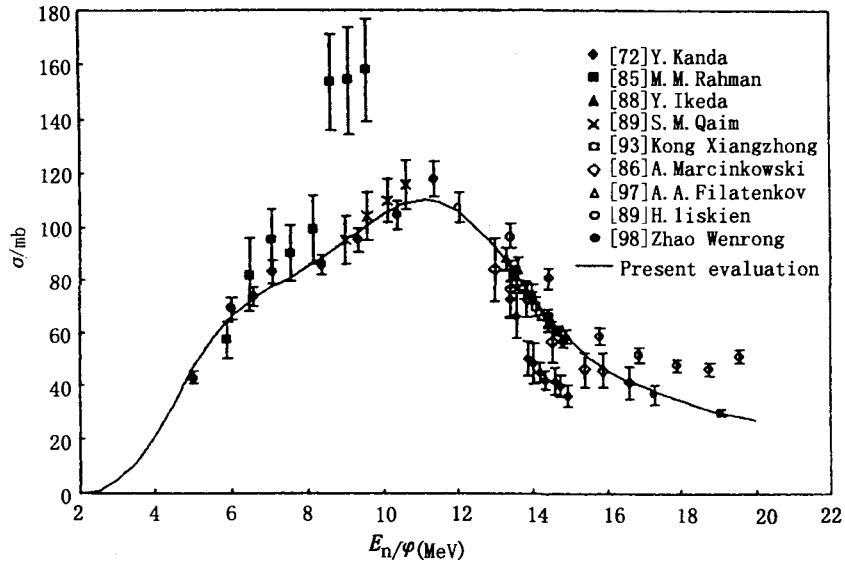

Fig.1 Cross section of ^{92}Mo(n,p) reaction

The cross sections are plotted as a function of neutron energy in Fig. 1 together with available values from literatures for comparison. The solid line presents this evaluation. Below 8 MeV, our data are in agreement with the data of Rahman[2]. From 8 to 12 MeV, the results of Qaim[3] are consistent with ours, while the cross sections of Rahman[2] are about 50% higher than ours. In about 14 MeV energy range, the data of Ikeda[4], Filatenkov[5], Kong[6] and present work fall into agreement. The data of Kanda[7] are much lower than others. Above 16 MeV, the tendency of the cross sections for Marcikowski[8] and ours is coincident. The results of Liskien[1] are higher than others in his whole measured energy range.

In the energy range of 18 to 20 MeV, the data of Liskien[1] increase with the neutron energy. In the same energy range in present work, a new T-Ti target was used and the correction was made by "gas out" irradiation for the effect of D-d low energy neutrons. The correction is 10% at 19 MeV neutron energy in our experimental condition. Therefore, the present cross sections are lower than Liskien[1], and the tendency of our measurements is decreased with neutron energy increasing.

The cross sections of $^{58}Ni(n,p)^{58}Co$ and $^{64}Zn(n,p)^{64}Cu$ reactions were also measured relative to $^{27}Al(n,\alpha)^{24}Na$ monitor reaction in high energy range. And the same tendency of the cross sections were obtained.

Because of the low threshold of $^{92}Mo(n,p)^{92m}Nb$ reaction, only 288 keV, the effect of D-d low energy neutrons is obvious in high energy range. The influence is increased with the neutron energy and strongly depends on the threshold of the specific reaction and the irradiated time. Therefore, the correction, by "gas out" irradiation, for the effect of low energy neutrons is very important for the reactions with low thresholds in high energy range of neutrons produced through $T(d,n)^4He$ reaction.

References

[1] H. Liskien, R. Wolfle, R. Widera, et al., Appl. Radiat. Isot. 1990, 41(1)83

[2] M. M.Rahman and S. M. Qaim, Nucl. Phys, 1985 A435(1), 43

[3] A. M. Qaim and R. Wolfle, Phys. Rev 1993, 40(5)1089

[4] Y. Ikeda, K. Konno, T. Nakamura, et al., JAERI Report 1988 1312

[5] A. A. Filatenkov, S. V. Chuvaev, V. N. Aksenov, et al., INDC1997 (ccp)-402

[6] Kong Xiangzhong, Wang Yougchang, Yuang Jungian, et al., "Cross Section Measurement for n+Mo", Private Communication, 1992

[7] Y. Kanda, Nncl. Phys, 1972, A 185, 177

[8] A. Marcinkowski, K. Stankiewics, U. Garuska, et al., Z. Phys, 1986, A 323, 91

CN9901203

II THEORETICAL CALCULATION

Progress Report on the Model Calculation of n+^{9}Be Reactions below 20 MeV

Zhang Jingshang Han Yinlu Shen Guangren Shen Qingbiao
(China Nuclear Data Center, CIAE)

Introduction

^{9}Be has long been selected as the material for controlled thermonuclear reactors[1]. The secondary particle energy spectra of n+^{9}Be reaction, especially the neutron spectrum needs further improvement to meet the needs of nuclear engineering and other applications. The neutron double differential cross sections have been measured by Drake et al. in 1977[2], Baba et al. in 1978[3] and Takahashi et al. in 1983[4]. Perkins et al. evaluated the measured data mentioned above in terms of Monte Carlo technique and set up ENDF/B-6 in 1985[5].

Because there is no suitable reaction model for the target nucleus with mass number about 10, which is too light for statistical theory and is too heavy for few body problem. So far the double differential neutron emission cross sections of n+^{9}Be were determined by the given representations of the multistage reactions in terms of the relative contributions of the various possible reaction channels based on the measured data and theoretical analysis[6]. A proper description of the double differential cross sections of neutron from n+^{9}Be reaction in terms of a realistic reaction model is one of the more complex problem that theorists and evaluators confront.

The emission processes from discrete levels in the pre-equilibrium state are the important reaction mechanism, which can be described by the unified Hauser-Feshbach and exciton model[7]. In this model the angular momentum dependent exciton model is used for conserving angular momentum in both equilibrium and pre-equilibrium reaction processes[8]. Meanwhile, the residual nuclei can decay spontaneously into two or three clusters, this is the characteristic for light nucleus reactions. Because of light mass, the recoil effect must be taken into account exactly to maintain the energy balance[9]. The improved pick-up mechanism was employed to calculate composite particle emissions in this model[10,11].

1 Reaction Channels of n+^{9}Be Reaction

In view of n+^{9}Be reactions for $E_n \leq 20$ MeV the reaction channels are listed as follows:

$$n+^{9}Be = \begin{cases} \gamma+^{10}Be & Q = 6.811\,MeV \\ p+^{9}Li(T_{1/2} = 178.3\,ms) & Q = -12.825\,MeV \\ \alpha+^{6}He(\beta_-, T_{1/2} = 806.7\,ms) & Q = -0.598\,MeV \\ d+^{8}Li(\beta_- + 2\alpha, T_{1/2} = 838\,ms) & Q = -14.663\,MeV \\ t+^{7}Li & Q = -10.439\,MeV \\ ^{5}He+^{5}He(2n+2\alpha) & Q = -3.362\,MeV \\ n,p+^{8}Li(\beta_- + 2\alpha, T_{1/2} = 838\,ms) & Q = -16.887\,MeV \\ 2n+^{8}Be(\alpha+\alpha) & Q = -1.665\,MeV \end{cases}$$

Reaction mechanism in the n+^{9}Be system leading to the decay into two neutrons and two α particles reactions may proceed via a number different reaction channels, either as sequential two-body reaction or as direct three-body or four body break-up processes. The different approach strongly differs each other in their respective neutron energy-angular distributions. The reaction channels to ^{9}Be(n,2n)2α channel involved in the calculation are as follows:

(a) $n+^{9}Be \rightarrow n+^{9}Be^{*}$
$^{9}Be^{*} \rightarrow n+^{8}Be^{*}$
$^{8}Be^{*} \rightarrow 2\alpha$

(b) $n+^{9}Be \rightarrow n+^{9}Be^{*}$
$^{9}Be^{*} \rightarrow +^{5}He^{*}$
$^{5}He^{*} \rightarrow n+\alpha$

(c) $n+^{9}Be^{*} \rightarrow ^{5}He^{*}+^{5}He^{*}$
$2^{5}He^{*} \rightarrow 2n+2\alpha$

(d) $n+^{9}Be^{*} \rightarrow \alpha+^{6}He^{*}$
$^{6}He^{*} \rightarrow n+n+\alpha$ (3 – body break - up)

(e) $n+^{9}Be^{*} \rightarrow ^{10}Be^{*} \rightarrow n+n+^{8}Be$ (direct 3 - body break - up)

The discrete level scheme of every reaction channels is taken from the "Table of Isotopes"[12] (1996).

2 Double Differential Cross Section from Discrete Levels to Discrete Levels

A new model has been developed for calculating nuclear reaction data of light nuclei[13]. In n+^{9}Be reactions all of emissions are carried out from discrete levels to discrete levels at $E_n \leq 20$ MeV.

The physical quantities used in this paper are defined as the following:

E^*: excitation energy;

E_n: incident neutron energy in L. S;

M_C, M_T: mass of compound nucleus and target;

m_1, m_2: mass of the first and the second emitted particle;

ε_1, ε_2: energy of the first and the second emitted particle;

M_1, M_2: mass of residual nucleus after the first and the second emitted particle;

E_1, E_2: energy of residual nucleus after the first and the second emitted particle;

B_1, B_2: binding energy of the first and the second emitted particle in its compound nucleus;

E_{k_1}, E_{k_2}: level energy with the level order number k_1, k_2 reached by the first and the second emitted particle;

$f_l^{m_1}(c)$, $f_l^{M_1}(c)$: Legendre expansion coefficient of the first emitted particle and its residual nucleus in C. M. S.;

$f_l^{m_2}(c)$, $f_l^{M_2}(c)$: Legendre expansion coefficient of the second emitted particle and its residual nucleus.

Obviously we have

$$f_l^{M_1} = (-1)^l f_l^{m_1} \tag{1}$$

Three motion systems are used in the model calculations, in which the physical quantity indicated by the superscript l, c, r and r for laboratory, center of mass, and recoil residual nucleus, respectively.

The Legendre expansion coefficients of the first emitted particle and its residual nucleus $f_l^{m_1}(c)$ and $f_l^{M_1}(c)$ can be obtained by the unified model. For low incident neutron energies ($\leq$ 20 MeV) the isotropic distribution of the second particle emissions is assumed in this model. The emitted energies of the first and second particles ε_1^c, ε_2^r (from k_1 level to k_2 level) are given by

$$\varepsilon_1^c = \frac{M_1}{M_c}(E^* - B_1 - E_{k_1}) \tag{2}$$

$$\varepsilon_2^r = \frac{M_2}{M_1}(E_{k_1} - B_2 - E_{k_2}) \tag{3}$$

The maximum and the minimum energies of the emitted second particle in C. M. S. are obtained by

$$\varepsilon_{2,\min}^c = \varepsilon_2^r(1-\gamma)^2 \tag{4}$$

$$\varepsilon_{2,\max}^c = \varepsilon_2^r(1+\gamma)^2 \tag{5}$$

where γ is defined by

$$\gamma = \sqrt{\frac{E_1^c m_2}{\varepsilon_2^r M_1}} \tag{6}$$

The Legendre expansion of the second emitted particle in C. M. S can be obtained by Ref. [13]

$$\frac{d^2\sigma}{d\varepsilon_2^c d\Omega_{m_2}^c} = \frac{\sigma}{4\pi}\sum_l (2l+1) f_l^{m_2}(\varepsilon_2^c) P_l(\cos\theta_{m_2}^c) \tag{7}$$

and

$$f_l^{m_2}(\varepsilon_2^c) = \frac{(-1)^l}{4\gamma\varepsilon_2^r} f_l^{m_1} P_l(\eta) \tag{8}$$

where

$$\eta = \sqrt{\frac{\varepsilon_2^r}{\varepsilon_2^c}} \frac{\frac{\varepsilon_2^c}{\varepsilon_2^r} - 1 + \gamma^2}{2\gamma} \tag{9}$$

In some reaction channels the residual nucleus is unstable and separated into two clusters spontaneously. For instance ^{8}Be=α+α with Q=0.092 MeV, ^{5}He=n+α with Q=0.894 MeV. We denote that m_3 and M_3 are the masses of the two clusters and $m_3+M_3=M_2$. If the residual nucleus is in a discrete level k_2, then the kinetic energies of the two clusters in the residual system are

$$\varepsilon_3^r = \frac{M_3}{M_2}(Q + E_{k_2}) \tag{10}$$

$$E_3^r = \frac{m_3}{M_2}(Q + E_{k_2}) \tag{11}$$

The two cluster separation can be treated as one cluster emission with isotropic distribution as that of second particle emissions. All of formulation can be found in Ref. [13].

3 Three-body Break-up Mode

The reaction mechanism of three-body break-up process is employed in n+^{9}Be reactions. The compound nucleus ^{10}Be contributes to total (n,2n) reaction with a probability through three-body break-up process. The nucleus ^{6}He* produced as a result of the (n,α) reaction on ^{9}Be. ^{6}He in ground state decays only by β. and contributes to the (n,α) reaction, so it does not contribute to the (n,2n) reaction. Since the first excited state of ^{6}He has the energy 1.797 MeV, the neutron binding energy in ^{6}He is 1.869 MeV, so it could not have the sequential decay by emission second neutron. Thus only sequential decay through three-body break-up process

contributes to the (n,2n) reaction.

The kinetics of the three-body break-up process has been given by Ohlsen[14] (1965). H. Fuchs explains Ohlsen's derivation by introducing the integration over the unobserved variables[15]. Meijer and Kamermens reviewed the three break-up process induced by He projectiles[16]. In the three break-up process, there are nine degrees of freedom. We can reduce the problem by four degrees of freedom using the momentum and energy conservation. Thus we only need to specify five independent variables in order to determine the kinetics of outgoing three-particles. Now we choose θ_1, Φ_1, θ_2, Φ_2 and ε_1 as the five independent variables, where θ_j, Φ_j represent the recoil nucleus system scattering angle variables for a particle of mass m_j and energy ε_j.

In the three break-up process of ^{6}He and ^{10}Be, ε_1, ε_2 are the outgoing two neutron energies, while the ε_3 represents the alpha particle and ^{8}Be, respectively. Following Ohlsen's notation, from the momentum and energy conservation $\varepsilon_1+\varepsilon_2+\varepsilon_3=Q$ and in $\vec{P}=\vec{P}_1+\vec{P}_2+\vec{P}_3=0$ system, which means that ^{10}Be is in C. M. S, while ^{6}He is in recoil residual system after the first α particle emission, the relation between ε_1 and ε_2 can be obtained

$$\frac{1}{m_3}\left[\varepsilon_1(m_1+m_3)+\varepsilon_2(m_2+m_3)+2\sqrt{m_1m_2\varepsilon_1\varepsilon_2}\cos\theta_{12}\right]=Q \qquad (12)$$

Where m_3 and ε_3 refer to the mass and energy of α particle or ^{8}Be. The Q-value is E_{k_1} –0.973 MeV for ^{6}He and E^*+8.477 MeV for ^{10}Be.

The triple-differential cross section for the observation of particle 1 with (θ_1, Φ_1, ε_1) simultaneously with particle 2 with (θ_2, Φ_2, ε_2) reads[14]:

$$\frac{\mathrm{d}^3\sigma}{\mathrm{d}\varepsilon_1\mathrm{d}\Omega_1\mathrm{d}\Omega_2}=\frac{2\pi}{\hbar}\frac{\mu_{\mathrm{in}}}{P_{\mathrm{in}}}\left|T_{ji}\right|^2\rho_1(\varepsilon_1) \qquad (13)$$

where

$$\rho_1(\varepsilon_1)=\frac{m_1m_2m_3p_1p_2}{2\pi\hbar^6\left[(m_2+m_3)+\dfrac{m_2(\vec{p}_1-\vec{P})\vec{p}_2}{p_2^2}\right]} \qquad (14)$$

μ_{in}= reduced mass in the incident channel,

P_{in}= momentum of the incident channel.

If the matrix element $|T_{ji}|$ can be considered as constant for the three break-up process, in this case the triple-differential cross section can be determined as a purely statistical spectrum of particle 1 at Ω_1 under the assumption that particle 2 is detected at Ω_2. Regardless energy of particle 2 for the fixed Q-value, by integrating over Ω_2, the double differential cross section of the first particle can be obtained by

$$\frac{d^2\sigma}{d\varepsilon_1 d\Omega_1} = \int \frac{d^3\sigma}{d\varepsilon_1 d\Omega_1 d\Omega_2} d\Omega_2 \tag{15}$$

From the relationship between ε_1 and ε_2 equation, the double differential cross section for the second neutron can be expressed as:

$$\frac{d^2\sigma}{d\varepsilon_2 d\Omega_2} = \int \frac{d^3\sigma}{d\varepsilon_1 d\Omega_1 d\Omega_2} \left|\frac{d\varepsilon_1}{d\varepsilon_2}\right| d\Omega_1 \tag{16}$$

4 Transformation from C. M. S to L. S

Since the emitted particle spectra from levels to levels are in ring-type form the Legendre expansion could not be used in L. S due to the forbidden area θ^1. The double differential cross sections have to be expressed by the two dimensions table of ε^1 and θ^1.

Denoting

$$\beta = \frac{\sqrt{m_1 m_n E_n}}{M_c} \tag{17}$$

For a given εl and $\mu^1=\cos\theta^1$ the corresponding quantities in C. M.S can be obtained by

$$\varepsilon^c = \varepsilon^1 + \beta^2 - 2\beta\sqrt{\varepsilon^1}\mu^1 \tag{18}$$

$$\mu^c = \cos\theta^c = \frac{\sqrt{\varepsilon^1}\mu^1 - \beta}{\sqrt{\varepsilon^1 + \beta^2 - 2\beta\sqrt{\varepsilon^1}\mu^1}} \tag{19}$$

The spectrum in C. M. S has its maximum and minimum values, the maximum and minimum values of $\varepsilon^1_{max}, \varepsilon^1_{min}$ can be given by

$$\varepsilon^1_{max} = (\sqrt{\varepsilon^c_{max}} + \beta)^2 \tag{20}$$

$$\varepsilon^1_{min} = \begin{cases} \left(\sqrt{\varepsilon^c_{min}} - \beta\right)^2 & \text{if } \beta < \sqrt{\varepsilon^c_{min}} < \sqrt{\varepsilon^c_{max}} \\ 0 & \text{if } \sqrt{\varepsilon^c_{min}} < \beta < \sqrt{\varepsilon^c_{max}} \\ \varepsilon^1_{min} = (\beta - \sqrt{\varepsilon^c_{max}})^2 & \text{if } \sqrt{\varepsilon^c_{min}} < \sqrt{\varepsilon^c_{max}} < \beta \end{cases} \tag{21}$$

The μ^1 is allowed in the area for a given ε^1

$$\max\left\{-1, \frac{\varepsilon^1 + \beta^2 - \varepsilon^c_{max}}{2\beta\sqrt{\varepsilon^1}}\right\} \le \mu^1 \le \min\left\{1, \frac{\varepsilon^1 + \beta^2 - \varepsilon^c_{min}}{2\beta\sqrt{\varepsilon^1}}\right\} \tag{22}$$

The double differential cross section in L. S can be given by

$$\frac{\mathrm{d}^2\sigma}{d\varepsilon^{\mathrm{l}}d\mu^{\mathrm{l}}}=\sqrt{\frac{\varepsilon^{\mathrm{l}}}{\varepsilon^{\mathrm{c}}}}\sum_l\frac{2l+1}{4\pi}f_l^{\mathrm{c}}(\varepsilon^{\mathrm{c}})P_l(\mu^{\mathrm{c}}) \tag{23}$$

5 Level Broadening Effect

For the first emission processes, the Gaussian expansion reads

$$\mathrm{G}(\varepsilon,k)=\frac{1}{\sqrt{2\pi}\Gamma_k}\exp(-\frac{(\varepsilon-\varepsilon_1^{\mathrm{c}})^2}{2\Gamma_k^2}) \tag{24}$$

where Γ_k refers to the width of the k_{th} level of residual nucleus. $\varepsilon_2^{\mathrm{c}}$ is the second particle emission energy from level k_1 to level k_2, the Gaussian expansion can be obtained by

$$\begin{aligned}\mathrm{G}(\varepsilon,k_1,k_2)&=\frac{1}{2\pi\Gamma_1\Gamma_2}\int_{-\infty}^{\infty}\mathrm{d}y\exp(-\frac{(\varepsilon-y)^2}{2\Gamma_2^2}-\frac{(y-\varepsilon_2^{\mathrm{c}})^2}{2\Gamma_1^2})\\&=\frac{1}{\sqrt{2\pi}\Gamma}\exp(\frac{(\varepsilon-\varepsilon_2^{c})^2}{2\Gamma^2})\end{aligned} \tag{25}$$

where

$$\Gamma=\sqrt{\Gamma_1^2+\Gamma_2^2} \tag{26}$$

Γ_1 and Γ_2 refer to the widths of level-k_1 and level-k_2, respectively. If the energy resolution ΔE in measurements is taken into account, the total width should be given by

$$\Gamma=\sqrt{\Gamma_1^2+\Gamma_2^2+\Delta E^2}$$

When a spectrum of outgoing particle is obtained by $S(\varepsilon')$, with energy region $\varepsilon_{\min}^{\mathrm{c}}\le\varepsilon'\le\varepsilon_{\max}^{\mathrm{c}}$, the Gaussian expansion at energy point ε reads

$$S_{\mathrm{G}}(\varepsilon)=\frac{\sqrt{2}}{\sqrt{\pi}\Gamma}\int_{\varepsilon_{\min}^{\mathrm{c}}}^{\varepsilon_{\max}^{\mathrm{c}}}\frac{\exp(-\frac{(\varepsilon-\varepsilon')^2}{2\Gamma^2})}{1+\mathrm{erf}(\frac{\varepsilon'}{\sqrt{2}\Gamma})}S(\varepsilon')\mathrm{d}\varepsilon' \tag{27}$$

to keep the value of cross section unchangeable,

$$\int_0^{\infty}S_{\mathrm{G}}(\varepsilon)\mathrm{d}\varepsilon=\int_{\varepsilon_{\min}^{\mathrm{c}}}^{\varepsilon_{\max}^{\mathrm{c}}}S(\varepsilon')\mathrm{d}\varepsilon' \tag{28}$$

where erf is the error function.

6 The Function of LUNF Code

The physical quantities calculated by LUNF code contain:

(1) cross sections of total, elastic scattering, compound elastic scattering, non-

elastic scattering and all reaction channels;

(2) elastic scattering angular distributions;

(3) the double differential cross sections of outgoing neutron and α particle from each reaction mechanism;

(4) the total double differential cross sections of emitted neutron and α particle from (n,2n) reaction channels.

(5) the ENDF/B-6 outputting is given.

7 Results and Discussion

The new model has been used for calculating the cross sections of n+^{9}Be reactions, including the total, elastic scattering, non-elastic scattering, (n,α), (n,d), (n,t) and (n,2n) cross sections. The cross section of (n,2n) is shown in Fig. 1. The model calculations also include the cross sections of (n,γ), (n,p), (n,np) and (n,n'γ), and in each channel the γ decaying competition is taken into account. In our interesting incident energy region (2 ~ 20 MeV), $\sigma_{n,\gamma}$< 0.1 mb, $\sigma_{n,n'}$< 0.4 μb and at 20 MeV $\sigma_{n,np}$=8 μb with the threshold energy of 18.78 MeV, all of them can be neglected. $\sigma_{n,p}$ is 13 mb at 20 MeV with the threshold energy of 14.26 MeV. The calculations of the double-differential cross sections of outgoing neutron and α particle from ^{9}Be(n,2n)2α reaction channel have been performed in a wide energy region and angles, which are listed in Table 1.

Table 1 The incident neutron energies and angles calculated for comparison with the experimental data

E_n / MeV	θ	Ref.
3.25	49.9	[3]
3.9	49.9	[3]
4.5	35.5 49.9 65.0 83.7 136.4	[3]
5.9	25. 35. 45. 60. 100. 125	[2]
6.4	25.9 49.9 83.7 92.7 115.4 136.4	[3]
7.05	25.9 44.4 58.4 83.7 136.4	[3]
10.1	25. 45. 60. 80. 100. 125.	[2]
14.1	15. 20. 30. 40. 50. 60. 70. 80. 90. 100. 113. 120. 130. 140. 150. 160.	[4]
14.1	25. 30. 37.5 45. 52.5 60. 80. 100. 120. 135. 150.	[3]
14.2	27.5 45. 60. 100. 125. 130. 145.	[2]

The plotting for E_n=10.1 and 14.1 are shown in Figs. 2 ~ 5, the comparisons of the calculated results with experimental data are all in good or reasonable agreements.

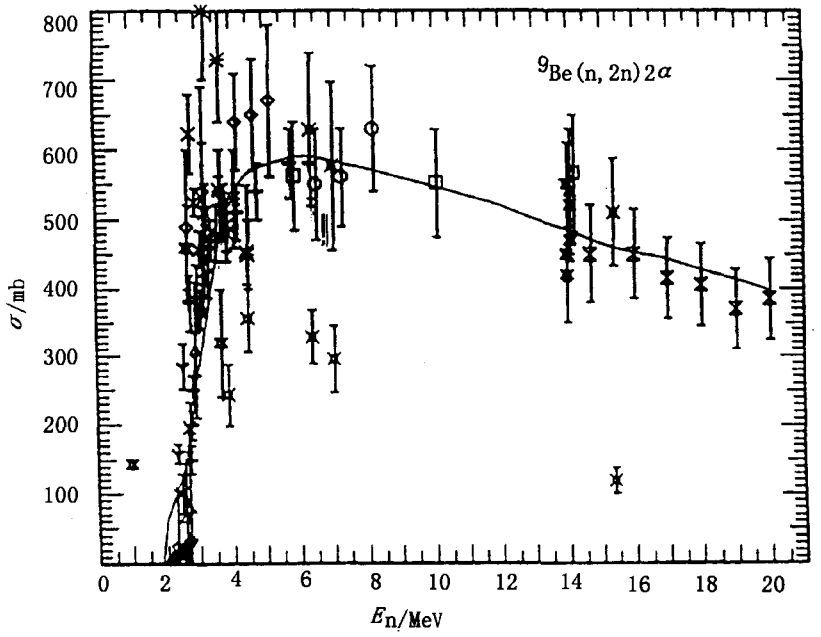

Fig. 1 The (n,2n) cross section of n+^{9}Be reaction
The data are taken from Refs. [2, 3].

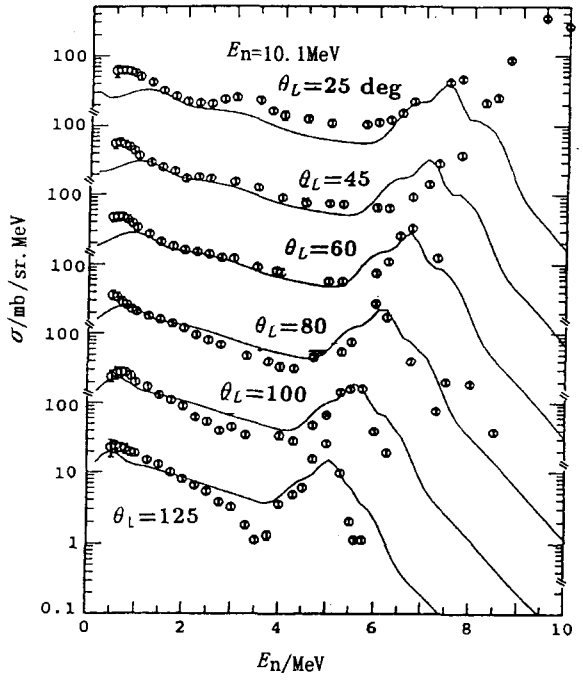

Fig. 2 The energy-angular spectra ^{9}Be(n,2n)2α at E_n=10.1 MeV.
The data are taken from Drake et al[2]

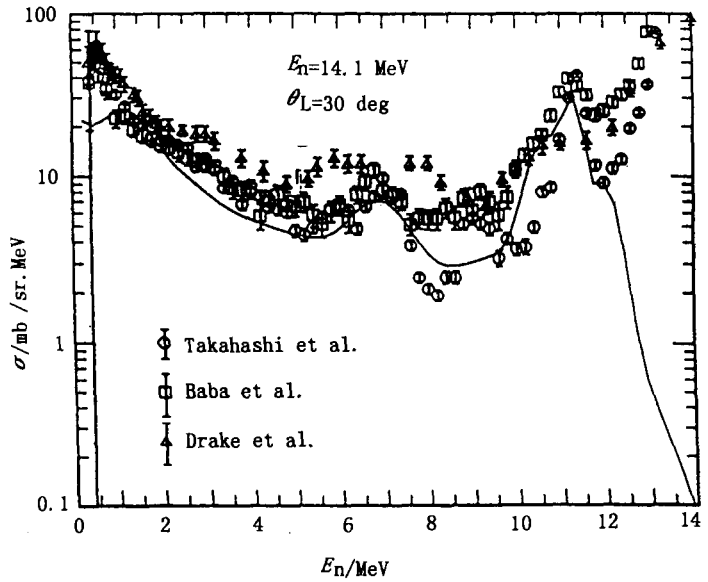

Fig. 3 The energy-angular spectra ^{9}Be(n,2n)2α E_n=14.1 MeV at θ=30

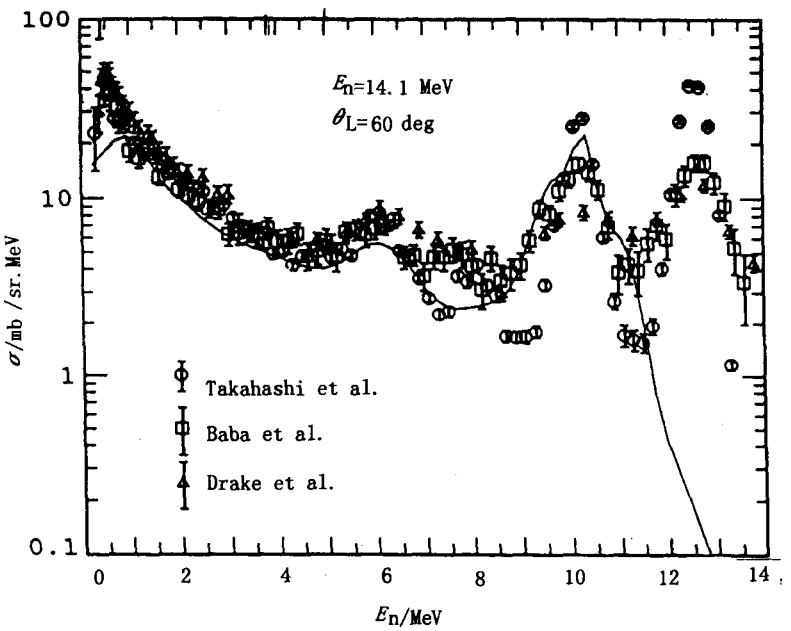

Fig. 4 The energy-angular spectra ^{9}Be(n,2n)2α E_n=14.1 MeV at θ=60

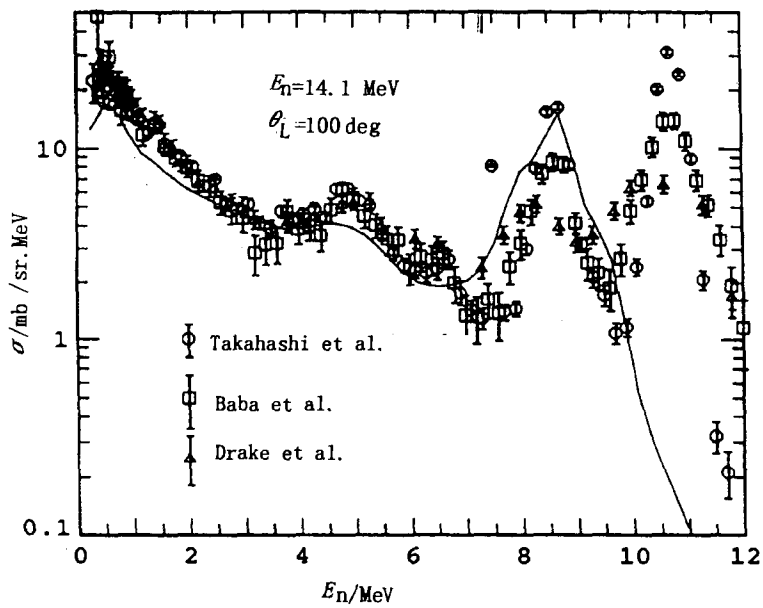

Fig. 5 The energy-angular spectra ^{9}Be(n,2n)2α E_n=14.1 MeV at θ=100

In this model sequential two-body reactions and the direct three-body processes are included, from which the different respective neutron energy-angular distributions are obtained as the components of the energy-angular spectrum of outgoing neutron and α particle. The direct 4-body break-up mechanism is not taken into account in the model calculation. The pre-equilibrium mechanism dominates reaction processes of ^{9}Be, while the equilibrium state only gives lightly implement even at low neutron incident energies (≤ 20 MeV). At E_n=14.1 MeV, as an example, the pre-equilibrium state occupies the percentage of $P_{pre\text{-}eq}$=84.31%, while equilibrium state only has P_{eq}=15.69 %. The parameter of exciton model K=100 MeV^3 is used in the calculations.

8 Conclusion and Remarks

A new model for neutron induced light nucleus reactions has been developed. The key point in this model is the description of the particle emissions from discrete levels to discrete levels in pre-equilibrium states. The pre-equilibrium emission mechanism dominants the reaction processes. The angular momentum conservation and parity conservation are taken into account in whole reaction processes and the energy balance is considered. The contribution to the (n,2n) reaction from three body break-up is small (< 10%). From fitting results the percentages of three body

break-up of ^{10}Be in the (n,2n) cross section are given as follows:

E_n / MeV	3.25	4.5	5.9	6.4	7.05	10.1	14.1	15.4
%	8.04	8.22	8.70	8.79	8.87	8.53	8.54	8.69

In this model the forward-angle emission is taken into account, it proved that the linear momentum dependent exciton state density can be employed in the light nucleus reaction to account for forward-angle emissions[17]. Since the light nucleus reactions have very strong recoil motion, the particles emitted from residual recoil nucleus have very strong backward tendency, while the first emitted particles have obvious forward tendency. Combining these effects the reasonable shapes of the energy-angular spectrum are obtained.

From the calculations we can see that the optical model still works well to give the emission branch from levels in the case of the light nucleus reaction. The emission probabilities can be obtained by a set of optical model parameters for both cross sections and double-differential cross sections.

The energy spectra of the second particle emissions from discrete levels to discrete levels have ring-type form in C. M. S.. In this case the Legendre expansion could not be used in laboratory system.

The pick-up mechanism is used in the composite particle emission. The excitation energy dependent formula is used in the calculation. The results indicate that E-dependent pre-formation formula is good for triton and deuteron emissions, but for α particle emission the pre-formation probability should be set by F_α=1.0, which drop a hint that Be has very strong cluster structure, the α cluster pre-formed already in the nucleus.

Since all the particle emissions are carried out from discrete levels to discrete levels so we do not need the level density parameters as the input model parameters except the compound nucleus. To fit experimental data of the double-differential cross sections of neutron the level broadening and the energy resolution must be included in the calculation accordingly. In our calculation the Gaussian expansion is used for the level broadening effect. The calculations of nuclear reaction data both of cross sections and energy-angular distributions of outgoing particles have being performed for ^{6}Li, ^{7}Li, ^{12}C and so on to test this new model.

References

[1] A. W. Schulke Jr (1985) Proc. 8*th* Mtg Int. Collaboration Advanced Neutron Sources (ICANS-VIII). Rutherford-Appleton Laboratory, Report No. RAL-85-110

[2] D. M. Drake., G. F. Auchampaugh., E. D. Ragan. and P. G. Young (1977) Nucl. Sci.

Engng 63 401
[3] M. Baba, T. Sakase, T. Nishitani, T. Yamada and T. Momota (1978) Proc. Conf. Neutron Phys. Nucl. Data Reactiona Appl. purposes, U. K. AEA, harwell. ICPR Neutron 79/9824, p198
[4] A. Takahashi, J. Xamamoto, T. Murakami, K. Oshima, H. Oda, Fujimoto and K. Sumita (1983)
[5] T. D. Beynon and B. S. Sim Ann. Nucl. Energy 15, 27-43 1988
[6] S. T. Perkins, E. F. Plechaty and R. J. Howerton (1985) Nucl. Sci. Engng. 90 83
[7] J. S. Zhang Nucl. Sci. Eng. 114, 55(1993)
[8] J. S. Zhang and Wen Yuanqi Chin. J. of Nucl. Phys. 16 153 (1994)
[9] J. S. Zhang "Fast Neutron Physics" p201
[10] J. S. Zhang Proc. Int. Conf. on Nuclear Data for Science and Technology. Gatlinburg, Tennesse. May 9-13, 1994 p932
[11] J. S. Zhang and S. J. Zhou Chin. J. of Nucl. Phys. 18 28 (1996)
[12] R. B. Firestone; V. S. Shirley "Table of Isotopes" 1996 Eighth Edition, A Wiley-interscience Publication JOHN WILEY and SONS. INC
[13] J. S. Zhang, Y. L. Han, G. R. Shen and Q. B. Shen "Model Calculation of n+^{9}Be Reaction Below 20 MeV" to be submitted in Phys. Rev. (1998)
[14] G. G. Ohlsen Nucl. Instrum. Meth. 37 240 1965
[15] H. Fuchs Nucl. Instrum. Meth. 200 361 1982
[16] R. J. Meijer and R. Kamermens Rev. mod. Phys. 57 147 1985
[17] M. B. Chadwick, P. Oblozinsky Phys. Rev. C 44 1740 (1991) Phys. Rev. C 46 2028 (1992)

CN9901204

Brief Report on the Model Calculation of n+^{12}C below 20 MeV

Zhang Jingshang Han Yinlu
(China Nuclear Data Center, CIAE)
Cao Ligang
(Department of Physics, Northwest University, Xi'an 710069)

Introduction

A new model was developed for calculating nuclear data of light nuclei, with which the cross sections and double differential cross sections of outgoing neutron of n+^{9}Be were calculated[1]. The results reproduce the experimental data successfully. Now we go on a step further to calculate the data for n+^{12}C to test this new model.

The reaction mechanism of light nucleus is more complicated. In the reaction processes of light nucleus the pre-equilibrium emissions dominate the reaction mechanism, while the equilibrium state only gives lightly implement even at low neutron incident energies. The emission processes from discrete levels in the pre-equilibrium state are the important reaction mechanism. In this model the angular momentum dependent exciton model is used for conserving angular momentum in both equilibrium and pre-equilibrium reaction processes[2]. Meanwhile, the residual nuclei can decay spontaneously into two clusters or carry out multi-particle break-up process, these are the characteristics for light nucleus reactions. Because of light mass, the recoil effect must be taken into account exactly to maintain the energy balance[3]. The improved pick-up mechanism is employed to calculate composite particle emission in this model[4,5].

In the case of $E_n < 20$ MeV, all of the reaction for n+^{12}C proceeds via several sequential decay process between discrete levels. The energy, spin and parity of the levels are taken from the "Table of Isotopes" (1996)[6].

Using LUNF code the calculated results of double differential cross sections of outgoing neutron at E_n=14.1 MeV and 18.0 MeV are shown in section 3. The optical parameters of all kinds of particles are obtained by APN94 code. Since the three-particle coincidence measurement of n+^{12}C→n+α at E_n=14.4 MeV has been performed[7], it is found that there is no evidence for this direct four body break-up process by the experiment analysis, for this reason the multi-particle break-up process is not taken into account in this calculation. The formulation of the reaction for light nucleus can be found in Ref. [1].

1 Reaction Channels of n+^{12}C

In view of n+^{12}C for $E_n < 20$ MeV the reaction channels are listed as follows:

$$\text{n+}^{12}\text{C}=\begin{cases}\gamma+^{13}C\\ \text{n}+^{12}\text{C}\\ \text{p}+^{12}\text{B}(\beta\_, T_{1/2}=20.0\,\text{ms})\\ \alpha+^{9}\text{Be}\\ \text{d}+^{11}\text{B}\\ ^{5}\text{He}+^{8}\text{Be}(2\alpha)\\ \text{n,p}+^{11}\text{B}\\ 2\alpha+^{5}\text{He}(\text{n}+\alpha)\end{cases}$$

The reaction channels of (n,t), (n,^{3}He), (n,2n) are not open due to the threshold energies > 20 MeV. The (n,α) reaction is reached by emitting an α to the ground state of ^{9}Be, while the excitation states of ^{9}Be decay to the (n,n)3α reaction. Reaction mechanism in the n+^{12}C system leading to the decay into one

neutron and three α particles reactions may proceed via a number of different reaction channels, such as sequential two-body reaction or two body break-up process; the different approach strongly differs each other in their respective neutron and α particle energy-angular distributions. The reaction channels to $^{12}C(n,n)3\alpha$ channel involved in the calculation are as follows:

(a) $n+^{12}C \longrightarrow \alpha+^{9}Be^*$

$^{9}Be^* \longrightarrow n+^{8}Be$

$^{8}Be \longrightarrow \alpha+\alpha$

(b) $n+^{12}C \longrightarrow \alpha+^{9}Be^*$

$^{9}Be^* \longrightarrow \alpha+^{5}He$

$^{5}He \longrightarrow n+\alpha$

(c) $n+^{12}C \longrightarrow n+^{12}C^*$

$^{12}C^* \longrightarrow \alpha+^{8}Be$

$^{8}Be \longrightarrow \alpha+\alpha$

(d) $n+^{12}C \longrightarrow ^{5}He+^{8}Be$

$^{8}Be \longrightarrow \alpha+\alpha$

$^{5}He \longrightarrow n+\alpha$

2 Calculated Results and Discussion

As an example of the cross section, the comparison of theoretical calculated results and experimental data[8~12] of ^{12}C (n,n+2α) reaction cross section is given in Fig. 1. The measured data have large discrepancy and the theoretical calculation curve pass through the measured data.

The comparisons of theoretical calculated double differential cross sections and the experimental data[13,14] of outgoing neutron are shown in Figs. 2 ~ 3 at neutron incident energy E_n= 14.1 MeV, for outgoing angular 30.0, 37.5, 45.0, 52.5, 60.0, 120.0, 135.0, 150.0 degree, respectively. The experimental data are taken from M. Baba in 1987 by circle and 1990 by triangle, respectively. Meanwhile, the comparisons of double differential cross sections between theoretical calculated results and experimental data[14] of outgoing neutron are given in Figs. 4 ~ 7 at neutron incident energy E_n=18.0 MeV, the outgoing angular of neutron are 20.0, 25.0, 30.0, 35.0, 40.0, 45.0, 52.5, 60.0, 75.0, 90.0, 105.0, 120.0, 135.0, 146.0 degrees, respectively. The experimental data are taken from M. Baba in 1990. In the calculated results the elastic peak is not involved. In Figs. 2 ~ 7 the calculated values of outgoing neutron double differential cross sections are in agreement with experimental data very well.

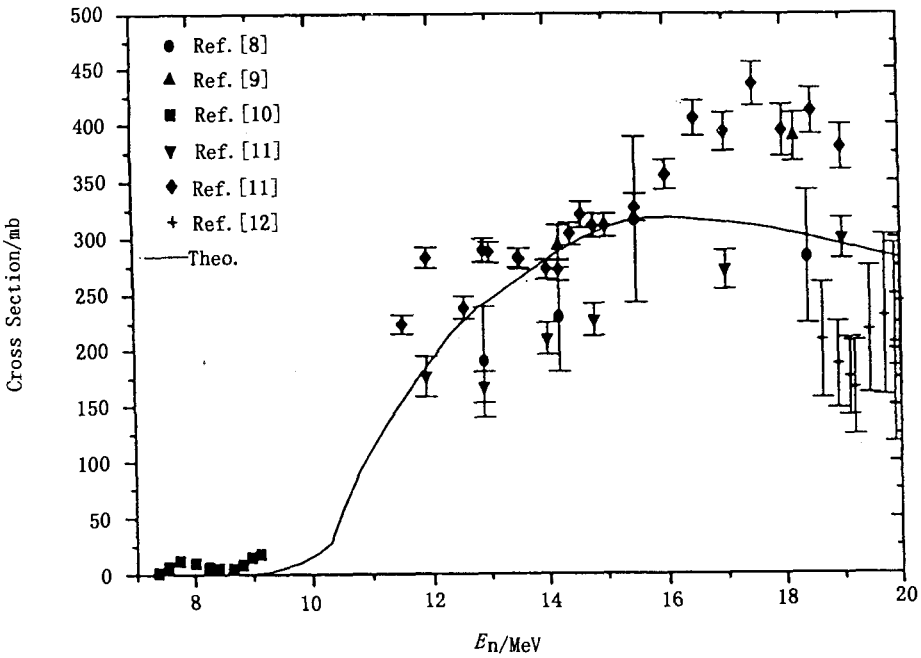

Fig. 1 Comparison of calculated $^{12}C(n,n+2\alpha)\alpha$ reaction cross section with experimental data

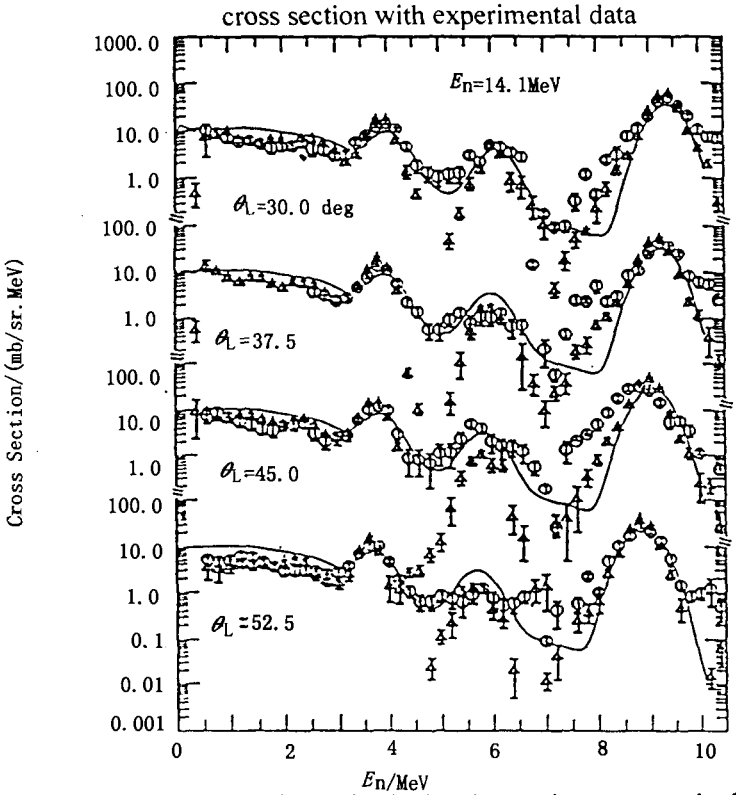

Fig. 2 Comparison of calculated outgoing neutron double differential cross section with experimental data

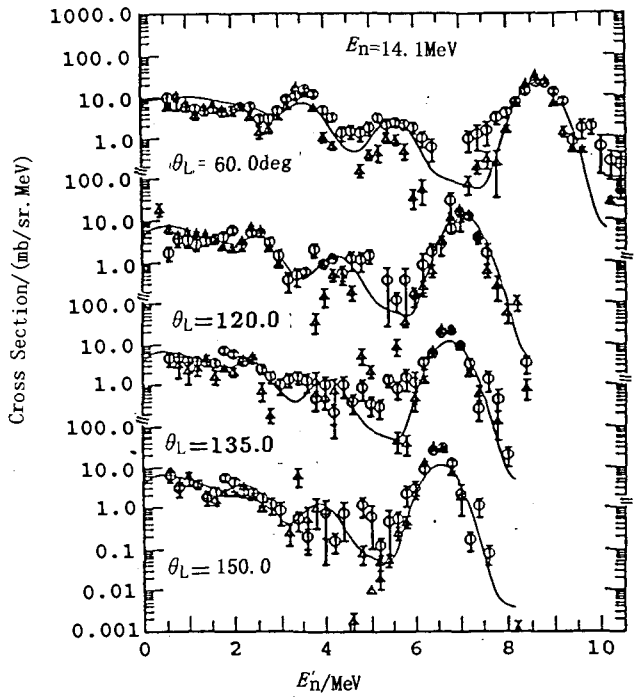

Fig. 3 Comparison of calculated outgoing neutron double differential cross section with experimental data

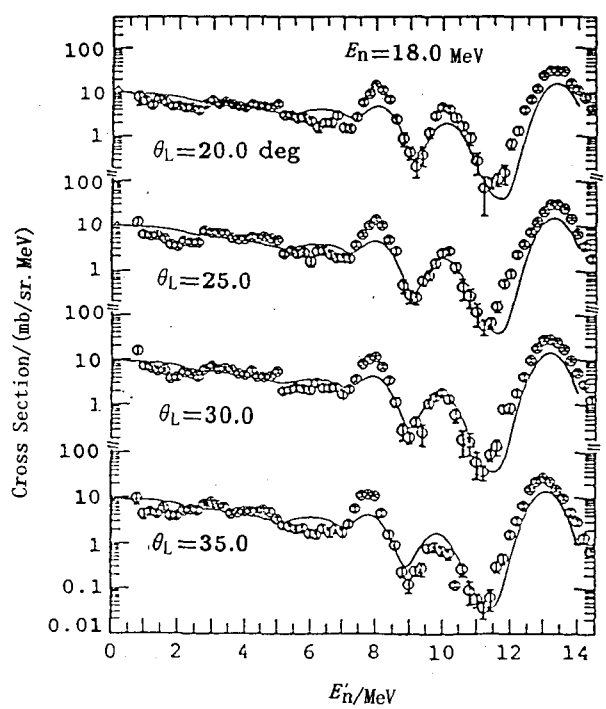

Fig. 4 Comparison of calculated outgoing neutron double differential cross section with experimental data

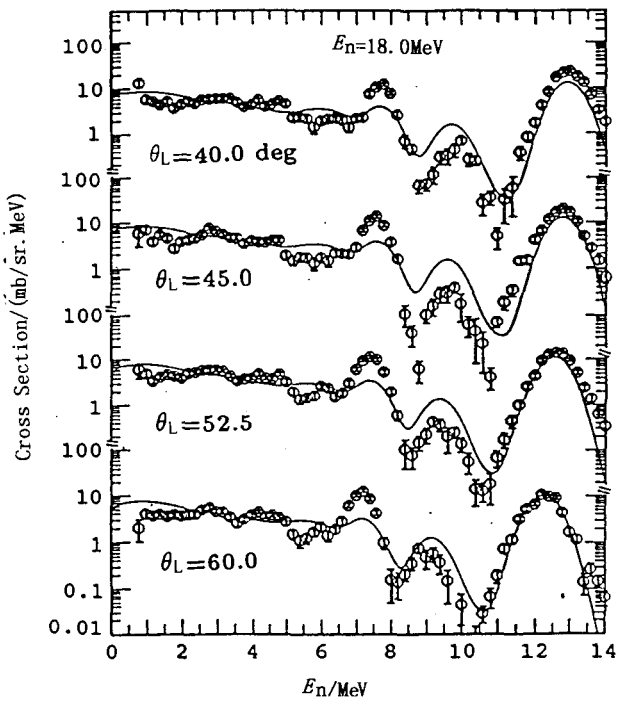

Fig. 5 Comparison of calculated outgoing neutron double differential cross section with experimental data

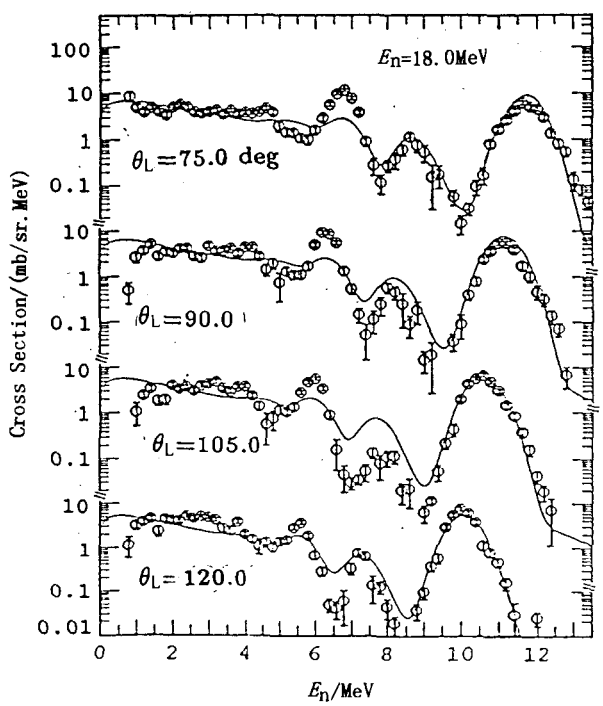

Fig. 6 Comparison of calculated outgoing neutron double differential cross section with experimental data

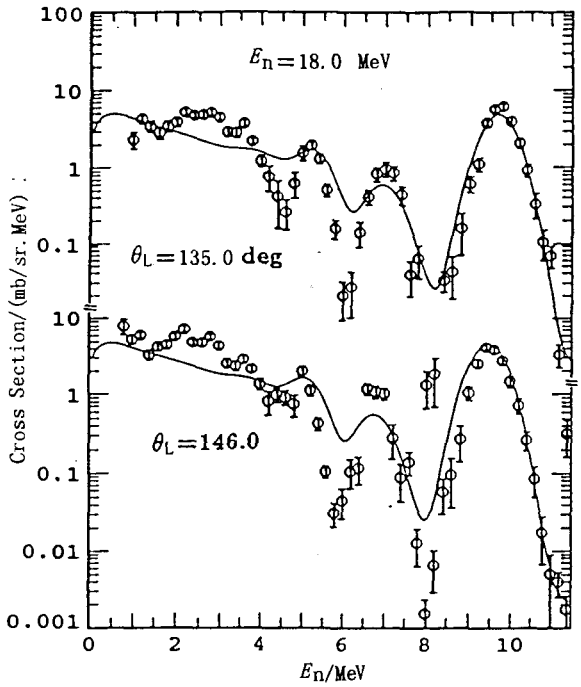

Fig. 7 Comparison of calculated outgoing neutron double differential cross section with experimental data

3 Conclusion

A new model for neutron induced light nucleus reactions has been developed. The key point in this model is the description of the particle emissions from discrete levels to discrete levels in pre-equilibrium states. The pre-equilibrium emission mechanism dominants the reaction processes. In whole reaction processes the angular momentum and parity are conserved and the energy balance is taken into account. To fit the experimental data the level broadening effect and the energy resolution must be considered. The comparison with experimental data of ^{12}C in a very wide incident neutron energies and energy-angular spectra have been performed. From the calculation we can see that the optical model still works well to give the emission branch from levels in the case of light nucleus reaction. The comparisons indicate that this new model can reproduce the nuclear data of $n+^{12}C$ successfully.

References

[1] J. S. Zhang et al. Phys. Rev. C (submitted to Phys. Rev. C)

[2] J. S. Zhang and Wen Yuanqi Chin. J. of Nucl. Phys. 16, 153 (1994)
[3] J. S. Zhang "Fast Neutron Physics" P201
[4] J. S. Zhang Proc. Int. Conf. on Nuclear Data for Basic Science and Technology. Gatlinburg, Tennesse. May 9-13 (1994) P932
[5] J. S. Zhang and S. J. Zhou Chin. J. of Nucl. Phys. 18, 28 (1996)
[6] R. B. Firestone V. S. Shirley "Table of Isotopes" 1996 Eighth Edition, A Wiley-interscience Publication John Wiley and Sonc. Sci.
[7] B. Antolkovic and Z. dolenec Nucl. Phys. A237, 235 (1975)
[8] G. M. Frye Gr et al. Phys. Rev. 99, 1375 (1955)
[9] M. Baba et al. Conf. on Nuclear Data for Basic & Applied Sci., Santa Fe, 1, 223 (1985)
[10] H. J. Brede et al. Nucl. Sci. Eng. 107, 22 (1991)
[11] B. Antolkovic et al. Nucl. Sci. Eng. 107 1 (1991)
[12] A. P. Stevens INIS Microfiches. Identification Assigned By I. A. E. A (1976)
[13] M. Baba NETU-49 (1987)
[14] M. Baba et al. JAERI-M-90-025, Tokai Reports, 383 (1990)

CN9901205

Fragment Angular Anisotropies and Inertia Parameters

A. N. Beehkami P. Nazarzaden

(Physics Department, Shiraz University, Shiraz, 71454 Iran)

Abstract

An analysis of selected fission fragment angular distributions of various target is made using exact theoretical expressions. Theoretical anisotropies obtained from the transition state model are compared with their corresponding values deduced from the statistical scission model. The nuclear moment of inertia extracted from the model calculations are compared with their estimated values from a microscopic theory, which includes the nuclear pairing interaction[1]. Single particle levels of Nilsson et al. are utilized. It is found that the value of the statistical parameter, $K_0^2 (K_0^2 = \Im_{\text{eff}} T / \hbar^2)$, is very sensitive to the energy gap parameter, Δ. The reduction of energy gap results in an increase in the moment of inertia. The effect of pairing interaction on the inertia parameters are illustrated and discussed.

Introduction

There is considerable evidence that the statistical transition model (TSM) provides a good representation of experimental fission fragment angular distributions at low spin values and moderate excitation energies. The fundamental assumption of this model is that the spin projection, K, on the nuclear symmetry axis remains unchanged during the fission process. For heavy reaction system where the angular momentum and excitation energy is large, fission fragment angular distributions are analyzed with the statistical scission model (SSM). Versions of this model have been published by Rossner et al.[2] and Bond[3]. Although the formal equation in the two models are of the same structure, variances in the distributions of angular momentum projections on the fission direction are established at very different stages on the fission process in the two models. The properties of transition state complex were studied by various authors[4~6]. Nuclear moments of inertia were extracted from the measured fission fragment anisotropies, Huizenga et al..[7] A sharp decreasing in $\Im_{sph}/\Im_{eff}$ with Z^2/A at relatively low spin values has been observed which calls for shell and / or pairing effects[8].

In the present work we have developed a special computer code to deduce the statistical parameter $K_0^2(K_0^2=\Im_{eff}T/\hbar^2)$, from experimental angular anisotropies using the exact theoretical expressions. The K_0^2 values have also been evaluated by employing the microscopic theory of interaction fermions using the single particle levels of Nilsson model. Our microscopic calculations of the inertia parameters are in satisfactory agreement with experiment, especially at lower spin values and moderate excitation energies. In Sec.1, we review the basic theoretical framework. Variances of the spin distribution obtained from model calculations based on the transition state model and in some cases the statistical scission models are presented in Sec. 2.a. In Sec. 2.b the dependence of K_0^2 on excitation energy and nuclear deformation is presented and the resulting inertia parameters obtained from microscopic theory, are compared with their corresponding experimental values.

1.1 Formalism of Transition State Moder at Excitation Energies

The excited levels in the transition nucleus are described by statistical theory. The K-distribution of these levels is predicted by Halpern et al.[9] to be Gaussian

$$F(K) \propto \exp\left(\frac{-K^2}{2K_0^2}\right) \tag{1}$$

and the variance of the distributions is

$$K_0^2 = \frac{\Im_{\text{eff}} T}{\hbar^2} \tag{2}$$

The effective moment of inertia is $\Im_{\text{eff}} = \Im_{\|}\Im_{\perp}/(\Im_{\perp} - \Im_{\|})$ where $\Im_{\perp}$ and $\Im_{\|}$ are nuclear moment of inertia about an axis perpendicular and parallel to symmetry axis and T is the temperature of the nucleus in the transition state.

With the assumption that the fragments separate along the symmetry axis and that K is a good quantum number during the fission process, then the fragment angular distribution from a state with quantum numbers K and M (projection of total spin I along the space fixed axis) is given by[10]

$$W_{M,K}^{I}(\theta) = [(2I+1)/4\pi]\left|d_{M,K}^{I}(\theta)\right|^2 \tag{3}$$

The normalized $d_{M,K}^{I}(\theta)$ functions are defined by[11]

$$d_{M,K}^{I}(\theta) = [(I+M)!(I-M)!(I+K)!(I-K)!]^{1/2} \sum_{X} \frac{(-1)^X (\sin(\theta/2))^{K-M+2X} (\cos(\theta/2))^{2I-K+M-2X}}{(I-K-X)!(I+M-X)!(X+K-M)!X!} \tag{4}$$

where the sum is over X=0,1,2... and contains all terms in which no negative value appears in the denominator of the sum for any one of the quantities in parentheses.

If the target and projectile spins are zero and no particle emission from the initial compound nucleus occur before fission (i.e.M=0), then the overall angular distribution for a fixed energy E, is given by Griffin[12].

$$W(\theta) \propto \sum_{I=0}^{\infty} (2I+1) T_I \sum_{K=-I}^{I} \left[(2I+1)\left|d_{M=0,K}^{I}(\theta)\right|^2 \exp\left(\frac{-K^2}{2K_0^2}\right) \Big/ \sum_{K=-I}^{I} \exp\left(\frac{-K^2}{2K_0^2}\right) \right] \tag{5}$$

where the transmission coefficients are written as T_l, since l=I when M=0. Eq.(5) is an exact theoretical expression for computation of fission fragment angular distribution when both the target and projectile spins are zero. If the target and projectile spins ate included, an exact expression for the fission fragment angular distribution is[11,12]

$$W(\theta) \propto \sum_{I=0}^{\infty} \sum_{M=-j_{\max}}^{+j_{\max}} \left[\sum_{l=0}^{\infty} \sum_{j=|I_0-s|}^{I_0+s} \sum_{\mu=-I_0}^{I_0} \frac{(2l+1)T_l \left|C_{M,0,M}^{j,l,I}\right|^2 \left|C_{\mu,M-\mu,M}^{I_0,s,j}\right|^2}{\sum_{l=0}^{\infty}(2l+1)T_l} \right] \sum_{K=-I}^{I} \left[(2I+1)\left|d_{M,K}^{I}(\theta)\right|^2 \exp\left(\frac{-K^2}{2K_0^2}\right) \Big/ \sum_{K=-I}^{I} \exp\left(\frac{-K^2}{2K_0^2}\right) \right] \tag{6}$$

The quantity I_0, s and j are the target spin, projectile spin and channel spin, respectively. The channel spin j is defined by the relation $j = I_0 \oplus s$. The total angular momentum I is given by the sum of the channel spin and orbital angular momentum; $I = j \oplus l$ The projection of I_0 on the space-fixed axis is given by μ, whereas the projection of j (and I) on this axis is M.

The use of equations (5) or (6), requires the evaluation of many $d^I_{M,K}(\theta)$ functions and the Clebsch-Gordan coefficients, hence these equations have rarely been used for data analysis. In the present paper, we have developed a special computer code to run these more cumbersome theoretical expressions and thereby to deduce the statistical variance K_0^2. We have found quite different values of K_0^2 as compared to their values from the approximate expression[13~15].

1.2 Formalism of the Statistical Scission Model

According to the statistical scission model, the relative cross-section, $W(\theta)$, for fission fragments to be emitted in the direction $\hat{n}$ forming angle θ with the beam axis, when the target and projectile spins are zero is given by Huizenga et al.[16]

$$W(\theta) \propto \sum_{I_{\min}}^{I_{\max}} (2I+1) T_I \frac{\sum_{m=-I}^{I} [(2I+1)/2] \left| D^I_{M=0,m}(\theta) \right|^2 \exp(-m^2/2S_0^2)}{\sum_{m=-I}^{I} \exp(-m^2/2S_0^2)} \tag{7}$$

here again the distribution of spin projection m (the projection of total angular momentum I along $\hat{n}$), is taken to be a Gaussian with variance S_0^2. Where S_0^2 for spherical fission fragments is given by either of the following Eqs.[2]

$$S_0^2 = \begin{cases} 2\sigma^2 \left\{ \left[2\sigma^2 + \left(\mu R_c^2 T/\hbar^2 \right) \right] / \left(\mu R_c^2 T/\hbar^2 \right) \right\}, \\ \left(2\Im_{\text{sph}} T/\hbar^2 \right) \left[(2\Im_{\text{sph}} + \mu R_c^2)/\mu R_c^2 \right] \end{cases} \tag{8}$$

where $\sigma^2 = \Im_{\text{sph}} T/\hbar^2 = \frac{2}{5} MR^2 T/\hbar^2$.

The quantities $\Im_{\text{sph}}$, T, M and R, are the moment of inertia, nuclear temperature, mass and radius of one of the symmetric fission fragments. R_c is the distance between centers of fragments at scission configuration and is equal to R_c=1.225$(A_1^{1/3} + A_2^{1/3})(c/a)^{2/3}$ (A_1 and A_2 are mass numbers of fission fragments). For a scission configuration of two unattached deformed fragments, the variance S_0^2 is given by either of two Eq.[2]

$$S_0^2 = \begin{bmatrix} 2\sigma_{\parallel}^2 \left\{ \left[2\sigma_{\perp}^2 + \left(T\mu R_c^2 / \hbar^2 \right) \right] \right/ \left[\left(\mu R_c^2 T / \hbar^2 \right) + 2\sigma_{\perp}^2 - 2\sigma_{\parallel}^2 \right] \\ \left(2\Im_{\parallel} T / \hbar^2 \right) \left[(2\Im_{\perp} + \mu R_c^2) / (\mu R_c^2 + 2\Im_{\perp} - 2\Im_{\parallel}) \right] \end{bmatrix} \tag{9}$$

where $\sigma_{\parallel}^2$, $\sigma_{\perp}^2$ $\Im_{\parallel}$ and $\Im_{\perp}$ are spin cut-off parameters and moments of inertia of a single fission fragment rotating about an axis parallel and perpendicular to the symmetry axis, respectively. The primary fission fragments are assumed to have spheroidal shapes with the principal one-half axes of magnitude in terms of their ratio *c/a* namely[16].

$$c = r_0 A^{1/3} (c/a)^{2/3} \quad \text{and} \quad a = r_0 A^{1/3} (c/a)^{-1/3} \tag{10}$$

where A is the mass number of each fission fragments. The formula (7) is similar to the corresponding equation in the transition state model. However as seen for equations (8) and (9) the variance S_0^2 is calculated in a completely different way. The total intrinsic excitation energy in the two fission fragments at scission is given by

$$E = E_{\text{c.m}} + Q - E_{\text{K}} - E_{\text{def}} - E_{\text{rot}} \tag{11}$$

where Q represents the difference in energy between the entrance channel nuclei and the ground state of the two fission fragments. $E_{\text{K}} + E_{\text{def}}$ is the sum of the kinetic and deformation energies at the instant of scission and E_{rot} is the rotational energy of the scission configuration. The kinetic energy is estimated by use of the expression

$$E_{\text{K}}(\text{MeV}) = 0.107 \frac{Z^2}{A^{1/3}} + 22 \tag{12}$$

where Z and A are the charge and mass number of composite system. The rotational energy E_{rot} of the system at scission configuration for spin I and projection m on the scission axis is

$$E_{\text{rot}} = \frac{\left[(I + 1/2)^2 - m^2 \right] \hbar^2}{2\mu R_c^2 + 4\Im_{\perp}} \tag{13}$$

μ is the reduced mass of the fission fragments. The temperature of each fission fragment was assumed being given by

$$T = [(E/2)/\text{LDP}]^{1/2} \tag{14}$$

The variances of the spin distribution can be estimated also, with a microscopic theory of interacting fermions using a realistic set of single particle levels. For deformed fission fragments with axial symmetry, the single particle states are from

the motion of a nucleon in the deformed average potential. They are characterized by the projection Ω of the angular momentum on the nuclear symmetry axis.

Employing the microscopic theory with nuclear pairing, the spin cut-off parameter $\sigma_{\|}^2(E)$ is defined by[2,17]

$$\sigma_{\|}^2(E) = \Im_{\|} T/\hbar^2 = \frac{1}{2}\left\{\sum_i \Omega_{\mathrm{pi}}^2 \sec h^2\left(\frac{1}{2}\beta E_{\mathrm{pi}}\right) + \sum_i \Omega_{\mathrm{ni}}^2 \sec h^2\left(\frac{1}{2}\beta E_{\mathrm{ni}}\right)\right\} \quad (15)$$

where $\beta = \frac{1}{T}$ (T is the nuclear temperature), $E_{\mathrm{pi}}(E_{\mathrm{ni}})$ is the proton (neutron) quasi particle energy. The quasi particle energies E_i are related to the single particle energies ε_i by $E_i = \left[(\varepsilon_i - \lambda)^2 + \Delta^2\right]^{1/2}$ where λ is the chemical potential and Δ is the ground state gap parameter. The quantity $\Im_{\|}$ is the moment of inertia about an axis parallel to the symmetry axis. The spin cut-off parameter $\sigma_{\|}^2(E)$ is determined by the properties of the intrinsic state. Hence Eq.(15) is a definition of the moment of inertia.

In so far as the neutron-proton superfluids are independent, then the values of the thermodynamic functions are the sum of those for neutrons and protons. For example the intrinsic excitation energy corresponding to a given temperature is

$$E_{\mathrm{int}} = E_{\mathrm{int}}^{\mathrm{P}} + E_{\mathrm{int}}^{\mathrm{n}} \quad (16)$$

Since the interaction between the neutron and proton is neglected, the value of the moment of inertia is the sum of the proton and neutron moments of inertia.

$$\Im = \Im_{\mathrm{p}} + \Im_{\mathrm{n}} \quad (17)$$

The temperature dependence of $\Im$ is investigated by examining the data on angular distribution of fission fragments. Such angular distribution depends on the statistical variance K_0^2 discussed in Sec.2.1. This quantity is

$$K_0^2 = \Im_{\mathrm{eff}} T/\hbar^2 = \left(\frac{T}{\hbar^2\sigma_{\|}^2} - \frac{1}{\Im_{\perp}}\right)^{-1} T/\hbar^2 \quad (18)$$

The dependence of K_0^2 upon excitation energy is therefore a good test of the persistence of super conducting effects to finite excitation energies. The dependence of K_0^2 versus the excitation energy for some typical cases of helium-induced fission reactions, has been tested and the results will be given in the next section.

2.1 Results and Discussions

Several fission reactions are chosen to deduce the statistical variance, K_0^2 by

fitting experimental fission fragment angular distributions with exact theoretical expressions, which do and don't include the target and projectile spins. Angular distributions have been studied for fragments in the fission of ^{209}Bi, ^{233}U, ^{234}U, ^{235}U, and ^{238}U by 51.5 MeV deuterons and in the fission of these same nuclei including ^{197}Au by 42.8 MeV and 103 MeV helium ions. Optical-model transmission coefficients are used in all calculations and the α-particle transmission coefficients, Huizenga and Igo[18], are kept fixed for the calculations with the different equations. The experimental anisotropy W(170)/W(90) for ^{238}U(He,f) reaction with 42.8 MeV is 1.52 taken from Gindler et al.[13]. The curve in Fig. 1 illustrates the theoretical dependence of anisotropy of K_0^2 extracted from Eq. (5), which assumes that both the target and projectile spins are zero. The experimental anisotropy W(174)/W(90) for ^{209}Bi(d,f) reaction with 51.5 MeV deuterons is 1.592. The curve in Fig. 2 illustrates the theoretical dependence of anisotropy on K_0^2 for this reaction deduced from Eq. (6), which includes the target and projectile spins. Similar results for ^{197}Au(He,f) reaction with 103 MeV helium ions is shown in Fig. 3. The fission fragment angular anisotropies together with the variances K_0^2, obtained from the listed anisotropies at 42.8 MeV helium ions, using the exact expressions are given in Table 1.

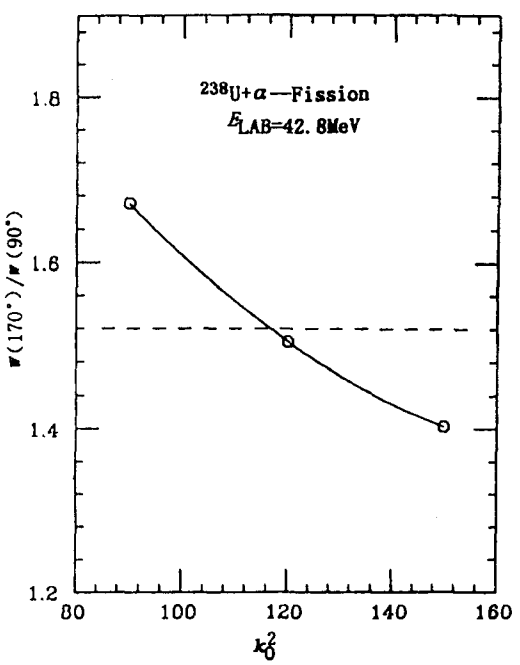

Fig. 1 Anisotropy W(170)/W(90) of fission fragments for ^{238}U(He,f) reaction with 42.8 MeV α-particles. The theoretical curve is calculated with Eq. (5)

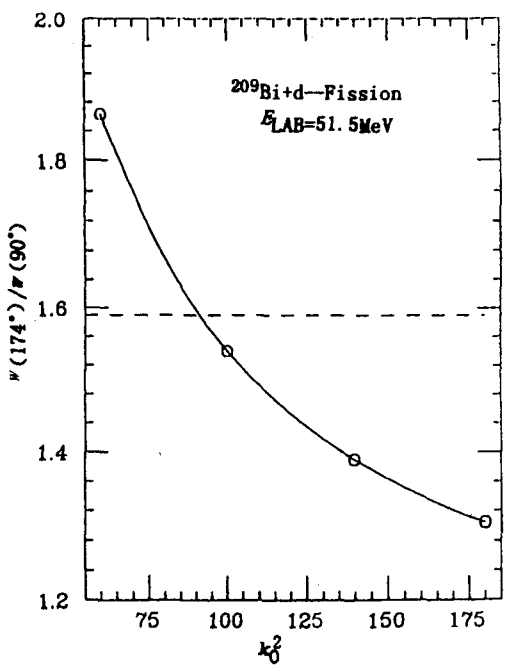

Fig. 2 Anisotropy W(174)/W(90) of fission fragments for ^{209}Bi(d,f) reaction with 51.5 MeV deuterons. The theoretical curve is calculated with Eq. (6)

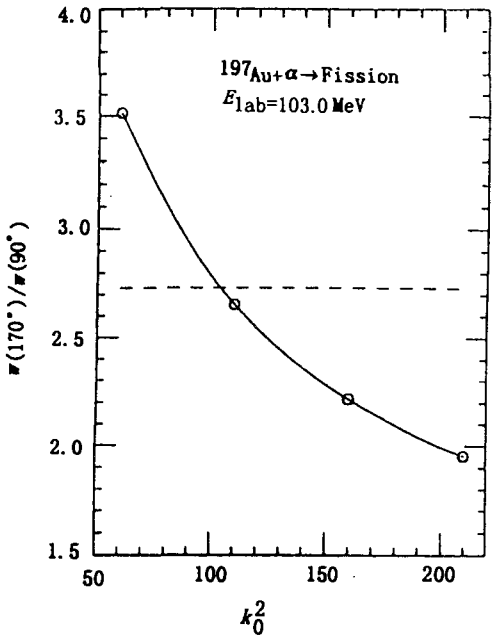

Fig. 3 Anisotropy W(170)/W(90) of fission fragments for ^{197}Au(He,f) reaction with 103 MeV α-particles.
The theoretical curve is calculated with Eq. (6)

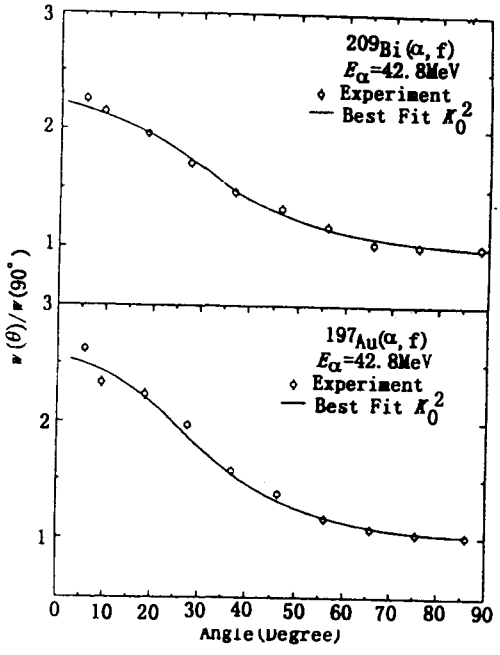

Fig. 4 The angular distributions of fragments in the helium-ion induced fission of ^{197}Au and ^{209}Bi. The experimental data are expressed by open circles. The solid curve shows the "best fit" K_0^2 calculated angular distributions.

Table 1 Anisotropies, K_0^2 and S_0^2 values determined from the exact theoretical fit to the data at 42.8 MeV helium ions

Target	$\frac{W(170)}{W(90)}$ (a)	K_0^2 (b)	K_0^2 (c)	S_0^2 (d)	S_0^2 (e)
^{197}Au	2.47	39	37.5	33.1	46.2
^{209}Bi	2.12	56	46.5	45.5	52.7
^{233}U	1.38	151	151.5	135	150
^{234}U	1.42	131	138	133	135.4
^{235}U	1.40	149	146	129	152.6
^{238}U	1.52	108	116.3	101	111

a) Anisotropy measurement taken from [13]
b) K_0^2 calculated from a polynomial fit to the data [13]
c) K_0^2 values obtained from the present work
d) Best fit values of S_0^2 with $I_f = 20\hbar$
e) Theoretical values of S_0^2

Examination of the K_0^2 given in Table 1, reveals that our K_0^2 values are in some cases smaller than their previously reported values. For example, the experimental anisotropy for ^{209}Bi(He,f) reaction is 2.12. The results of our exact

theoretical calculation with spin of target and projectile included, is 46.5 as compared to its reported value of 56, which is about 17% small. This demonstrates the error introduced by neglecting the target and projectile spins. The fission anisotropies and their corresponding variances K_0^2, obtained from the listed anisotropies at 51.5 MeV deuterons and 103 MeV helium ions, using the exact expressions are listed in Table 2. The values of K_0^2 reported in Table 1 and 2 were calculated from the listed anisotropies since these anisotropies may result not only from first chance but also second and third chance fission The values of K_0^2 represent for some type of average value for the various fissioning nuclei, not for the initial compound nucleus.

Table 2 Anisotropies and K_0^2 values determined from the exact theoretical fit to the data

Target	W(174) [a] / W(90)	51.5 MeV deuterons K_0^2 [b]	K_0^2 [c]	W(170) [a] / W(90)	103 MeV helium ions K_0^2 [b]	K_0^2 [c]
^{197}Au	--	--	--	2.73	113	102
^{209}Bi	1.592	105	91	2.56	132	116
^{233}U	1.270	226	213	1.57	371	283
^{234}U	1.299	198	192	1.55	381	398
^{235}U	1.211	299	276	1.62	345	353
^{238}U	1.348	172	170	1.60	353	369

a) Anisotropy measurement taken from [13]
b) K_0^2 calculated from a polynomial fit to the data [13]
c) K_0^2 values obtained from the present work

Again, comparison of the K_0^2 values listed in Table 2 shows that variances, K_0^2 deduced from exact calculations are generally smaller than their corresponding values reported previously[13,16]. The experimental anisotropy for ^{209}Bi(d,f) reaction with 51.5 MeV deuterons is 1.592 the results of our analysis using Eq. (6) is 91, as compared to its previously reported values of 105 which is about 15% small.

The measured fission fragment angular distributions at 42.8 MeV helium-induced fission of ^{197}Au and ^{209}Bi, taken from Chaudhry et al.[19] are fitted using the "best fit" values of K_0^2 from Table 1, the results are displayed in Fig. 4. It is seen that the exact theoretical calculations give an excellent fit to the experimental fission fragment angular distributions.

Variance S_0^2, has been evaluated at 42.8 MeV helium ions fitting the listed experimental fission fragment angular distributions using Eq. (7) by assuming $I_f = 20\hbar$. Our best fit values are given in Table 1. It is seen that in some cases the deduced values of S_0^2 is close to the values of K_0^2 calculated from the TSM model. The variances S_0^2 have also been calculated, assuming spheroidal fragments at the

scission configuration. These theoretical values of S_0^2 are computed with Eq.(9) by assuming r_0=1.225 fm, a=A/8 and E_{def}=10 MeV. Our theoretical values of S_0^2 for deformed fragments are considerably smaller than their corresponding experimental values for uranium reactions. In order to bring the predicted values in agreement with the experimental variances, the level density parameter "a" would need to be changed from A/8 up to A/20. The results are shown in the last column of Table 1.

We conclude that the variances K_0^2 produced by the TSM model for the 42.8 MeV helium-ion reactions give generally a good agreement relative to the SSM model. This reestablished the applicability of this model for systems with well defined deformation and lower spin values at moderate energies.

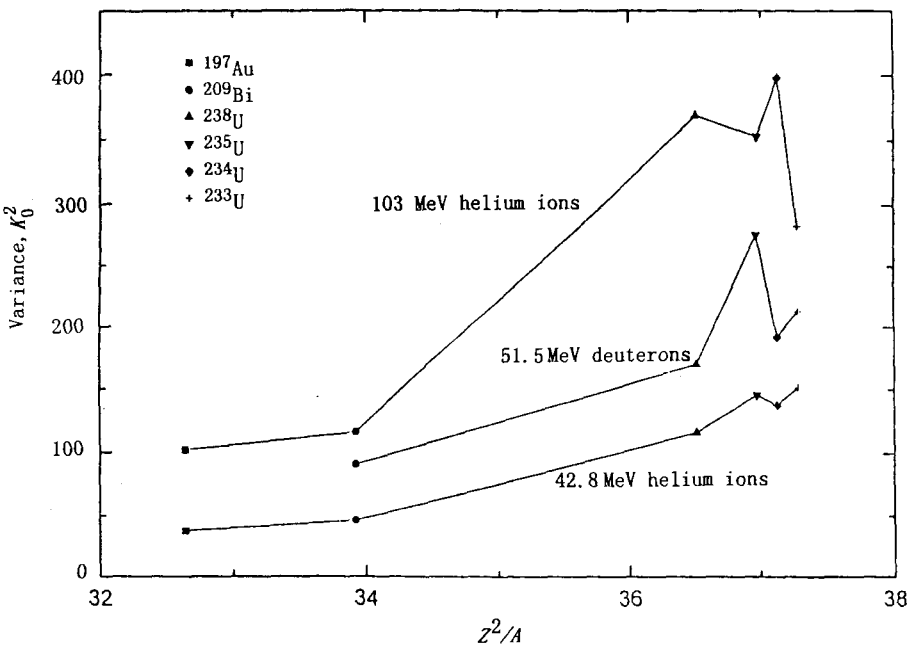

Fig. 5 Values of K_0^2 as a function of Z^2/A of the fissioning nucleus for reactions listed in Table 1 and 2. The calculated variances are labeled according to the target nucleus.

Variances K_0^2 determined from the listed angular anisotropies at 42.8 and 103 MeV helium-ion and 51.5 MeV deuterons induced fission of various targets under study, are plotted in Fig. 5 as a function of Z^2/A of the fissioning nucleus. From the study of Fig. 5 the following general trends are observed (i) the variance K_0^2 for given target and projectile is larger for the high energy projectiles, (ii) the K_0^2 value for a given projectile energy tends to increase as the parameter Z^2/A of the

compound nucleus increase. This is related to an increase in $\Im_{eff}$ with Z^2/A. We have converted our "best fit" values of K_0^2 to values of $\Im_{sph}/\Im_{eff}$ using Eq. (2) for 42.8 MeV helium ions induced fission reactions by utilizing the appropriate nuclear temperature, T. We have estimated the temperature for first and second chance fission. In Fig. 6 we show results only for the assumption of first chance fission.

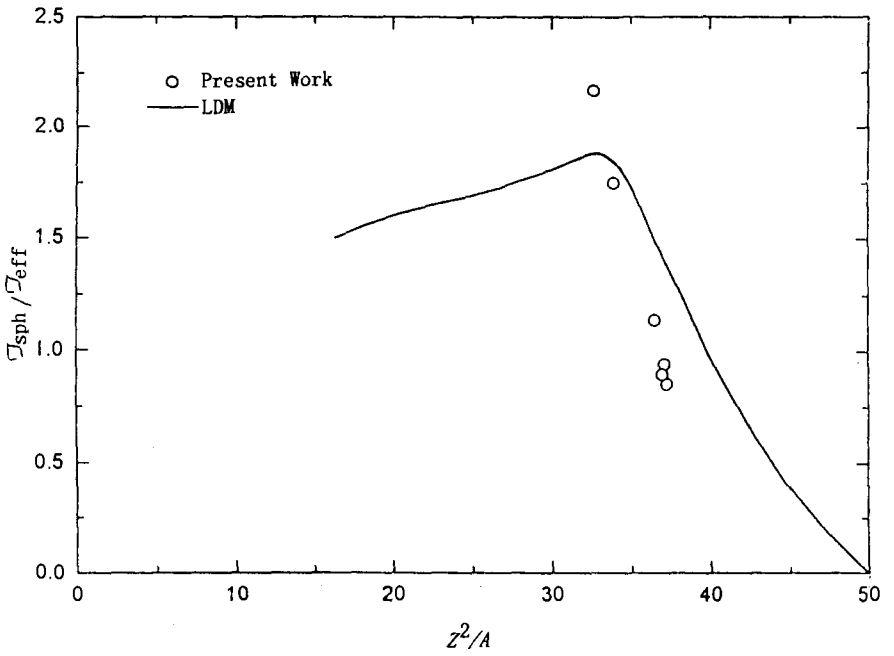

Fig. 6 Comparison of the experimental values of $\Im_{sph}/\Im_{eff}$, determined from helium-ion induced reactions with the liquid drop model at 42.8 MeV helium ions. Solid line curve represents the theoretical non-rotating (LDM) model values of $\Im_{sph}/\Im_{eff}$ as a function of Z^2/A.

It is clear from Fig. 6 that there is a distinct increase of $\Im_{sph}/\Im_{eff}$ with decreasing Z^2/A. This is the effect which was observed by Simmons et al.[20] and confirmed by others[21] and discussed in connection with dependence of K_0^2 on the excitation energy above fission barrier. The proposed explanation involves pairing energy and/or shell effects, which will be discussed next.

2.2 Inertia Parameters

For determination of fission fragment anisotropies in the super conducting model, the most important parameter to be calculated is $\Im_{\|}T/\hbar^2$. This quantity is

directly related to the average of K_0^2 over the particle spectrum and is given by the spin cut-off parameter, $\sigma_{\|}^2 = \Im_{\|} T / \hbar^2$. The microscopic theory is used to compute $\sigma_{\|}^2(E)$ by way of Eq. (15). The energies and spins of the single particle levels for a given deformations δ, were calculated with a program and parameters of Nilsson et al.[22]. The initial values of the gap parameters, Δ_n and Δ_p, were obtained from the newest mass table of G. Audi. et al.[23]. The chemical potential, λ, were evaluated by a procedure outlined in our pervious publications[24,25]. Values of $\sigma_{\perp}^2(E)$ are calculated with the rigid body moment of inertia. K_0^2 Values are deduced as a function of excitation energies for the case of helium induced fission of ^{197}Au, ^{209}Bi and ^{238}U target nuclei. The temperature dependence of gap parameters for ^{242}Pu fissioning nucleus with Δ_n=1.23 MeV and Δ_p=1.37 MeV is shown in Fig. 7. The moment of values of inertia for 242Pu is plotted as a function of nuclear temperature in Fig. 8. The experimental values of K_0^2 versus the excitation energy for ^{201}Tl, ^{213}At, and ^{242}Pu fissioning nucleus together with theoretical curves calculated from the super conducting model are displayed in Figs. 9 ~ 11. In the case of ^{242}Pu, the calculations are made for shapes corresponding to deformation parameter δ=0.37 and δ=0.65. It is seen that the agreement between the calculations and experiment is very good. The results from LDM model are also plotted for comparison.

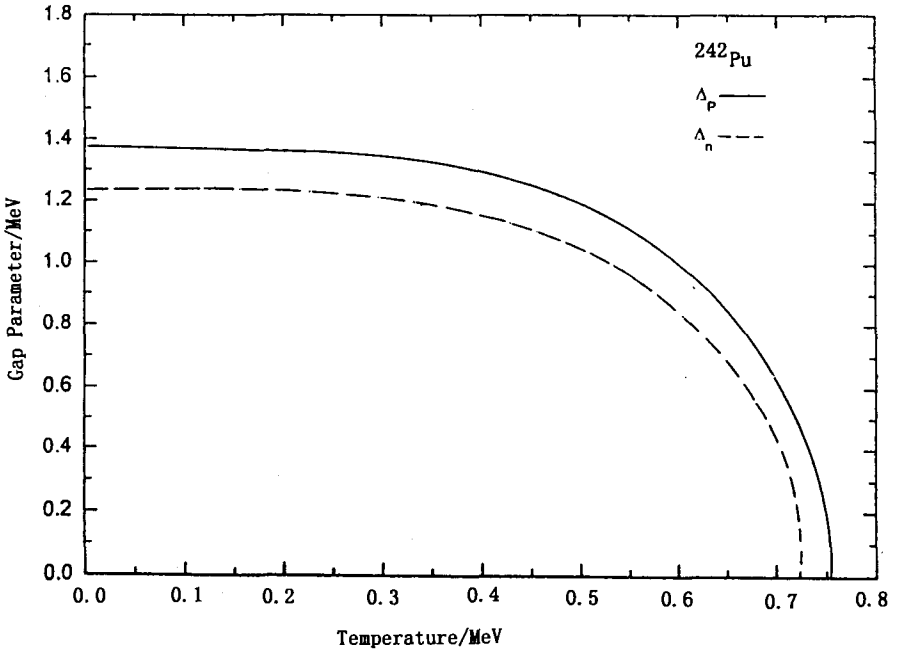

Fig. 7 Temperature dependence of the neutron and proton energy gap parameters of ^{242}Pu nucleus.

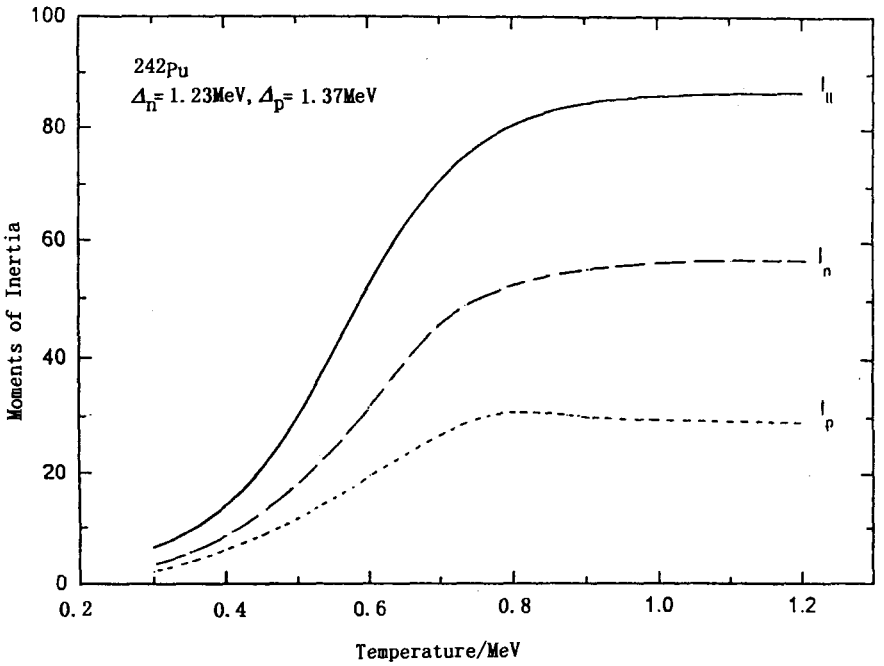

Fig. 8 Temperature dependence of moments of inertia for ^{242}Pu nucleus.

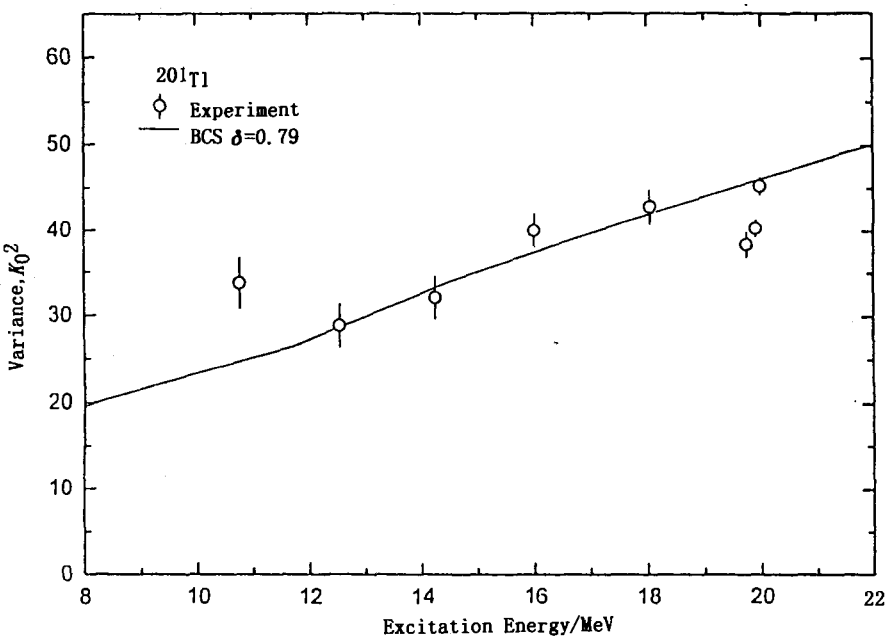

Fig. 9 Variation of K_0^2 with the excitation energy of the nucleus ^{201}Tl. The experimental points are taken from [19]. The calculated values of K_0^2 corresponding to the deformation (δ=0.79) is shown by solid line.

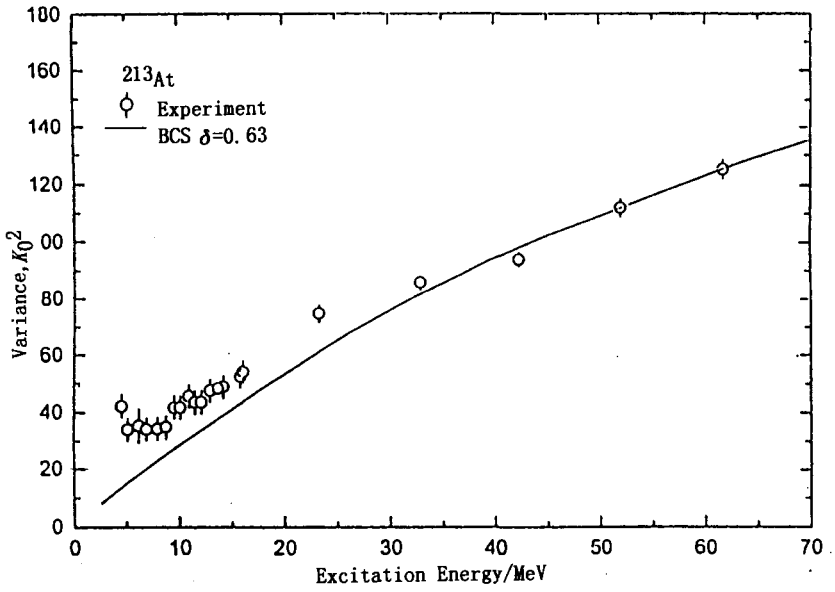

Fig. 10 Same as Fig. 9 for the ^{213}At nucleus. The experimental points are taken from [26]. The solid line curve gives the theoretical energy dependence from a microscopic theory for δ=0.63 by assuming $1/\sigma_{\perp}^2$ to be small.

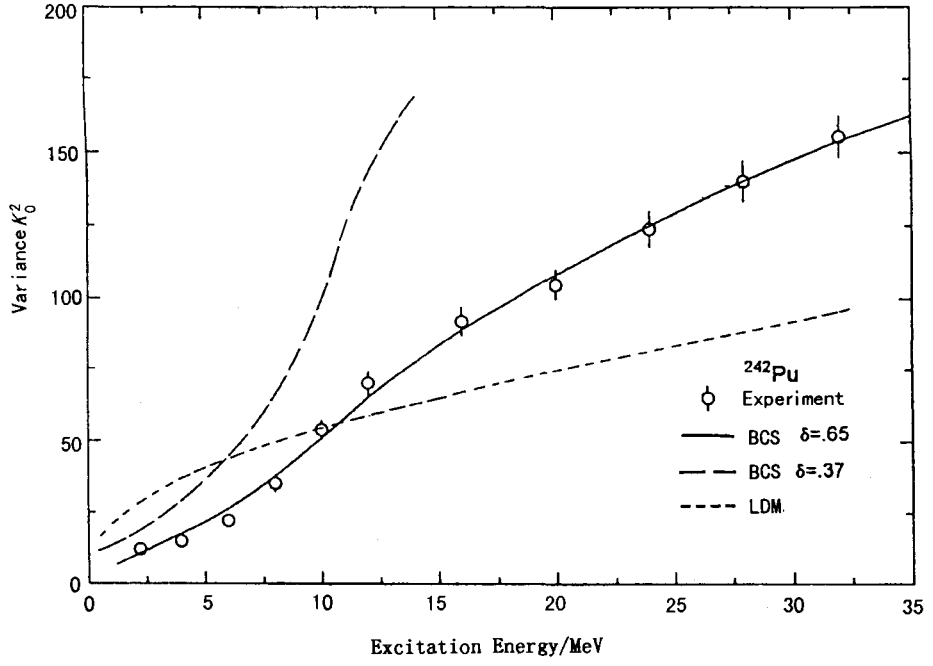

Fig. 11 Variation of K_0^2 with the excitation energy of the nucleus ^{242}Pu. The experimental points are taken from [21]. The calculated values of K_0^2 corresponding to the barrier I (δ=0.37) and barrier II (δ=0.65) are shown by dashed and solid line respectively.

In summery, by considering the various statistical interpretation of fission fragment angular anisotropies, we have concluded that the TSM model gives generally a good representation of experimental angular anisotropies at moderate excitation energies.

The exact theoretical expressions including target and projectile spins as given in Eqs. (5) and (6) provides more precise information on the fission fragment angular anisotropies. The rather encouraging results obtained by applying microscopic theory for several fission reactions may serve as means of calculating the total cross-sections and angular distributions of fission fragments. We intend to extend such investigations to anisotropies produced in heavy ion reactions.

References

[1] J. Bardeen, L. N. Cooper and J. R. Schrieffer, Phys. Rev. 106, (1957)162
[2] H. Rossner, J. R. Huizenga and W. U. Schroder, Phys. Rev. C, Vol. 33, No. 2 (1985)560
[3] P. D. Bond, phys. Rev. Lett. 52, (1984)414
[4] R. Vandenboch and J. R. Huizenga, Nuclear Fission (Academic, New York, 1973)
[5] H. Rossner et al., Phy. Rev. C27, (1981) 2666
[6] V. S. Ramamuthy and S. S. Kapoor, Phys. Lett. 54, (1985)178
[7] J. R. Huizenga et al., Phys. Rev, Vol. 177, No. 4, (1969)1826
[8] L. C. Vaz and J. M. Alexander. Phys. Report, 97, (1983)1
[9] I. Halpern, Ann. Rev. Nucl. Sci 9, (1959)245
[10] J. R. Huizenga, A. N. Behkami, J.W. Meadows, JR and E.D. Klema, Phys. Rev, Vol. 174, No. 4, (1968)1539
[11] J. R. Huizenga, L. G. Moretto and A. N. Behkami, Phys. Rev, Vol. 177, No. 4, (1969)1826
[12] J. J. Griffin, Phys. Rev. B354 (1965)139
[13] J. Gindler et al., Nucl. Phys. A145 (1970)337
[14] M. B. Tsang et al., Phys. Rev. C28 (1983)747
[15] M. Prakash et al., Phys. Rev. Lett 52 (1984)990
[16] J. R. Huizenga, H. H. Rossner and W. U. Schroder, J. Phys. Soc. JPN. 54, (1985)257
[17] J. R. Huizenga et al., Nucl. Phys. A123, (1974)589
[18] J. R. Huizenga and J. Igo, Nucl. Phys.29 (1962)462
[19] R. Chaudhry et al., Phys. Rev.126, (1962)220
[20] J. E. Simmons and H. Hofman, Nucl. Phys. A394, (1983)477
[21] M. Sano and M. Wakai, Progress of Theoretical Physics, Vol. 48, No. 1, (1972)160
[22] S. G. Nilsson et al., Nucl. Phys. A131, (1969)1
[23] G. Audi, A. H. Wapstra, Nucl. Phys. A566, (1993)1
[24] A. N. Behkami, Z. Kargar, 1992, J. Phys. G, Nucl. Particle.18, 1223
[25] A. N. Behkami et al., Bull. Am. Phys. Soc, Vol.41, No. 5, (1996), AD13
[26] S. S. Kapoor et al., Phys. Rev, Vol. 149, (1966)965

CN9901206

Calculations of Complete Data for n+^{89}Y in the Energy Region 0.001 ~ 20 MeV

Cai Chonghai
(Department of Physics, Nankai University, Tianjin 300071)
Shen Qingbiao
(China Nuclear Data Center, CIAE)

Abstract

All reaction cross sections, secondary neutron spectra and elastic scattering angular distributions of n+^{89}Y in E_n=0.001 ~ 20 MeV are calculated. Pretty good results in accordance with experimental data are obtained. And the data results are given in ENDF/B-6 format.

Introduction

Among the large number of fission product nuclides, ^{89}Y is one of several very important nuclides for which there are abundant experimental data for σ_{tot} and elastic scattering angular distributions, sufficient experimental data for $\sigma_{n,\gamma}$ and $\sigma_{n,2n}$, some data for σ_{el}, $\sigma_{n,n'}$, $\sigma_{n,p}$ and $\sigma_{n,\alpha}$. There are no experimental data for other reaction cross sections and secondary neutron spectra. All of the experimental data were taken from EXFOR. The universal optical potential parameters for six channels used in calculations are given in Table 1.

Firstly, the code APMN[1] was used to automatically get the optimum parameters of optical potential for neutron channel. There are no experimental σ_{non} for ^{89}Y to search for the optimum optical potential parameters. They were calculated from experimental σ_{el} and $\sigma_{n,\gamma}$. The final optimum set of optical potential parameters for neutron channel are (the parameters not listed here are taken the same values as in Table 1):

V_0 = 55.46697998, V_1 = –0.62699956, V_2 = 0.01931670, V_4 = –0.09212393,
W_0 = 4.56148911, W_1 = 0.23274532,
U_0 = –0.21403342, U_1 = 0.38227317, U_2 = –0.08095945,
a_r = 0.44500044, a_s = 0.40294382, a_v = 0.77707744,
r_r = 1.27821732, r_s = 1.37984145, r_v = 1.10318673.

Table 1 The universal optical potential parameters for six channels

channel	n	p	t	^{3}He	d	α
a_r	0.75,	0.75,	0.72,	0.72,	0.71,	0.520,
a_s	0.58,	0.51,	0.84,	0.88,	0.78,	0.520,
a_v	0.58,	0.51,	0.84,	0.88,	0.78,	0.520,
a_{SO}	0.75,	0.75,	0.72,	0.72,	0.71,	0.520,
r_r	1.17,	1.17,	1.20,	1.20,	1.17,	1.442,
r_s	1.26,	1.32,	1.40,	1.40,	1.30,	1.442,
r_v	1.26,	1.32,	1.40,	1.40,	1.30,	1.442,
r_{SO}	1.01,	1.01,	1.20,	1.20,	0.64,	1.442,
r_c	1.25,	1.25,	1.30,	1.30,	1.30,	1.250,
V_0	56.30,	54.00,	165.00,	151.90,	90.60,	164.700,
V_1	−0.32,	−0.32,	−0.17,	−0.17,	0.00,	0.000,
V_2	0.00,	0.00,	0.00,	0.00,	0.00,	0.000,
V_3	−24.00,	24.00,	−6.40,	50.00,	0.00,	0.000,
V_4	0.00,	0.40,	0.00,	0.00,	0.00,	0.000,
V_{SO}	6.20,	6.20,	2.50,	2.50,	7.13,	0.000,
W_0	13.00,	11.80,	46.00,	41.70,	12.00,	0.000,
W_1	−0.25,	−0.25,	−0.33,	−0.33,	0.00,	0.000,
W_2	−12.00,	12.00.	−110.00,	44.00,	0.00,	0.000,
U_0	−1.56,	−2.70,	0.00,	0.00,	0.00,	22.400,
U_1	0.22,	0.22,	0.00,	0.00,	0.00,	0.000,
U_2	0.00,	0.00,	0.00,	0.00,	0.00,	0.000,

Secondary, the code DWUCK4[2] was used to calculate the cross sections and angular distributions of direct inelastic scattering to 6 levels. These direct inelastic scattering data and the optimum set of optical potential parameters were taken as the input data of the kernel program SUNF[3]. Through adjusting some parameters in the input data of SUNF by hand again and again, the cross sections $\sigma_{n,\gamma}$, $\sigma_{n,n'}$, $\sigma_{n,2n}$, $\sigma_{n,p}$ and $\sigma_{n,\alpha}$ were made in optimum agreement with experimental data.

The final optimum values of the adjusted parameters we got are:

C_k=2350 (the parameter for exciton model);

C_{el}=0.34 (the multiplied factor in $\sigma_{n,\gamma}$);

The optical potential parameters for p, α were adjusted as follows:

for p channel, a_r and a_{SO} to 0.63, a_s and a_v to 0.51, r_s and r_v to 1.24;

for α channel, a_s and a_v to 0.55, r_r and r_{SO} to 1.40, r_s and r_v to 1.39;

The change of energy density parameters are as follows:

$a_{n,n'}$ from 9.37206 to 10.37206, $a_{n,p}$ from 9.92813 to 12.88813, $a_{n,\alpha}$ from 11.21302 to 13.35302, $a_{n,d}$ from 9.76237 to 10.36237, $a_{n,2n}$ from 10.81555 to 15.81555;

The change of pair energy corrections are as follows:

$\Delta_{n,\gamma}$ from 0.39 to 0.19, $\Delta_{n,n'}$ from 1.49 to 0.49;

The calculated σ_{tot}, σ_{non} and σ_{el} with the experimental data are given in Fig. 1(a) and (b), from which we can see that calculated σ_{tot} are in very good accordance with experimental data except in E_n<0.4 MeV energy region, σ_{non} and σ_{el} are also in reasonable good accordance with experimental data. The results of $\sigma_{n,\gamma}$ are given in Fig. 2, from which we can see that the calculated values are in pretty good agreement with experimental data except in E_n>5 MeV energy region. The calculated and experimental $\sigma_{n,n'}$ and $\sigma_{n,2n}$ are given in Fig. 3, from which we can see that the calculated $\sigma_{n,2n}$ are in very good agreement with experimental data and B. S. Yu's evaluated values, the calculated $\sigma_{n,n'}$ are also in pretty good consistent with experimental data. The calculated and experimental $\sigma_{n,p}$ and $\sigma_{n,\alpha}$ are given in Fig. 4, from which we can see that the calculated $\sigma_{n,\alpha}$ are in very good agreement with experimental data, and the calculated $\sigma_{n,p}$ are not in very good accordance with experimental data because the experimental data themselves are some divergent. All calculated cross sections are plotted in Fig. 5, which are of reasonable values. There are experimental and calculated elastic scattering angular distributions at 60 energy points, only ten of them are given in Fig. 6 to Fig. 8, from which we can see that calculated values are in pretty good agreement with experimental data (for other 50 energy points, calculated values are in similar accordance with experimental data). The calculated secondary neutron spectra of continuous inelastic scattering (MT=91) and (n,2n) reaction (MT=16) at E_n=8.0, 14.0 MeV and 20.0 MeV are plotted in Fig. 9 and Fig.10, respectively. These secondary neutron spectra are of reasonable shapes in physics, though there are no experimental data to compare with.

References

[1] Shen Qingbiao, APMN, a code for automatically searching for a set of optimal optical potential parameters of medium and heavy nucleus (unpublished)

[2] P. D. Kunz, DWBA code DWUCK4, University of Colorado, USA (unpublished)

[3] Zhang Jingshang, SUNF, a code for comprehensive calculations of fission product nucleus based on unified model, CNDC, CIAE (unpublished)

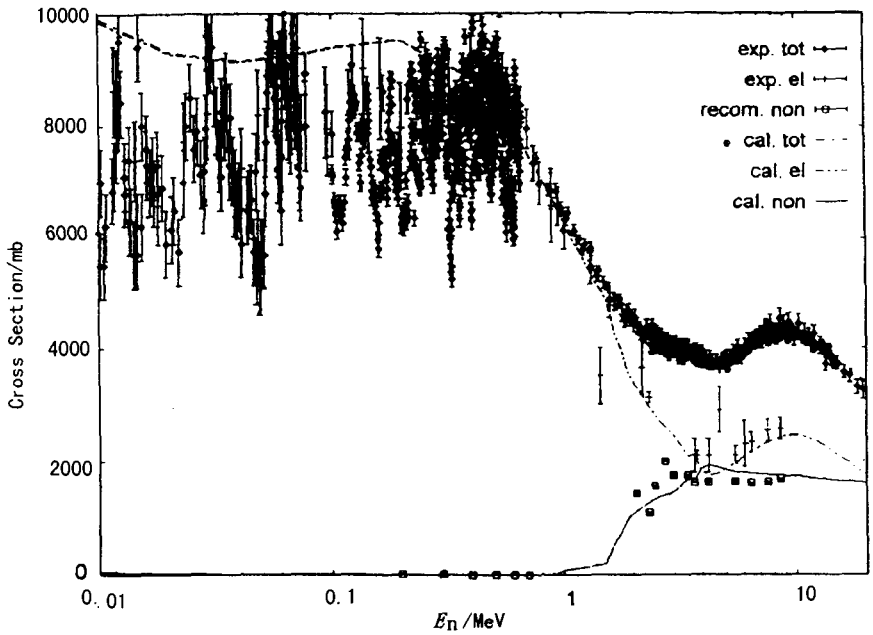

Fig. 1 ^{89}Y total, elastic and nonelastic cross sections energies of incoming neutron in L-frame (MeV)

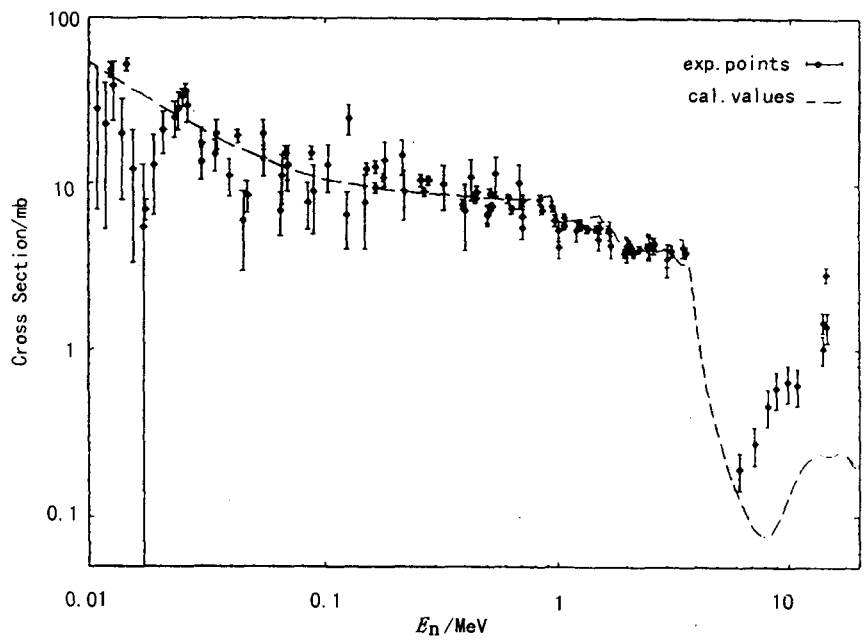

Fig. 2 ^{89}Y(n,γ) cross sections energies of incoming neutron in L-frame (MeV)

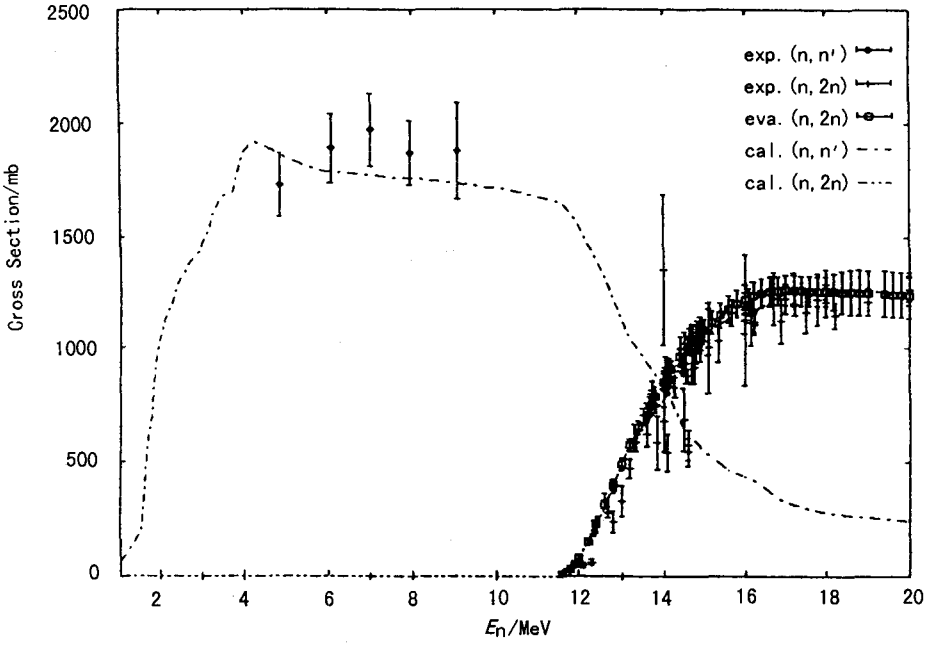

Fig. 3 ^{89}Y(n,n') and (n,2n) cross sections energies of incoming neutron in L-frame (MeV)

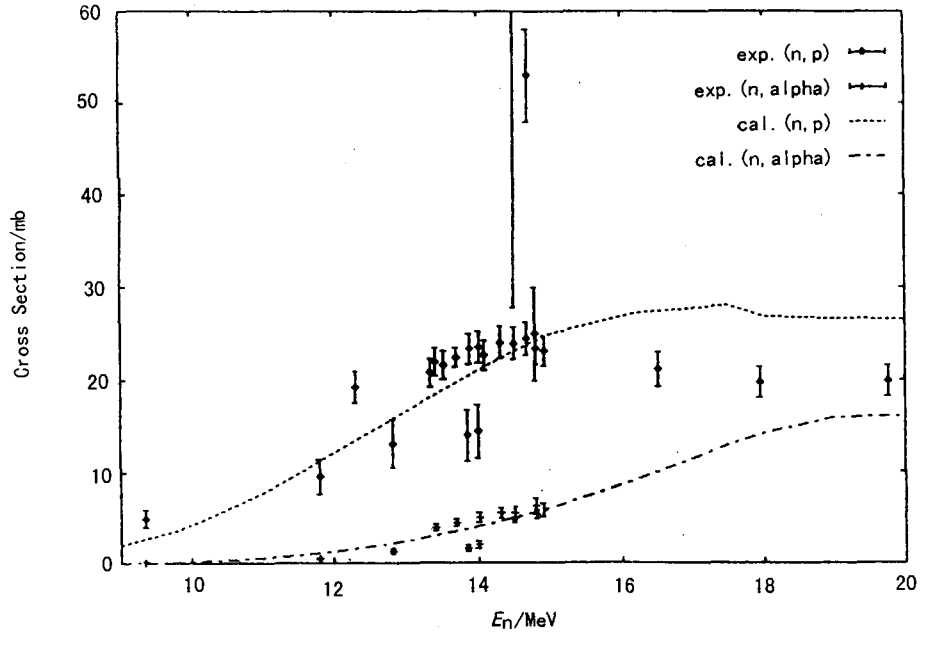

Fig. 4 ^{89}Y(n,p) and (n,α) nonelastic cross sections energies of incoming neutron in L-frame (MeV)

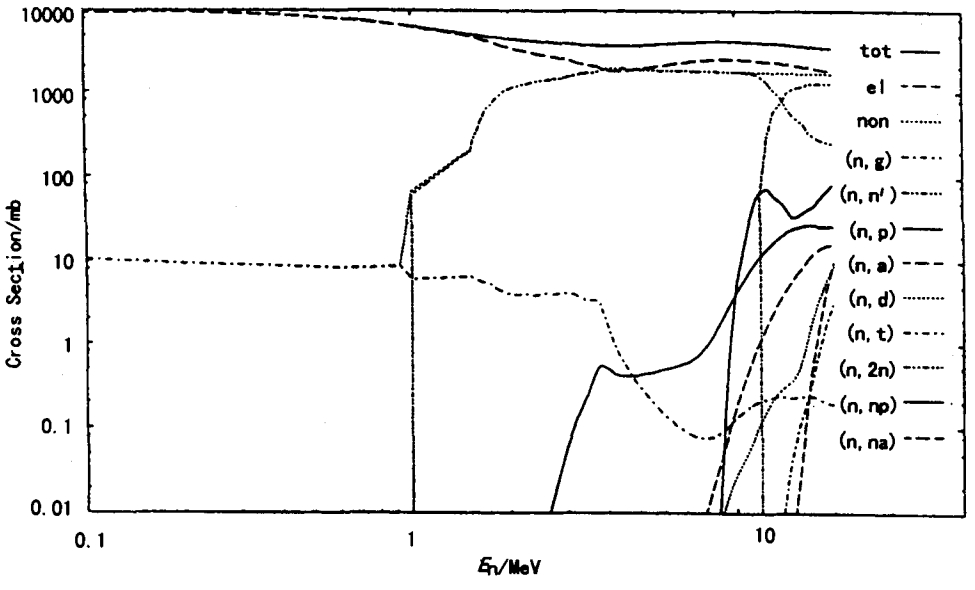

Fig. 5 n+^{89}Y cross sections energies of incoming neutron in L-frame (MeV)

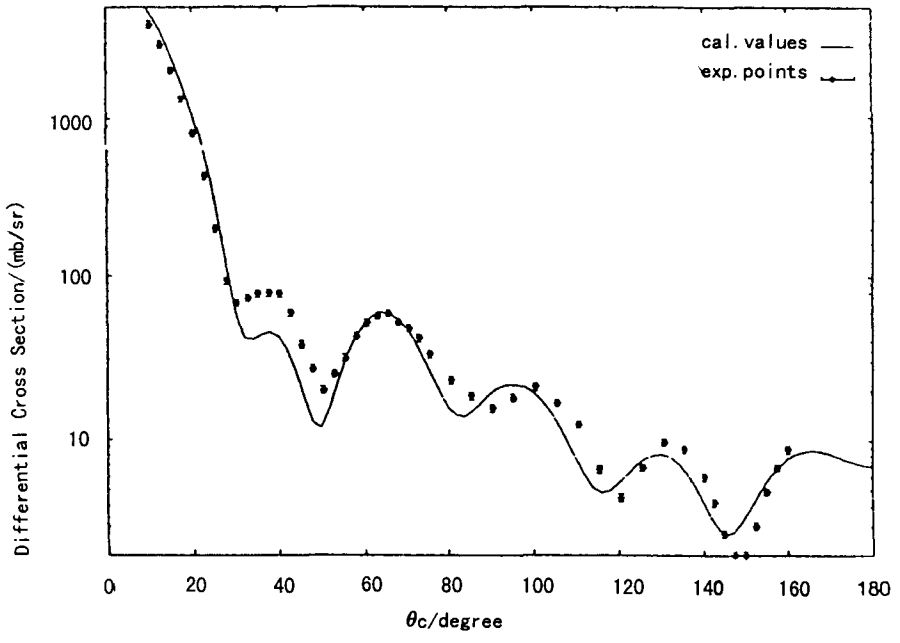

Fig. 6 ^{89}Y elastic differential C. S. at E_l=21.6 MeV angles (degree) of outgoing n in CM-frame (MeV)

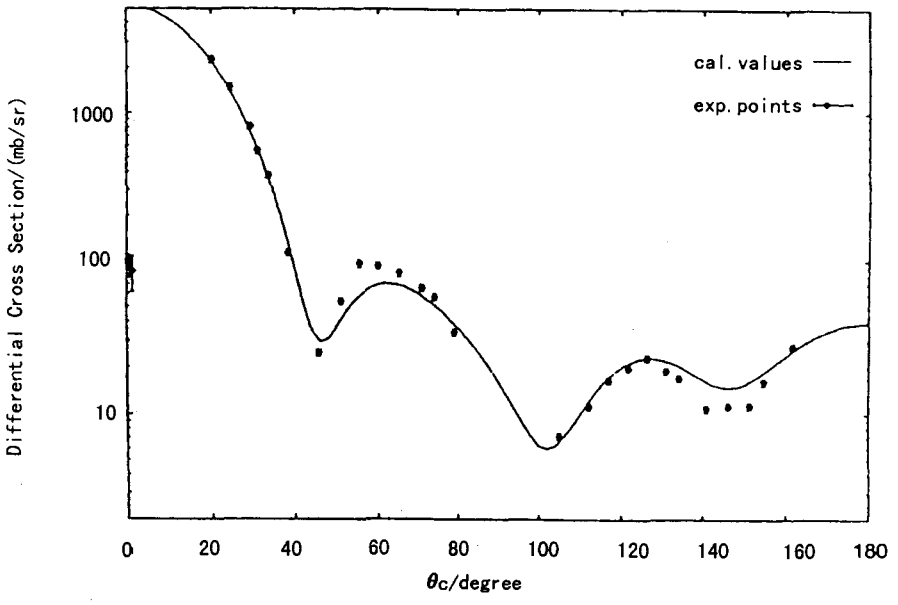

Fig. 7 ^{89}Y elastic differential C. S. at E_f=9.95 MeV angles (degree) of outgoing n in CM-frame (MeV)

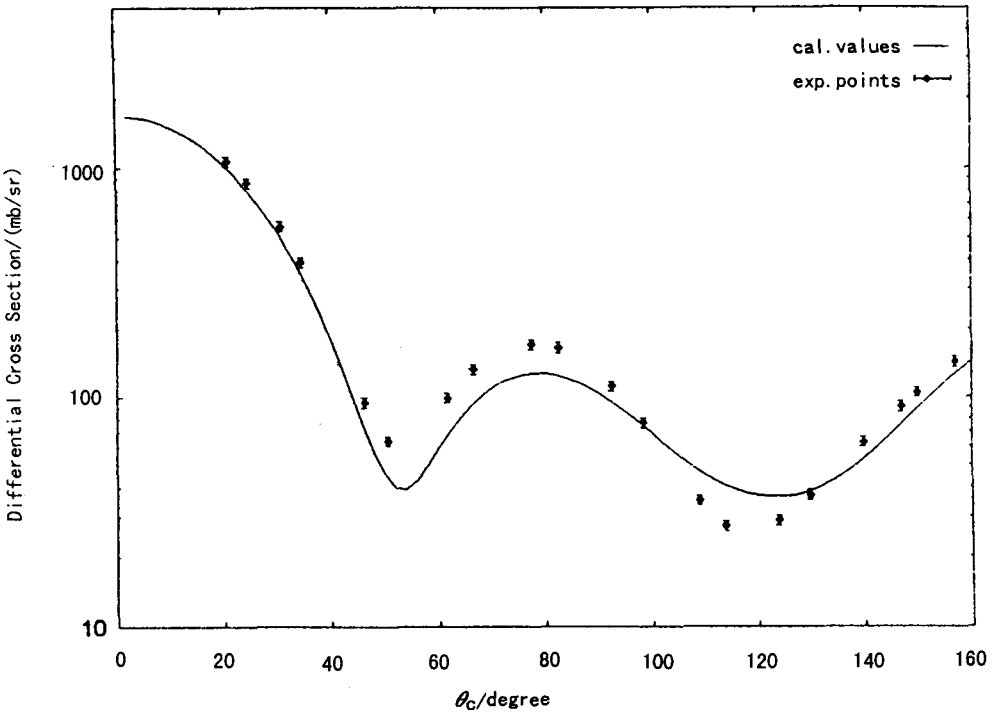

Fig. 8 ^{89}Y elastic differential C. S. at E_f=3.72 MeV angles (degree) of outgoing n in CM-frame (MeV)

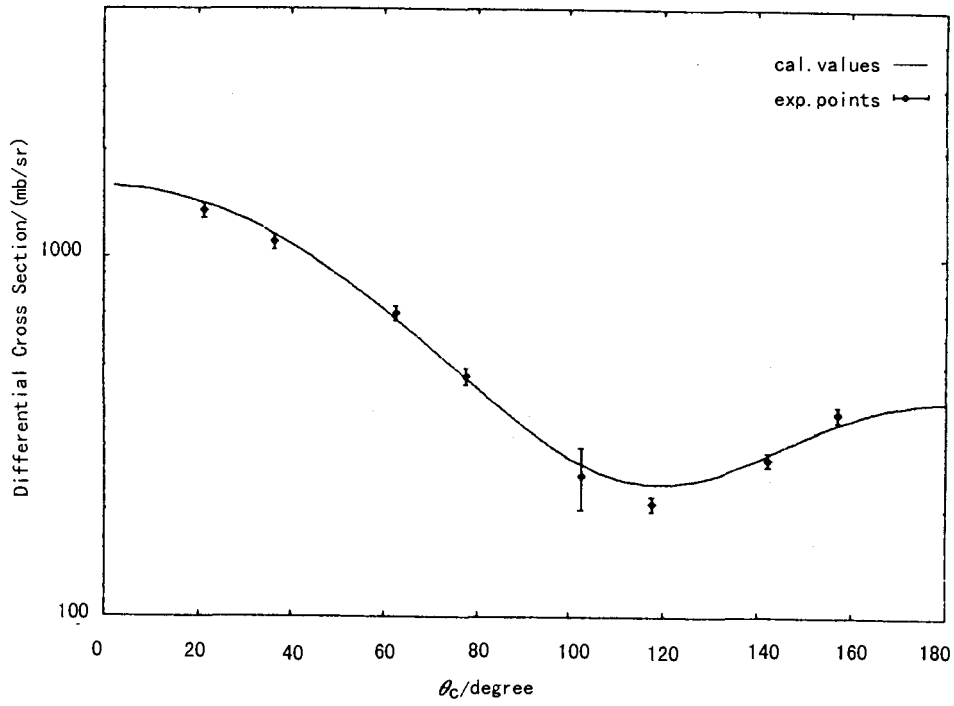

Fig. 9 ^{89}Y elastic differential C. S. at E_{Γ}=0.889 MeV angles (degree) of outgoing n in CM-frame (MeV)

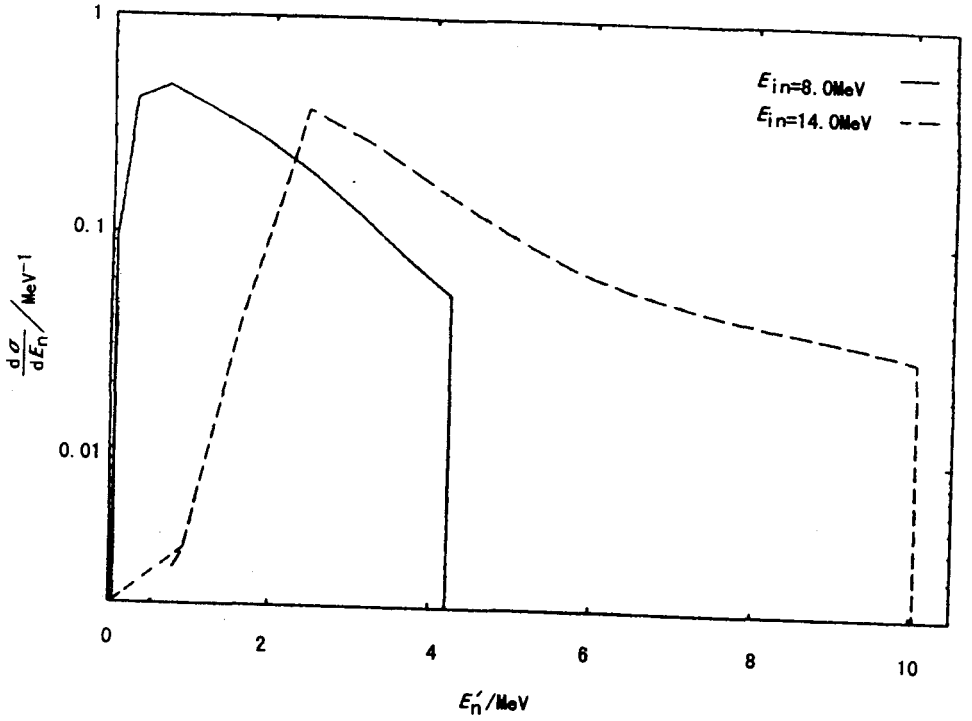

Fig. 10 ^{89}Y energy spectra of continuous inelastic scattering energies of outgoing neutron (MeV)

CN9901207

Calculations of all Reactions for n+^{88}Sr, ^{89}Sr and ^{90}Sr in E_n=0.001 ~ 20 MeV

Cai Chonghai
(Department of Physics, Nankai University, Tianjin 300071)
Shen Qingbiao
(China Nuclear Data Center, CIAE)

Abstract

All reaction cross sections, secondary neutron spectra and elastic scattering angular distributions of n+^{88}Sr, ^{89}Sr and ^{90}Sr in E_n=0.001 ~ 20 MeV are calculated, rather good results in accordance with experimental data are obtained, and the data are given in ENDF/B-6 format.

Introduction

The natural element Sr has 4 stable isotopes: ^{88}Sr, ^{87}Sr, ^{86}Sr, and ^{84}Sr, the abundances of which are 82.58%, 7.00%, 9.86% and 0.56%, respectively. As fission product nuclei, this time we need to calculate 3 isotopes: ^{88}Sr, ^{89}Sr and ^{90}Sr, the later two of which are unstable. There are abundant experimental data of σ_{tot} for natural element, some very divergent experimental σ_{tot} for ^{88}Sr near E_n=0.01 MeV; few experimental σ_{el} for natural element; some experimental data of $\sigma_{n,\gamma}$ for ^{88}Sr and natural element; sufficient experimental data of $\sigma_{n,p}$ for ^{88}Sr; sufficient experimental data of elastic scattering angular distributions for natural element at E_n=0.886, 1.0, 3.2, 3.66, 4.37, 11.0 and 14.76 MeV. There are no experimental data for other reaction cross sections and secondary neutron spectra. All of the experimental data we were taken from EXFOR. The universal optical potential parameters for six channels used in calculations are given in Table 1 of Ref. [1].

Firstly, The code APMN[2] is used to automatically get the optimal parameters of optical potential for neutron channel. Because there are only some very divergent experimental σ_{tot} for ^{88}Sr near $E_n \approx 0.01$ MeV, the experimental σ_{tot} and elastic scattering angular distributions for natural element are used to determine the optimal optical potential parameters of ^{88}Sr for neutron channel in running the code APMN. The final same set optimal parameters of optical potential for neutron channel used for calculations of ^{88}Sr, ^{89}Sr and ^{90}Sr are:

V_0= 56.09614944, V_1= –0.27418378, V_2= –0.02068655, V_4= –0.42493716,

$W_0 = 8.03748131$, $W_1 = 0.16873387$,
$U_0 = -0.20045300$, $U_1 = 0.17602199$, $U_2 = -0.04169800$,
$a_r = 0.66182411$, $a_s = 0.47570482$, $a_v = 0.64955997$,
$r_r = 1.26379693$, $r_s = 1.22453^{88}0$, $r_v = 1.25863004$.

Secondary, the DWBA code DWUCK4[3] is used to calculate the direct inelastic scattering cross sections and angular distributions of 5 levels for ^{88}Sr, 11 levels for ^{89}Sr, and 5 levels for ^{90}Sr. These direct inelasti scattering data and the optimum set of optical potential parameters are taken as the input data of the kernel program SUNF[4]. Through adjusting some parameters in the input data of SUNF for ^{88}Sr by hand again and again, we can make $\sigma_{n,\gamma}$ and $\sigma_{n,p}$ for ^{88}Sr in optimum agreement with experimental data.

The final optimal values of the changed parameters for ^{88}Sr we got are:

C_k (the parameter for exciton model)=950.0;

C_{el} (the multiplied factor in $\sigma_{n,\gamma}$)=0.55;

The change of level density parameter for ^{88}Sr is a $\sigma_{n,p}$ from 9.97920 to 10.37920.

The pair energy corrections and optical potential parameters for charged particles channels are not changed for ^{88}Sr.

For ^{89}Sr and ^{90}Sr, there are no experimental data for all cross sections, elastic scattering angular distributions and secondary neutron spectra at all, we take C_k=950.0 (the same as for ^{88}Sr) and C_{el}=1.0, the optical potential parameters are the same as for ^{88}Sr, the level density parameters and pair energy corrections are not changed (kept the input values).

The calculated σ_{tot}, σ_{non} and σ_{el} for ^{88}Sr, ^{89}Sr and ^{90}Sr as well as the experimental σ_{tot} and σ_{el} for ^{88}Sr and natural element are given in Fig. 1, from which we can see that the calculated σ_{tot} are in very good accordance with experimental data, the calculated σ_{el} are also in rather good accordance with experimental data. The results of $\sigma_{n,\gamma}$ for ^{88}Sr, ^{89}Sr and ^{90}Sr are given in Fig. 2, from which we can see that the calculated values are not in good agreement with experimental data, because the experimental data are very divergent. The calculated $\sigma_{n,p}$ for ^{88}Sr, ^{89}Sr and ^{90}Sr and experimental $\sigma_{n,p}$ for ^{88}Sr are given in Fig. 3, from which we can see that the calculated value for ^{88}Sr are in very good agreement with experimental data, the calculated for ^{89}Sr and ^{90}Sr are also reasonable in physics. The calculated elastic scattering angular distributions for ^{88}Sr and the experimental data for natural element at E_n=0.886, 3.66, 11.0 and 14.76 MeV are given in Fig. 4(a) to 4(d), from which we can see that the calculated values are in pretty good agreement with experimental data. All kinds of the calculated cross sections are plotted in Fig. 5 for ^{88}Sr, in Fig. 6

for ^{89}Sr and in Fig. 7 ^{90}Sr. The calculated secondary neutron spectra of continuous inelastic scattering (MT=91) and (n,2n) reaction (MT=16) at E_n=8.0 MeV, E_n=14.0 MeV and E_n=20.0 MeV are plotted in Fig. 8(a) and (b) for ^{88}Sr, in Fig. 9(a) and (b) for ^{89}Sr, in Fig. 10(a) and (b) for ^{90}Sr, respectively. These secondary neutron spectra are of reasonable shapes in physics, though there are no experimental data to be compared with.

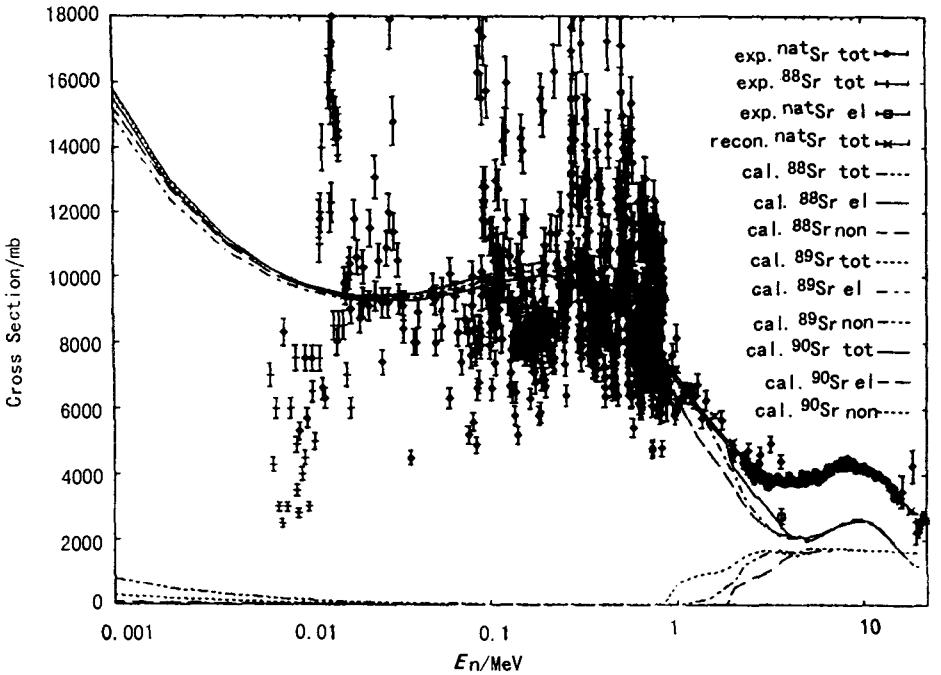

Fig. 1 ^{88,89,90}Sr total, elastic and nonelastic cross sections

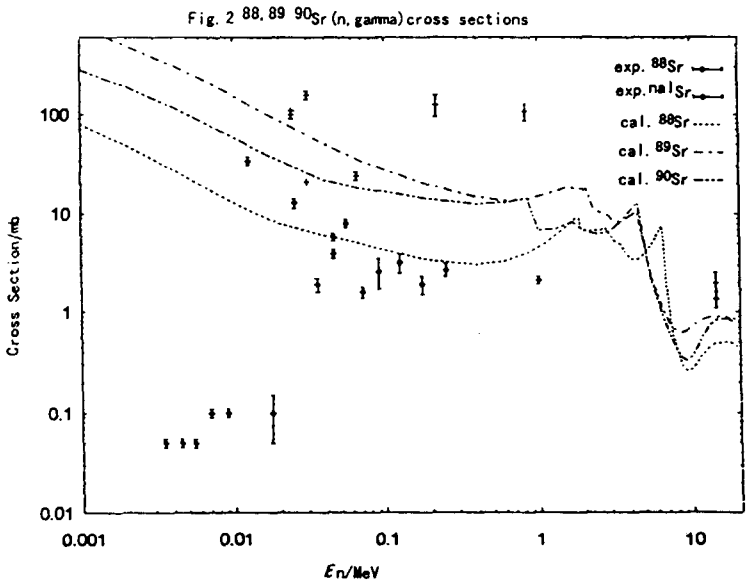

Fig. 2 ^{88,89,90}Sr (n,γ) cross sections

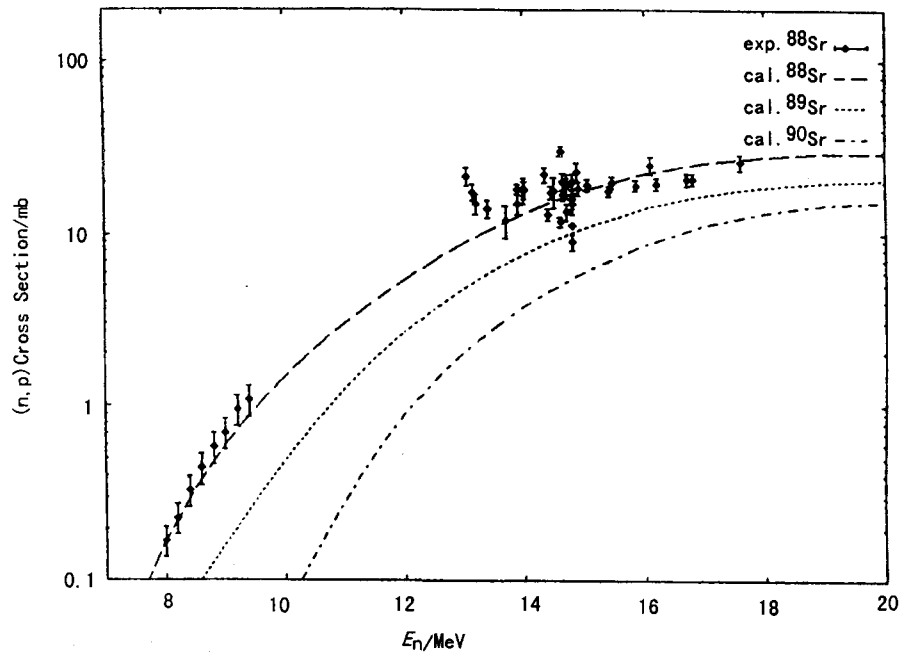

Fig. 3 ^{88,89,90}Sr (n,p) cross sections

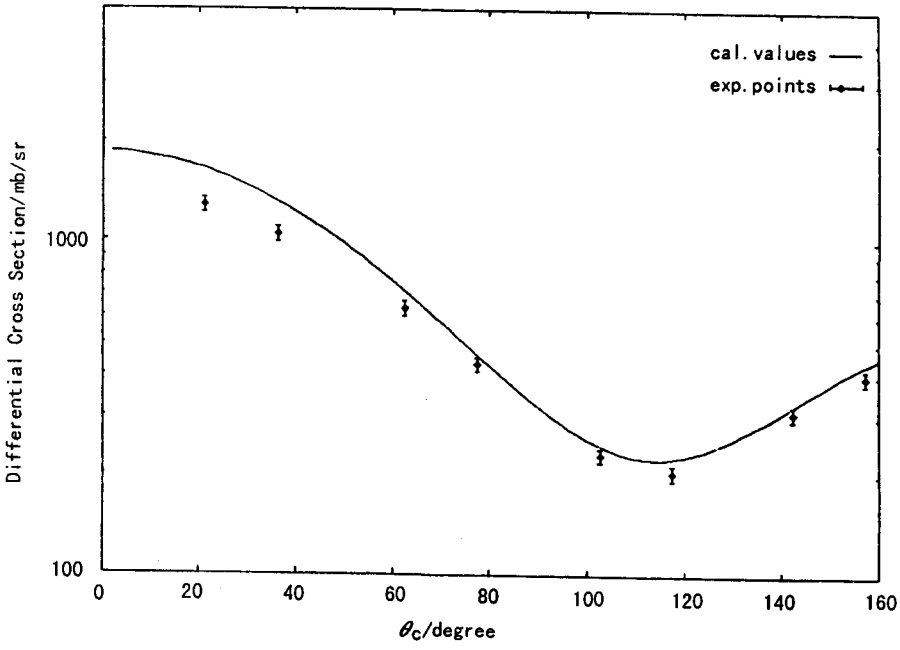

Fig. 4(a) ^{88}Sr elastic differential C. S. at E_l=0.886 MeV

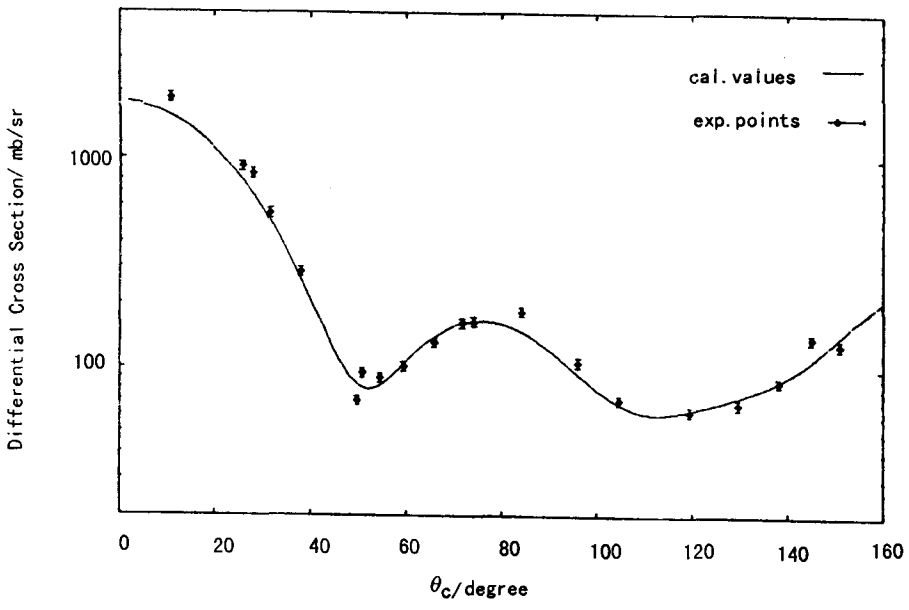

Fig. 4(b) ^{88}Sr elastic differential C. S. at E_l=3.66 MeV

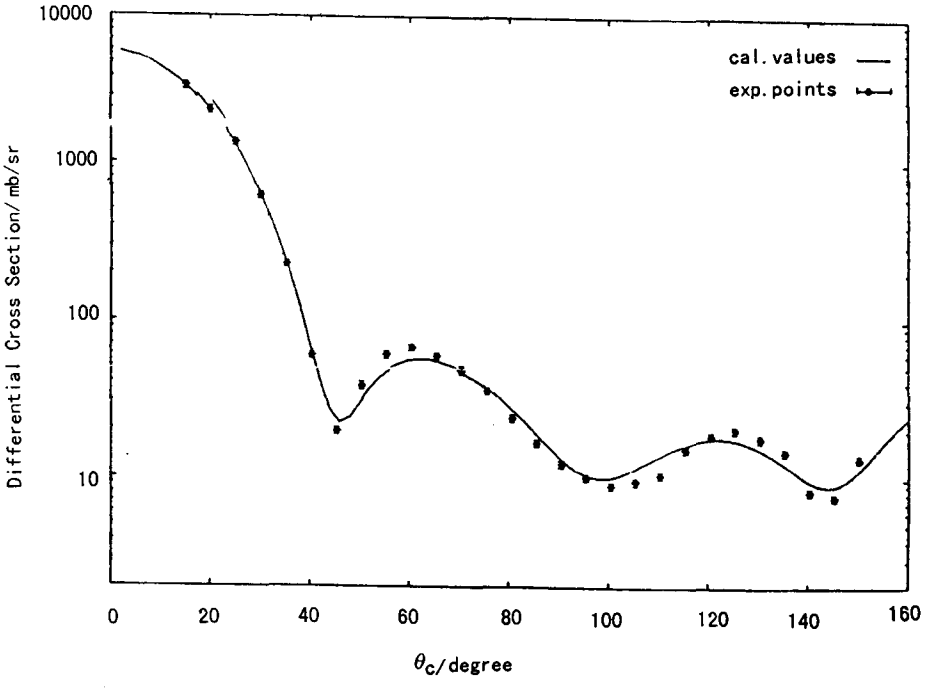

Fig. 4(c) ^{88}Sr elastic differential C. S. at E_l=11.0 MeV

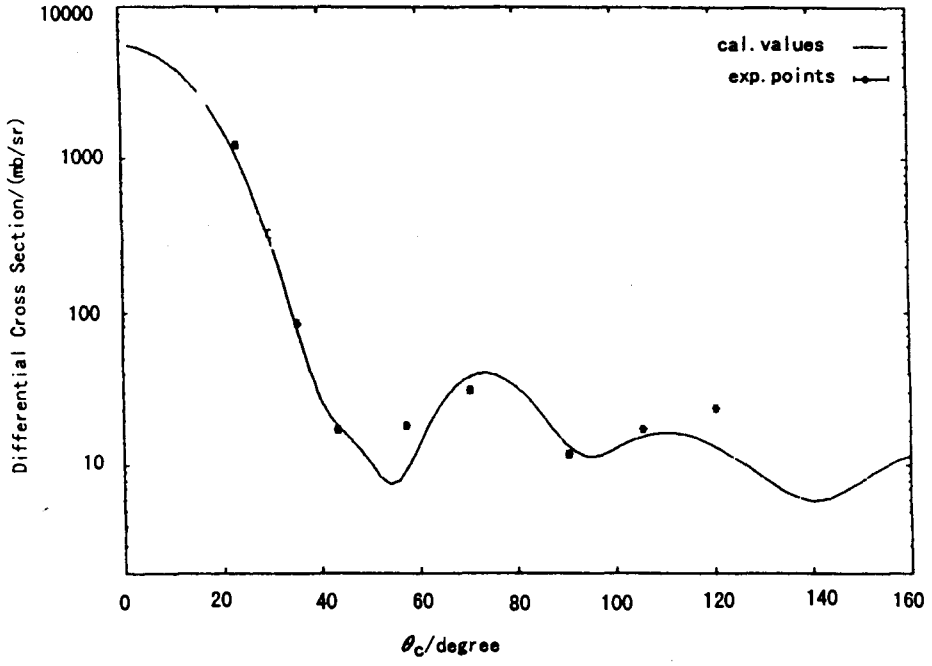

Fig. 4(d) ^{88}Sr elastic differential C. S. at E_l=14.76 MeV

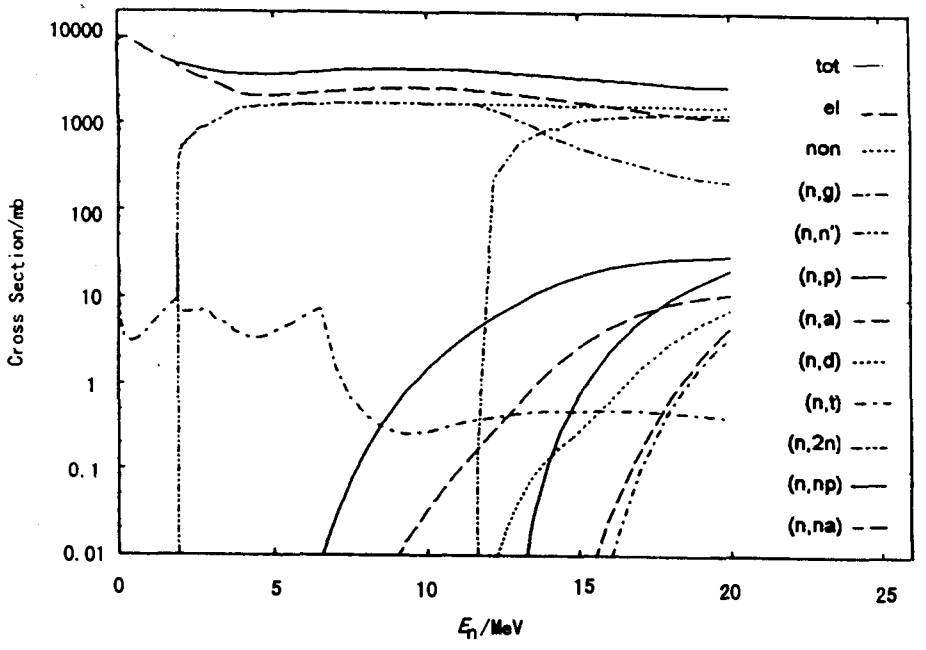

Fig. 5 all calculational cross sections of ^{88}Sr

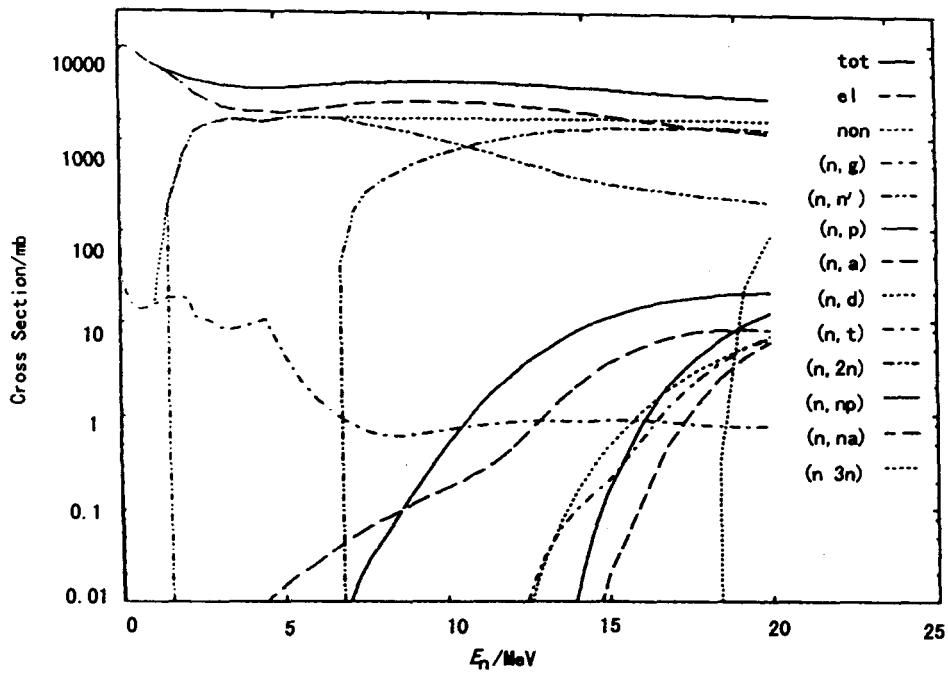

Fig. 6 all calculational cross sections of ^{89}Sr

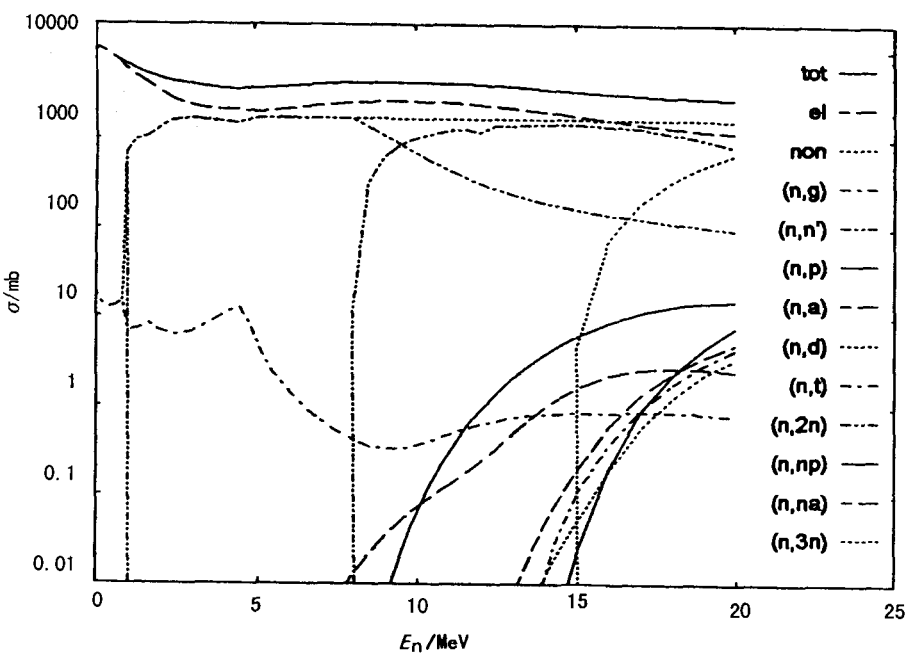

Fig. 7 all calculational cross sections of ^{90}Sr

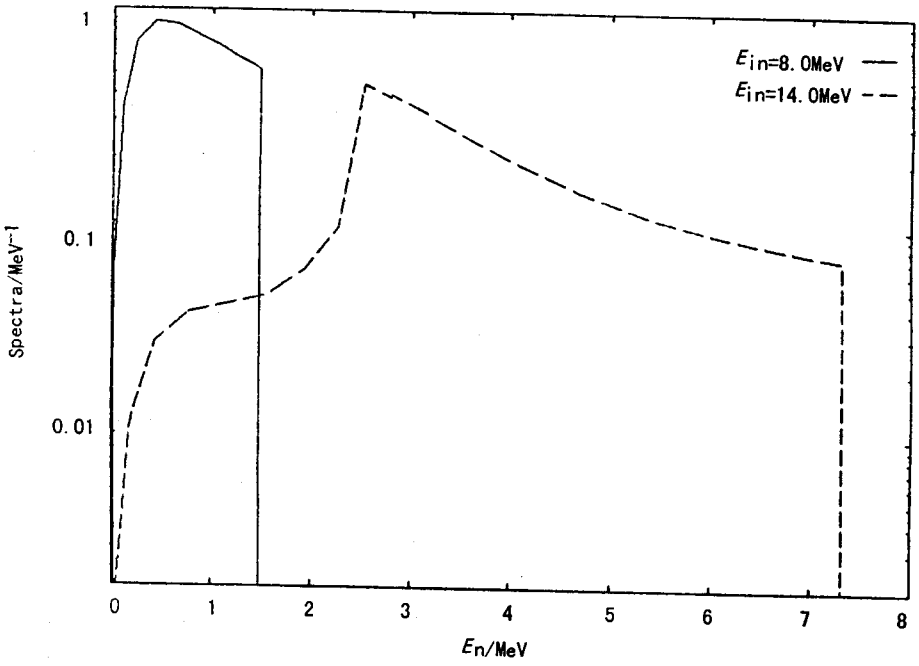

Fig. 8(a) ^{88}Sr (n,n') and (n,2n) energies spectra

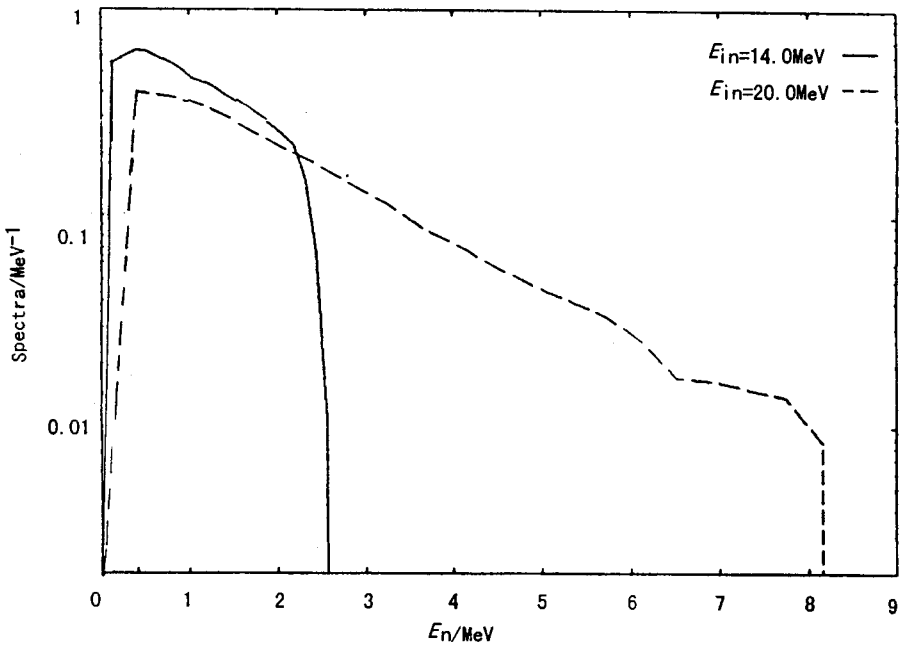

Fig. 8(b) ^{88}Sr (n,n') and (n,2n) energies spectra

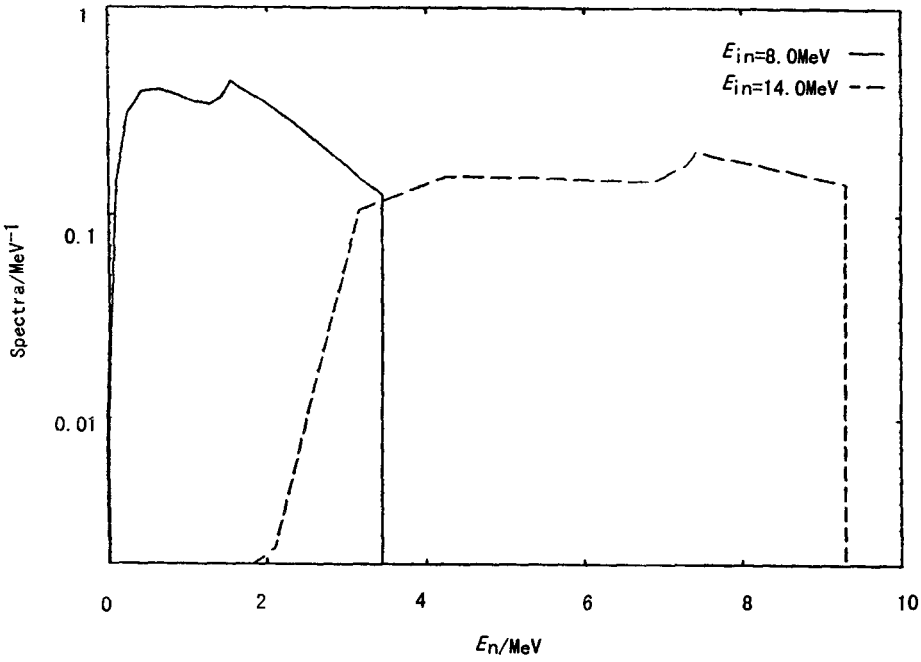

Fig. 9(a) ^{89}Sr (n,n') and (n,2n) energies spectra

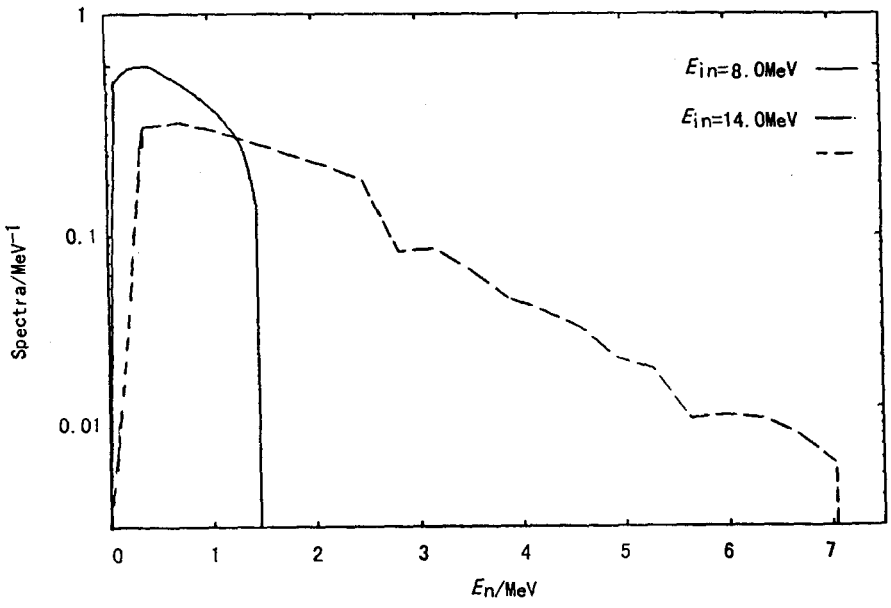

Fig. 9(b) ^{89}Sr (n,n') and (n,2n) energies spectra

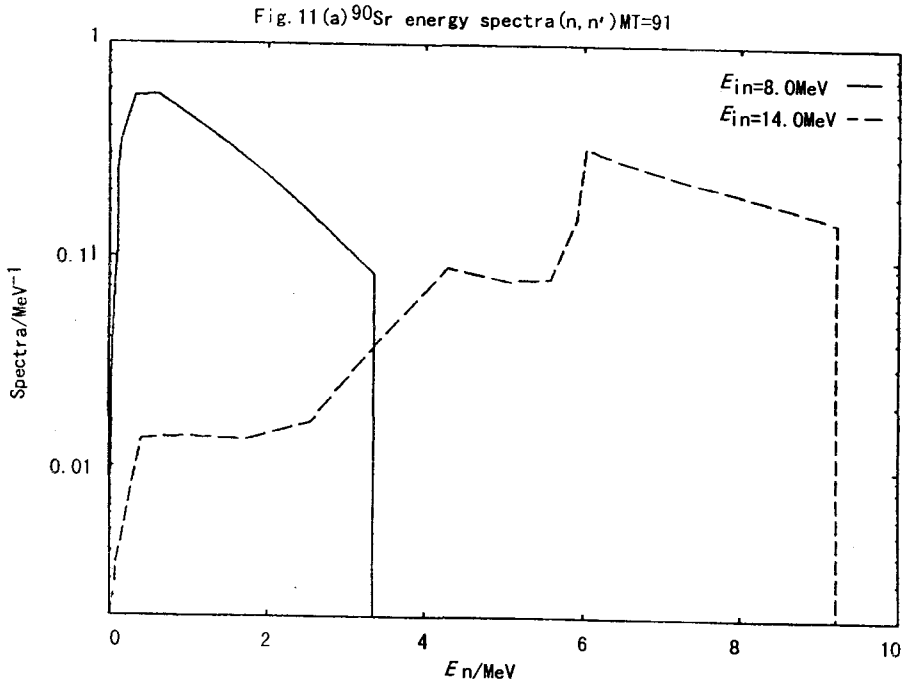

Fig. 10(a) ^{90}Sr (n,n') and (n,2n) energies spectra

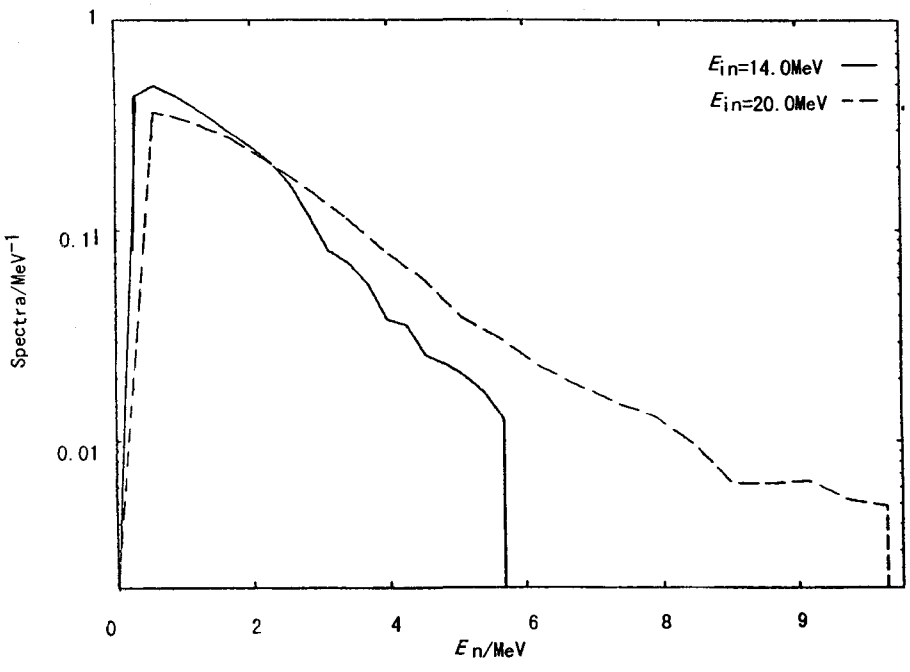

Fig. 10(b) ^{90}Sr (n,n') and (n,2n) energies spectra

References

[1] Cai Chónghai and Shen Qingbiao, Comprehensive Calculations of all Reactions for n+^{89}Y in E_n=0.001 ~ 20 MeV, to be published in CNDP

[2] Shen Qingbiao, APMN, a code for automatically searching for a set of optimal optical potential parameters of many medium and heavy nucleus (unpublished)

[3] P. D. Kunz, DWBA code DWUCK4, University of Colorado, USA (unpublished)

[4] J. S. Zhang, SUNF, a code for comprehensive calculations of fission product nucleus based on unified model, CNDC, CIAE (unpublished)

CN9901208

Neutron Spherical Optical Potential Parameters for $^{238\sim242}$Pu below 20 MeV

Wang Shunuan Yu Baosheng

(China Institute of Atomic Energy, CIAE)

Abstract

A set of neutron spherical optical potential parameters for $^{238\sim242}$Pu below 20 MeV is obtained by using the auto-searching optimum optical potential parameters code APFO96[1] based on latest available experimental data of total cross sections σ_t, nonelastic cross sections σ_{non}, elastic differential cross sections $\sigma_{el}(\theta)$, and systematics. The calculated results of σ_t, σ_{non}, $\sigma_{el}(\theta)$ for $^{238\sim242}$Pu are compared with available experimental data, CENDL-2 and other evaluated data files. Theoretical calculations and experimental data are in agreement fairly good. The set of neutron spherical optical potential parameters for $^{238\sim242}$Pu below 20 MeV are recommended for CENDL-3 actinides nuclei FUNF preequilibrium and equilibrium statistical calculations and evaluations.

In order to perform evaluations of actinides for CENDL-3, a set of neutron spherical optical potential parameters for $^{238\sim242}$Pu below 20 MeV was obtained by using the auto-searching optimum optical potential parameters code APFO96[1] (with 14 adjusted parameters) and its adapted Alpha computer AUTOFOPT system[2] connected with EXFOR, Model Parameters Library to produced two input data files for APFO96. The searched parameters are based on all of available experimental data of total cross sections σ_t, nonelastic cross sections σ_{non}, elastic differential cross sections $\sigma_{el}(\theta)$.

In the auto-searching optimum optical potential parameters, the latest available experimental data were used. There are enough σ_t data and $\sigma_{el}(\theta)$ data at 23 incident

neutron energy points (E_n=0.5 ~ 14.1 MeV) for ^{239}Pu. The σ_{non} data of n+^{239}Pu found from EXFOR are not correct not only for the magnitude but also the tendency, and they are not consistent with the sum of the all open reaction channels existing experimental data or evaluated data. Therefore, in the present paper, the σ_{non} excitation function, which are more reasonable and more consistent with the sum of the all open reaction channels existing experimental data, are evaluated and recommended for ^{239}Pu optical potential parameters adjustment. There are some σ_t data for ^{240}Pu only, and some σ_t data and $\sigma_{el}(\theta)$ data at three neutron energy points for ^{242}Pu only. There are no any available data for ^{238}Pu and ^{241}Pu. By using APFO96 code and AUTOFOPT system and the available data mentioned above, a set of neutron spherical optical potential parameters for ^{239}Pu, ^{240}Pu and ^{242}Pu at $E_n \leq 20$ MeV are firstly obtained respectively. According to the systematics of ^{239}Pu and ^{241}Pu (both are same Z and odd A), the parameters for ^{241}Pu was taken as the completely same as for ^{239}Pu. According to the systematics of ^{242}Pu, ^{240}Pu and ^{238}Pu (they are same Z and even A), the extrapolation of the 14 adjusted parameters from ^{242}Pu and ^{240}Pu was made to get the parameters for ^{238}Pu. From the later on comparison between the calculated results and experimental data, the systematics described above works well and successfully.

Table 1 Neutron ($E_n \leq 20$ MeV) Spherical Optical Potential Parameters for $^{238\sim242}$Pu

	^{242}Pu	^{240}Pu	^{238}Pu	^{239}Pu, ^{241}Pu
V_0	48.92297363	49.24069595	49.55841827	50.59375000
V_1	−0.40507239	−0.38750157	−0.36993075	−0.38913181
V_2	0.02700651	0.01600822	0.00500993	−0.01268969
r_r	1.25547445	1.26970696	1.28393947	1.25164747
a_r	0.58439469	0.61144131	0.63848793	0.59236091
W_{S0}	5.61328173	5.94410181	6.27492189	4.00000000
W_{S1}	0.34281868	0.19266422	0.04250976	0.11215307
r_s	1.39045620	1.35386860	1.31728100	1.27787423
a_s	0.52507484	0.50842720	0.49177956	0.80000001
W_{V0}	2.21182537	1.16506124	0.11829711	1.65087783
W_{V1}	−0.37751999	0.06561940	0.50875879	0.08693016
W_{V2}	−0.00947707	0.00000000	0.00947707	0.00000000
r_V	1.35027134	1.04229474	0.73431817	1.17236149
a_V	0.36000001	0.36000001	0.36000001	0.36000001
	(14 adjusted parameters)			
V_3	−24.0			
V_4	0.0			
W_2	−12.0			
V_{SO}	6.2			
$a_{SO}=a_r$				
$r_{SO}=r_r$				
	(6 fixed parameters)			

As far as it goes, a set of reasonable neutron spherical optical potential parameters for $^{238\sim242}$Pu below 20 MeV are shown in Table 1.

The calculated results of σ_t, σ_{non}, $\sigma_{el}(\theta)$ for $^{238\sim242}$Pu are compared with available experimental data, CENDL-2 and other evaluated data files shown in Figs. 1 ~ 9. Figs. 1 ~ 2 show the comparison of calculated total cross sections with experimental data and JENDL-3.2, CENDL-2.1, ENDF/B-6, respectively, for n+^{239}Pu below 20 MeV. It can be seen from Figs. 1 ~ 2 that our results fit the experimental data prety well, and they are more clossed to ENDF/B-6 and slightly better than CENDL-2 at 15 ~ 20 MeV. The calculated $\sigma_{el}(\theta)$ at E_n=0.5, 0.7, 0.8, 1.0, 1.2, 1.4, 1.5, 1.6, 1.8, 1.9, 2.0, 2.2, 2.3, 2.4, 2.6, 2.8, 3.0, 3.5, 4.0, 4.5, 5.0, 5.5, 14.1 MeV for ^{239}Pu are agreement with experimental data well. Figs. 3 ~ 6 show the $\sigma_{el}(\theta)$ results compared with experimental data and JENDL-3, CENDL-2.1, ENDF/B-6 at E_n=0.5, 1.9, 4.0, 14.1 MeV, respectively. Fig. 7 shows the calculated σ_t compared with experimental data and CENDL-2. It can be pointed out that the total cross sections at 3 ~ 20 MeV for ^{240}Pu calculated in the present paper fit the experimental data better than the one given in Ref. [3]. Figs. 8 ~ 9 show the σ_t at E_n=1 ~ 20 MeV and $\sigma_{el}(\theta)$ at E_n=0.57, 1.0, 1.5 MeV for ^{242}Pu, respectively. The comparison of calculated results with experimental data for ^{242}Pu is also fairly good. It can be concluded that the comparisons between theoretical optical model calculations and available experimental data are satisfied. The set of neutron parameters for $^{238\sim242}$Pu at $E_n \leq 20$ MeV could be recommended to CENDL-3 actinides nuclei FUNF preequilibrium and equilibrium statistical calculations and avaluations.

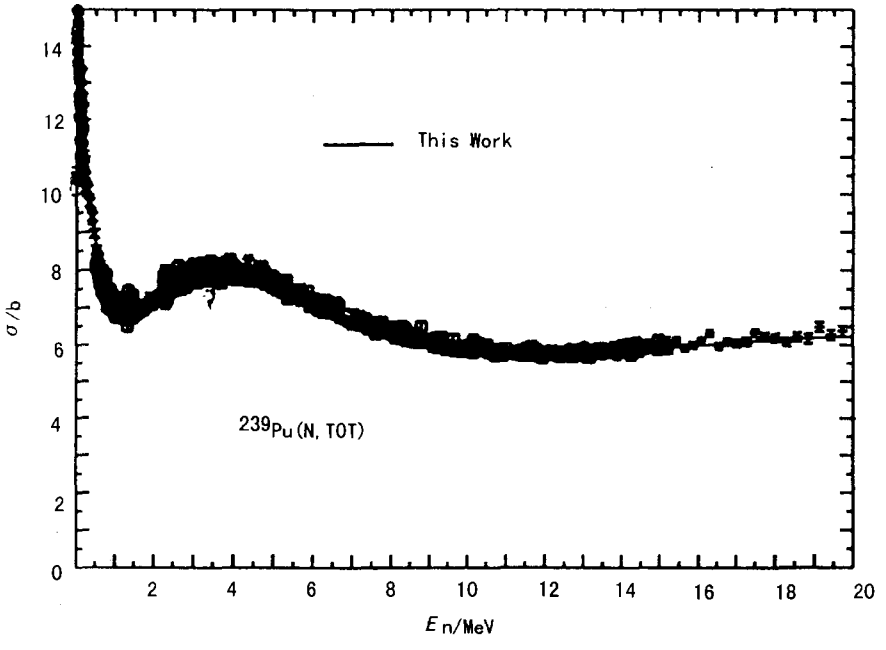

Fig. 1 Comparison of evaluated and measured data for ^{239}Pu(n,tot)

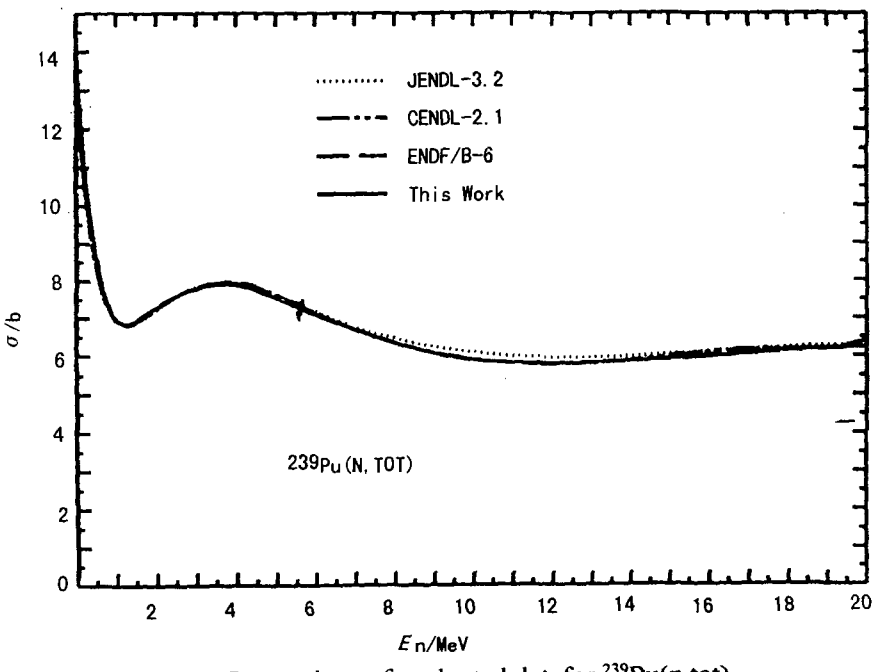

Fig. 2 Comparison of evaluated datafor ^{239}Pu(n,tot)

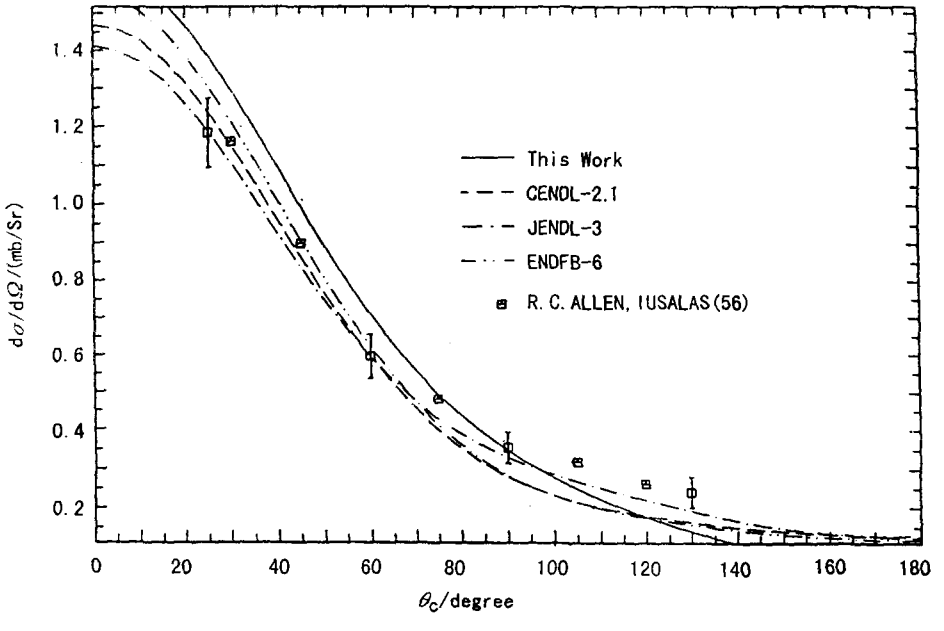

Fig. 3 ^{239}Pu elastic scattering differential cross section at 0.5 MeV

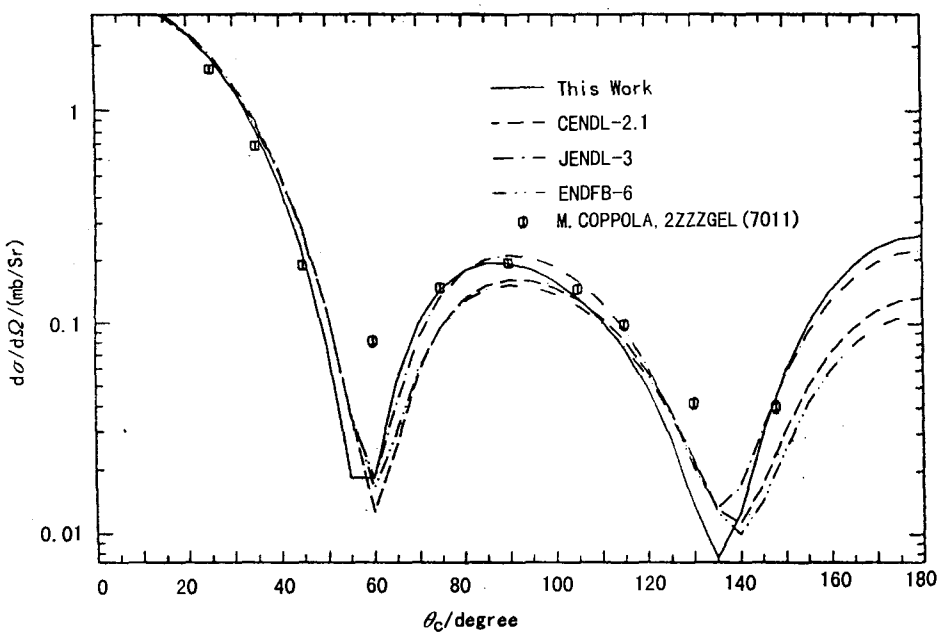

Fig. 4 ^{239}Pu elastic scattering differential cross section at 1.9 MeV

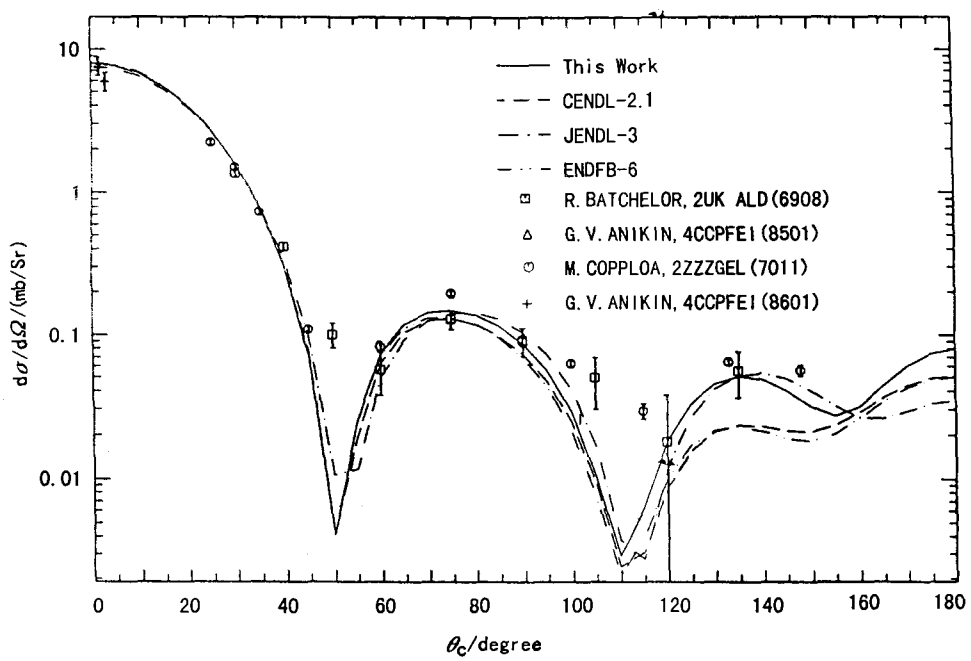

Fig. 5 ^{239}Pu elastic scattering differential cross section at 4.0 MeV

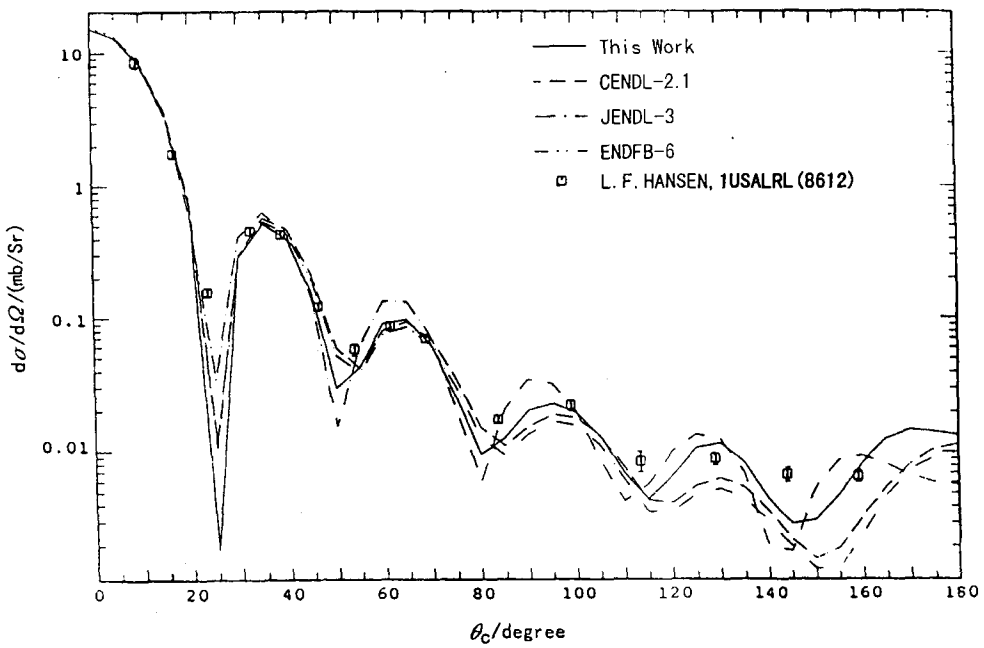

Fig. 6 ^{239}Pu elastic scattering differential cross section at 14.1 MeV

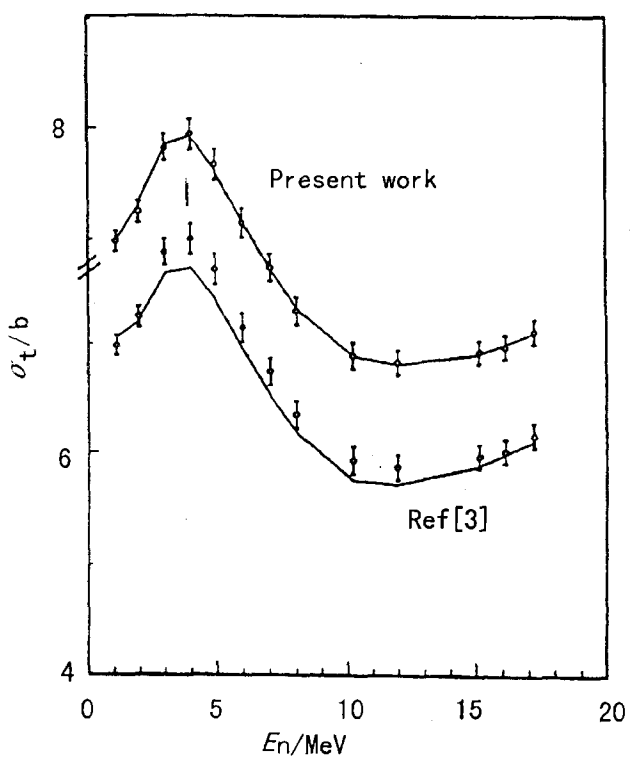

Fig. 7 n+^{240}Pu total cross section optical model calculation

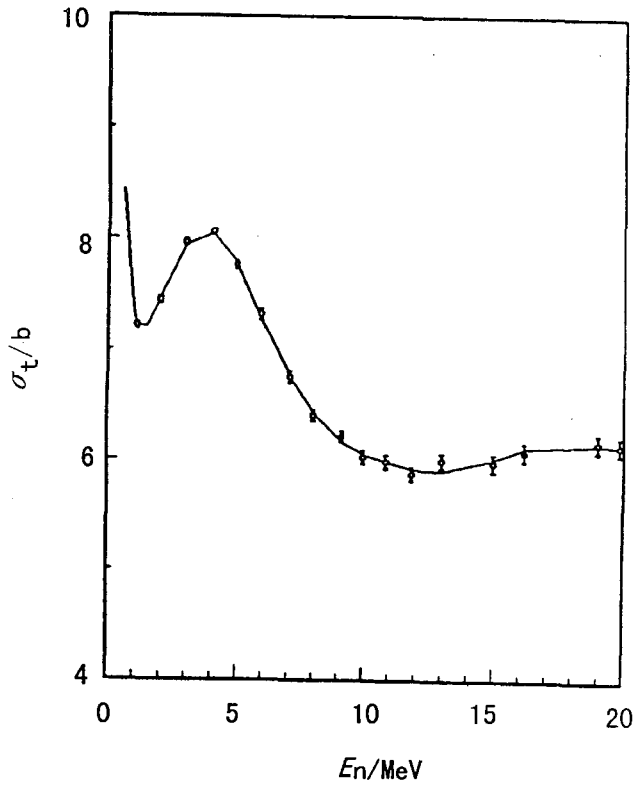

Fig. 8 n+^{242}Pu total cross section optical model calculation

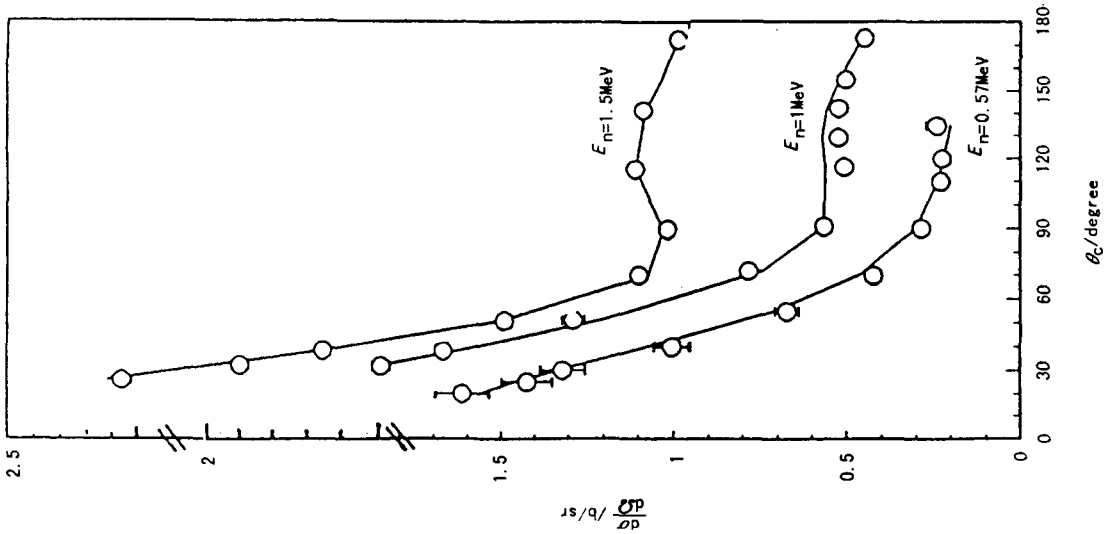

Fig. 9 n+^{242}Pu elastic angular distrlbution calculation and compared with exp. data

References

[1] Shen Qingbiao, APFO96 code, CNDC, 1996
[2] Liu Tong, AUTOFOPT System, CNDC, 1996
[3] Yan shi wei et al., Commu. of Nucl. Data Progress, No. 12, 14 (1994)

CN9901209

Calculation of Neutron Induced Reaction on ^{115}In in Energy Region from 0.01 to 20 MeV

Zhang Zhengjun Sun Xiuquan Zhang Jianshu Cao Ligang
(Department of Physics, Northwest University, Shaanxi)
Han Yinlu Shen Qingbiao
(China Nuclear Data Center, CIAE)

Abstract

A set of neutron optical potential parameters for ^{115}In in energy region of 0.01 to 20 MeV was obtained with available experimental data. Various cross sections of n+^{115}In reactions are calculated. Theoretical results are compared with experimental data.

Introduction

Calculating the cross sections of neutron induced reaction on ^{115}In is significant. There are few experimental data of total cross sections, nonelastic cross sections, elastic scattering cross sections and elastic scattering angular distributions of ^{115}In, but there are more experimental data of ^{Nat}In. In this paper a good set of optical potential parameters are presented and the calculated data of all cross sections and elastic scattering angular distributions of ^{115}In are given.

1 Theories and Parameters

The optical model, evaporation model and pre-equilibrium emission theory exciton model are used in our calculation.

In this calculations. The experimental data are taken from EXFOR library. The nuclear discrete levels are taken from Ref. [1]. The parameters of nuclear level densities and giant dipole resonance are taken from Ref. [2].

With the aid of code APOM94[3] the neutron optical potential parameters can be adjusted automatically with fitting experimental total, nonelastic cross section and elastic scattering angular distributions, then a set of best ones can be obtained. Because the experimental data of total, nonelastic cross section and elastic scattering angular distributions of ^{115}In are less, but there are more on ^{Nat}In, and the abundance of ^{115}In is 95.7 %, the experimental total cross sections, nonelastic cross sections and elastic scattering angular distributions of ^{Nat}In were used to play the roles of experimental data of ^{115}In. A set of optimum neutron optical potential parameters of ^{115}In are obtained as follows:

$V = 55.67852 - 0.079936E - 0.029445E^2 - 24.0(N-Z)/A$
$W_s = \max\{0.0, 8.23697 + 0.69874E - 12.0(N-Z)/A\}$
$W_v = \max\{0.0, -1.56148 + 0.21883E - 0.74522E^2\}$
$U_{SO} = 6.2$
$r_r = 1.19637$, $r_s = 1.31798$, $r_v = 1.26103$, $r_{SO} = 1.19637$,
$a_r = 0.67477$, $a_s = 0.44005$, $a_v = 0.58002$, $a_{SO} = 0.67477$.

The direct inelastic scattering cross sections were calculated by code DWUCK4[4] on the basis of this set of neutron optical potential parameters. Through adjusting the optical potential parameters of proton, alpha, ^{3}He, deuteron and triton particles, level densities and giant dipole resonance parameters, all cross sections of n+^{115}In reaction are calculated by the code SUNF[5].

In exciton model, the parameters K is taken as 600 MeV^3.

2 Calculation Results and Analyses

Fig. 1 shows the comparison of total cross sections between the calculated results and experimental data in the energy region from 0.01 to 20 MeV. The theoretical values are in good agreement with the experimental data. Fig. 2 shows the comparison of the calculated elastic scattering cross sections with the experimental data, the calculated results basically agree with the experimental data, but in energy region from 0.1 to 0.3 MeV, the theoretical curve is a little lower than experimental data. The calculated results are reasonable. The comparison between calculated values and experimental data of the elastic scattering angular distributions are shown in Figs. 3a, 3b, 3c. The theoretical values are in good agreement with the experimental data. Fig. 4 shows the comparison of the calculated inelastic scattering cross sections with the experimental data, experimental data is higher than theoretical curve. Because the theoretical values of total cross sections, elastic

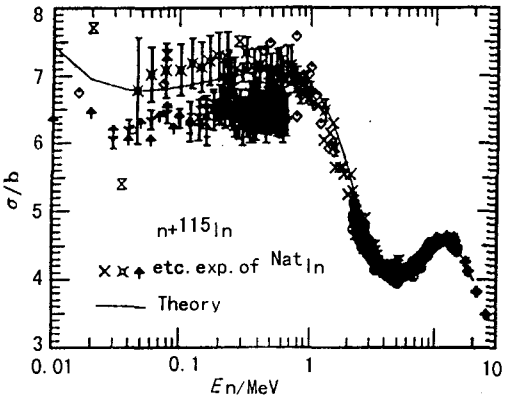

Fig. 1 Comparison of neutron total cross section between the calculated values of ^{115}In and the experimental data of ^{Nat}In

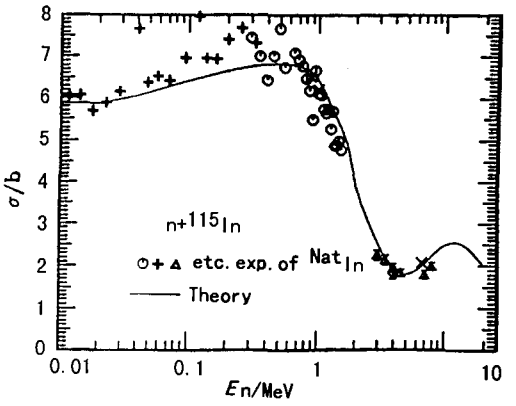

Fig. 2 Comparison of neutron elastic cross section between the calculated values of ^{115}In and the experimental data of ^{Nat}In

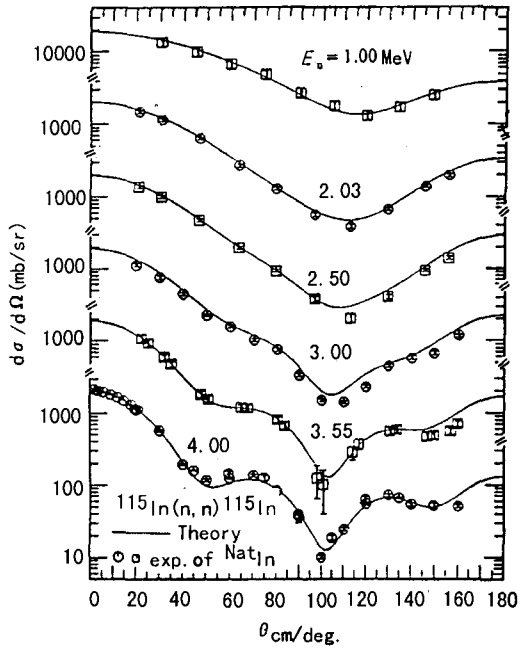

Fig. 3a Comparison of neutron elastic scattering angular distribution between the calculated values of ^{115}In and the experimental data of ^{Nat}In

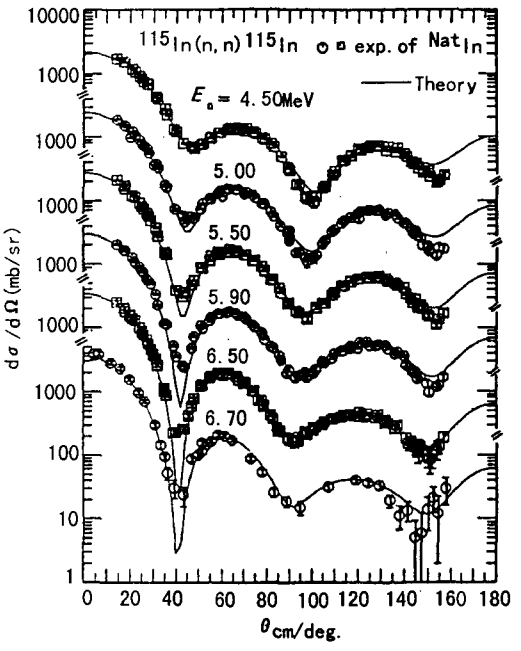

Fig. 3b Comparison of neutron elastic scattering angular distribution between the calculated values of ^{115}In and the experimental data of ^{Nat}In

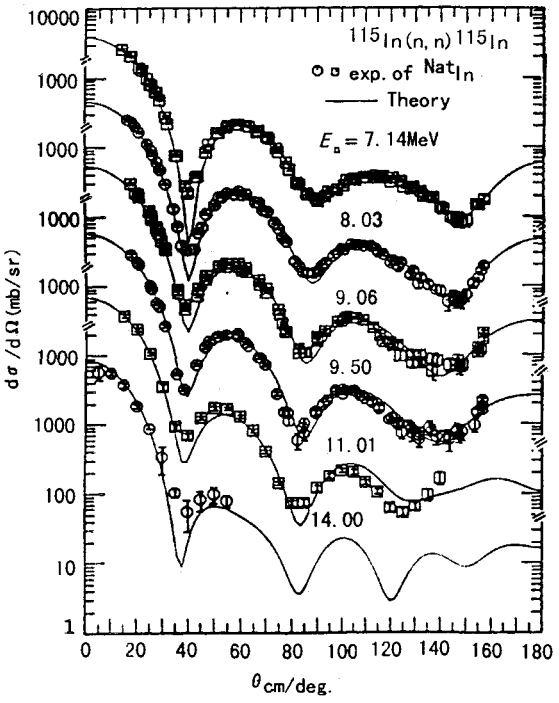

Fig. 3c Comparison of neutron elastic scattering angular distribution between the calculated values of ^{115}In and the experimental data of ^{Nat}In

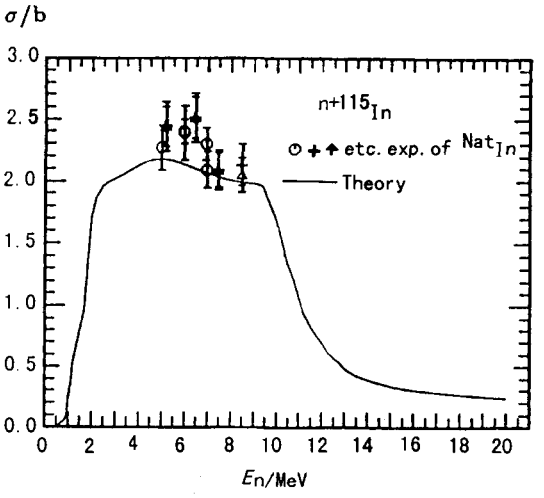

Fig. 4 Comparison of the inelastic cross section between the calculated values of ^{115}In and the experimental data of ^{Nat}In

scattering angular distributions and elastic scattering cross sections are in good agreement with experimental data, the calculated inelastic cross sections are reasonable. The theoretical values and experimental data of (n,γ) cross section of ^{115}In are shown in Fig. 5. The calculated results are in agreement with the experimental data for energy E_n<1.0 MeV. Figs. 6 and 7 give the comparison of calculated and experimental cross sections of (n, p) and (n,α) respectively. The calculated results of (n,α) are in agreement with the experimental data. Fig. 8 shows the theoretical values and experimental data of (n,2n). The theoretical values reproduce the experimental data[6,7,8] well. In Ref. [7], the experimental data of ground state and isomeric state are given, respectively. Thus, we give the sum of ground state and isomeric state data. Fig. 9 gives the total secondary neutron spectrum at energy E_n=14.625 MeV. The shape of theoretical curve is in agreement with experimental data. Fig. 10 shows all cross sections of n+^{115}In.

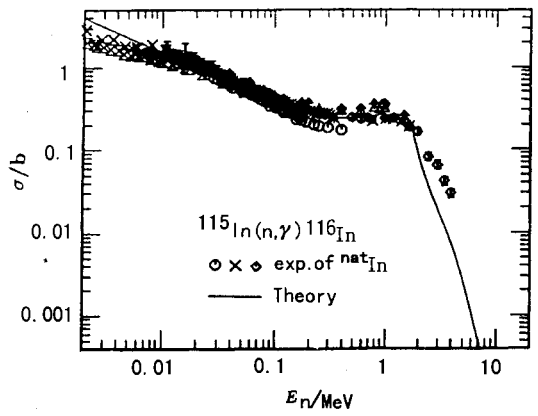

Fig. 5 The (n,γ) cross section

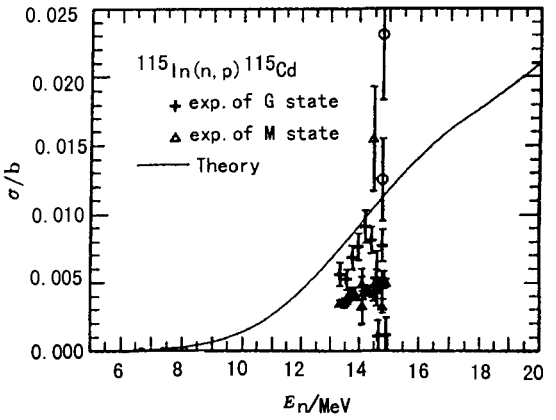

Fig. 6 The (n, p) cross section

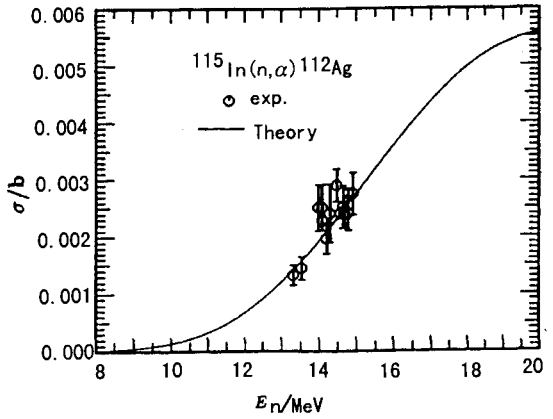

Fig. 7 The (n,α) cross section

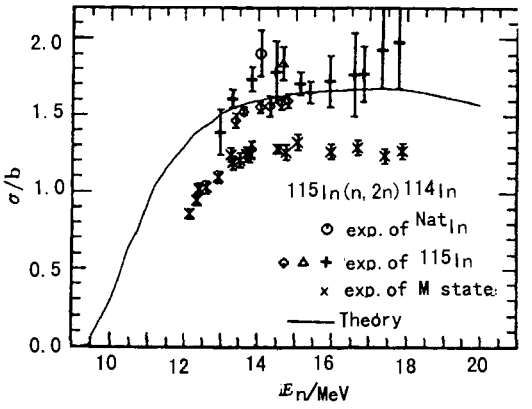

Fig. 8 The (n,2n) cross section

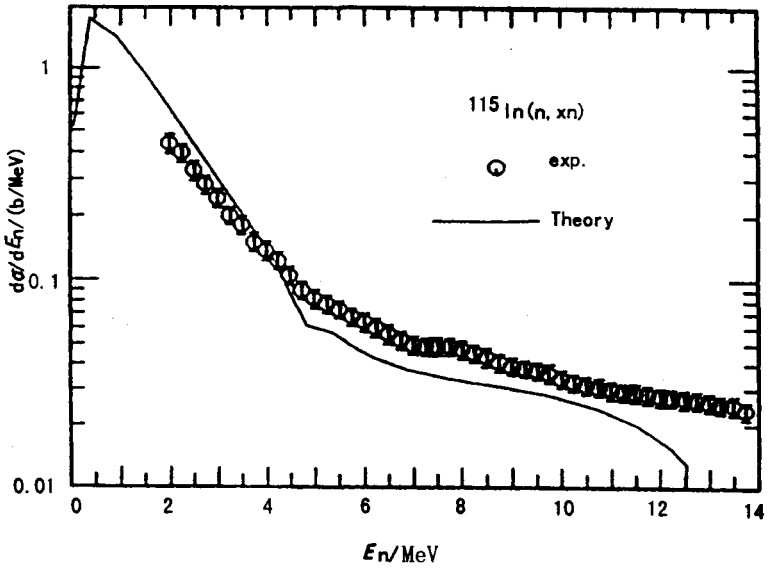

Fig. 9 The spectrum of total secondary neutron at E_n=14.625 MeV

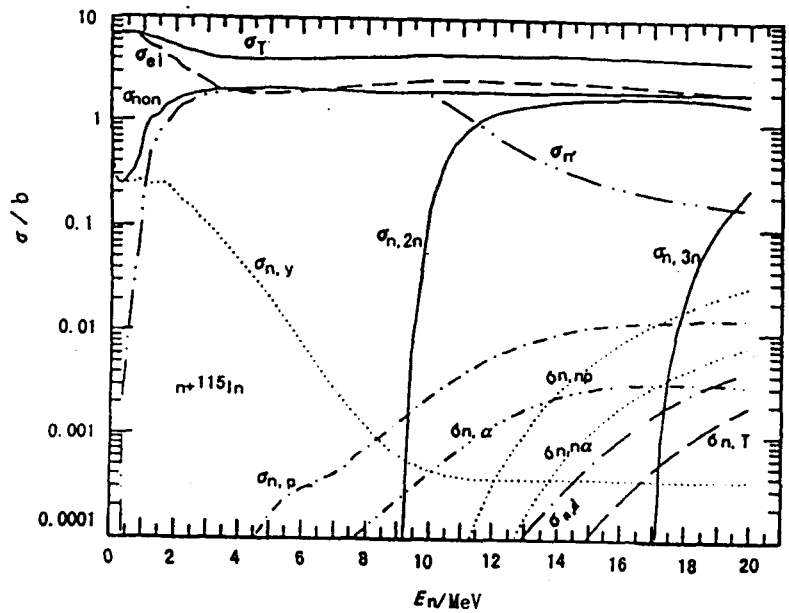

Fig. 10 The reaction cross section of n+^{115}In

3 Summary

Based on the available experimental data of ^{Nat}In, a set of neutron optical potential parameters was obtained for ^{115}In in the energy region from 0.01 to 20 MeV. Mentioned above results show that calculated values basically agree with the experimental data except inelastic cross section. The analysis was shows that the calculated inelastic cross sections are correct. It is possible that the experimental data of inelastic cross sections include some elastic scattering contribution. These theoretical results have important reference value to experimental scientists.

References

[1] Su Zongdi et al., Commun. Nucl. Data Progress, 12, 83 (1994)
[2] Su Zongdi et al., Chin. J. Nucl. Phys., 8, 149 (1986); INC (CPR)-2, 1986
[3] Shen Qingbiao, Commun. Nucl. Data Progress, 7, 43 (1992)
[4] P. D. Kunz, "Distorted Wave Code DWUCK4", University of Colorado
[5] Zhang Jingshang, Commun. Nucl. Data Progress, 17, 18 (1997)
[6] Grochulski et al., INR-1172
[7] J. Csikai, Zs. Lantos et al., Chin. J. Nucl.Phys., 11(3), 11 (1989)
[8] Ke Wei, Lu Hanlin et al., Z. fuer Phys., 337, 39 (1990)

CN9901210

Calculations of Complete Data for n+^{85,87,Nat}Rb in E_n=0.001 ~ 20 MeV

Cai Chonghai
(Department of Physics, Nankai University, Tianjin 300071)
Shen Qingbiao
(China Nuclear Data Center, CIAE)

Abstract

All reaction cross sections, secondary neutron spectra and elastic scattering angular distributions of n+^{85}Rb, ^{87}Rb and natural Rb in E_n=0.001 ~ 20 MeV are calculated, rather good theoretical results in accordance with experimental data are obtained, and all calculated results for ^{85}Rb and ^{87}Rb are given in ENDF/B-6 format.

Introduction

^{85,87}Rb are the only two stable isotopes of natural element Rb which belongs to fission product nuclides. The abundances of ^{85}Rb and ^{87}Rb are 72.165 and 27.835, respectively. There are sufficient experimental data of σ_{tot} for natural element, some experimental data of σ_{tot} for ^{85}Rb and ^{87}Rb in E_n<0.03 MeV region; sufficient experimental data of $\sigma_{n,\gamma}$ for ^{85}Rb, ^{87}Rb and natural element; sufficient experimental data of $\sigma_{n,2n}$ for ^{85}Rb and ^{87}Rb; some experimental data of $\sigma_{n,p}$ for ^{87}Rb and natural element; some experimental data of $\sigma_{n,\alpha}$ for ^{85}Rb and natural element. There are no experimental data for other reaction cross sections, elastic scattering angular distributions, and secondary neutron spectra. All of the experimental data are taken from EXFOR. The universal optical potential parameters for six channels used in calculations are given in Table 1 of Ref. [1].

Firstly, The code APMN[2] is used to automatically get the optimal parameters of optical potential for neutron channel. Because there are only some very divergent experimental data of σ_{tot} for ^{85}Rb and ^{87}Rb in E_n<0.03 MeV region and no experimental data for σ_{non} and elastic scattering angular distributions at all, the experimental data of σ_{tot} for natural element are used to determine the optimal optical potential parameters for neutron channel by using the code APMN. The optimal same set of optical potential parameters for neutron channel used for calculations of ^{85}Rb and ^{87}Rb are:

V_0= 49.664341, V_1= –0.201245, V_2= –0.009378, V_4= 0.081837,
W_0= –2.381331, W_1= 0.174407,

$U_0 = 1.949484$, $U_1 = 0.212028$, $U_2 = 0.009705$,
$a_r = 0.617588$, $a_s = 0.587063$, $a_v = 0.681305$,
$r_r = 1.279039$, $r_s = 1.238257$, $r_v = 1.200825$.

Secondary, the code DWUCK4[3] is used to calculate the cross sections and angular distributions of 10 levels for ^{85}Rb, 5 levels for ^{87}Rb, in direct inelastic scattering. These direct inelastic scattering data and the optimum set of optical potential parameters are taken as the input data of the kernel program SUNF[4]. SUNF can only calculate single isotope, so a small program is used to get the cross sections of natural element from the output of ^{85}Rb and ^{87}Rb. Through adjusting some parameters in the input data of SUNF for ^{85}Rb and ^{87}Rb $\sigma_{n,\gamma}$, $\sigma_{n,2n}$, $\sigma_{n,p}$ and $\sigma_{n,\alpha}$ for ^{85}Rb, ^{87}Rb as well as natural element in good agreement with experimental data are obtained.

The optimal values of the parameters we got are:

C_k (the parameter for exiton model) = 570.0 for ^{85}Rb, 600.0 for ^{87}Rb;

C_{el} (the multiplied factor in $\sigma_{n,\gamma}$) = 0.119 for ^{85}Rb, 0.50 for ^{87}Rb;

Some optical potential parameters for p, α channels are as follows:

for ^{85}Rb:

for p channel, a_r and a_{SO}=0.60, a_s and a_v=0.55, r_v=1.25;

for α channel, a_r, a_s, a_v and a_{SO}=0.65, r_r and r_{SO}=1.35, r_s and r_v=1.40;

for ^{87}Rb:

for p channel, a_r and a_{SO}=0.50, a_s and a_v=0.45, r_s and r_v=1.15;

for α channel, a_r, a_s, a_v and a_{SO}=0.60, r_r, r_s, r_v and r_{SO}=1.39;

The level density parameter is as follows:

for ^{85}Rb, $a_{n,p} = 11.48064$, $a_{n,\alpha} = 11.10343$, $a_{n,d} = 9.22576$, $a_{n,t} = 11.89621$, $a_{n,2n} = 14.21238$;

for ^{87}Rb, $a_{n,p} = 11.78000$, $a_{n,2n} = 12.51302$;

The pairing energy correction is as follows:

for ^{85}Rb, $\Delta_{n,n'} = 1.20$;

for ^{87}Rb, $\Delta_{n,n'} = 0.45$.

The calculated σ_{tot}, σ_{non} and σ_{el} as well as the experimental data of σ_{tot} for ^{85}Rb, ^{87}Rb and natural element are given in Fig. 1, from which we can see that the calculated σ_{tot} are in good agreement with experimental data. The results of $\sigma_{n,\gamma}$ for ^{85}Rb, ^{87}Rb and natural element are given in Fig. 2, from which we can see that the calculated values are in good agreement with experimental data except in E_n>2 MeV energy region. The calculated and experimental $\sigma_{n,p}$ are given in Fig. 3, from which we can see that the calculated value are in good agreement with experimental data for ^{87}Rb, but not in good agreement with experimental data for natural element. We

guess that the experimental $\sigma_{n,p}$ in E_n>14.5 MeV energy region possibly includes $\sigma_{n,pn}$, because in this energy region the $\sigma_{n,p}$ should gradually decrease in company with the increase of $\sigma_{n,pn}$. The calculated and experimental $\sigma_{n,\alpha}$ are given in Fig. 4, from which we can see that the calculated value are difficult to compare with experimental data, because the experimental $\sigma_{n,\alpha}$ for both ^{85}Rb and natural element are rather divergent. The calculated $\sigma_{n,n'}$ and $\sigma_{n,2n}$ and experimental $\sigma_{n,2n}$ for ^{85}Rb and ^{87}Rb are given in Fig. 5, from which we can see that the calculated $\sigma_{n,2n}$ are in good agreement with experimental data for ^{85}Rb and ^{87}Rb and H. R. Yuan's evaluated values for ^{85}Rb. All the calculated cross sections are plotted in Figs. 6 ~ 8 for natural element, ^{85}Rb and ^{87}Rb, respectively. The calculated secondary neutron spectra of continuous inelastic scattering (MT=91) at E_n=8.0 and 14.0 MeV and (n,2n) reaction (MT=16) at E_n=14.0 and 20.0 MeV are plotted in Fig. 9 and Fig. 10 for ^{85}Rb, in Fig. 11 and Fig. 12 for ^{87}Rb, respectively. The shape of these secondary neutron spectra are reasonable in physics, though there are no experimental data to compare with.

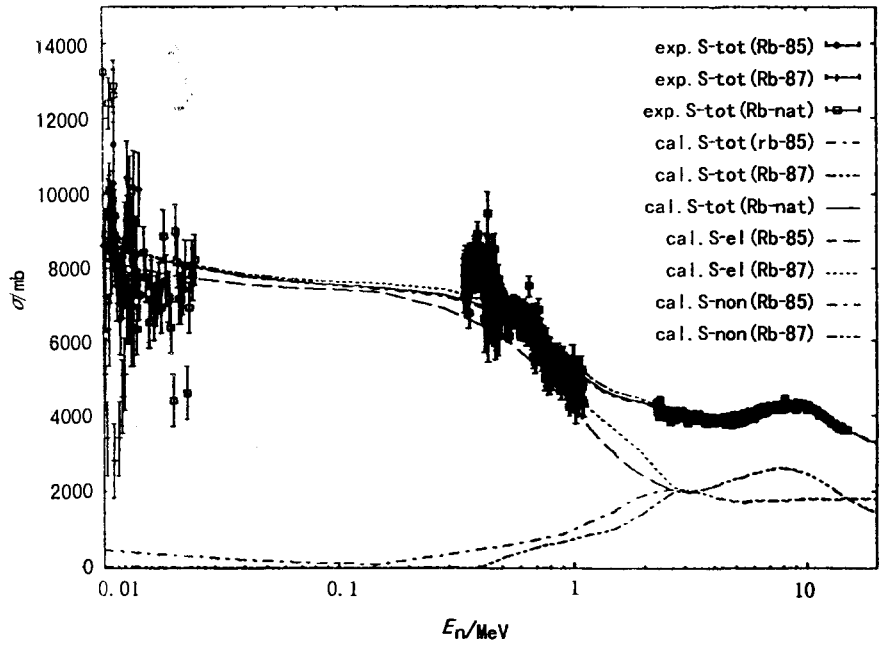

Fig. 1 Rb total, elastic and nonelastic cross sections energies of incoming neutron in L-frame (MeV)

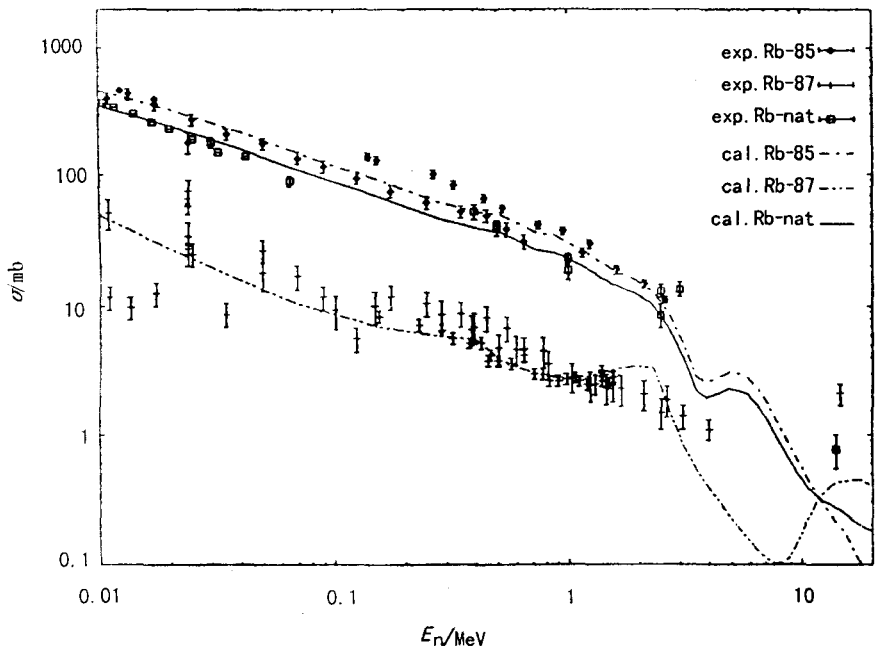

Fig. 2 Rb (n,γ) cross sections energies

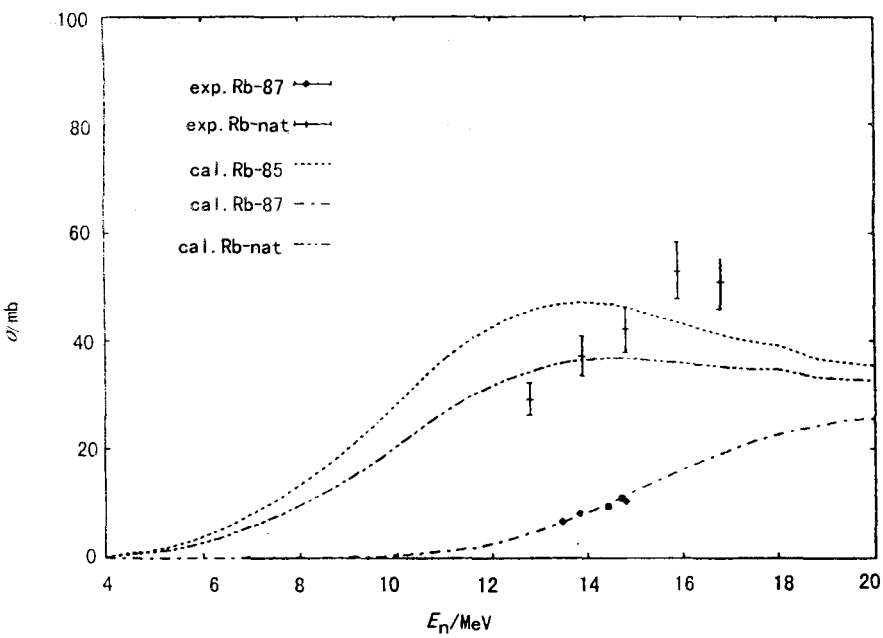

Fig. 3 Rb (n,p) cross sections energies

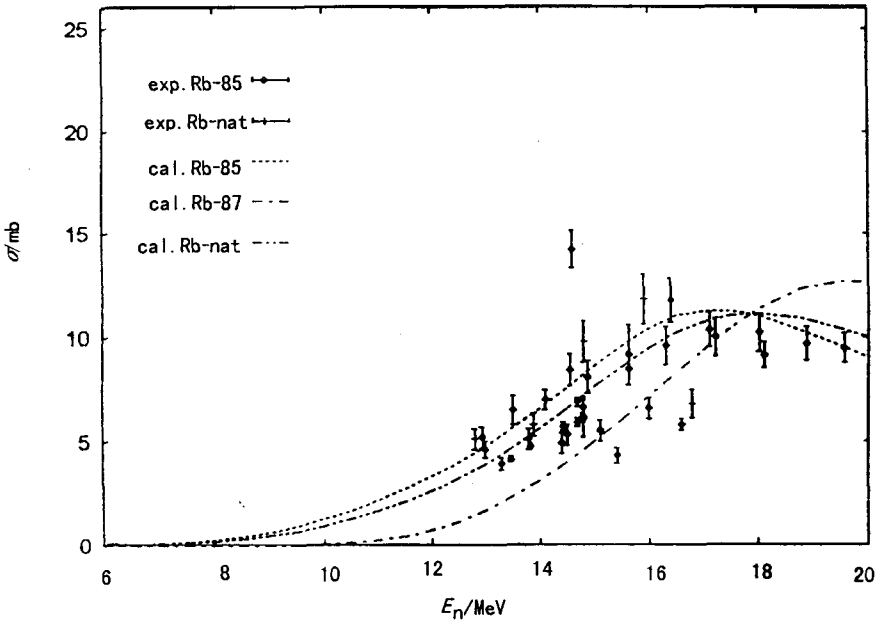

Fig. 4 Rb (n,α) cross sections energies

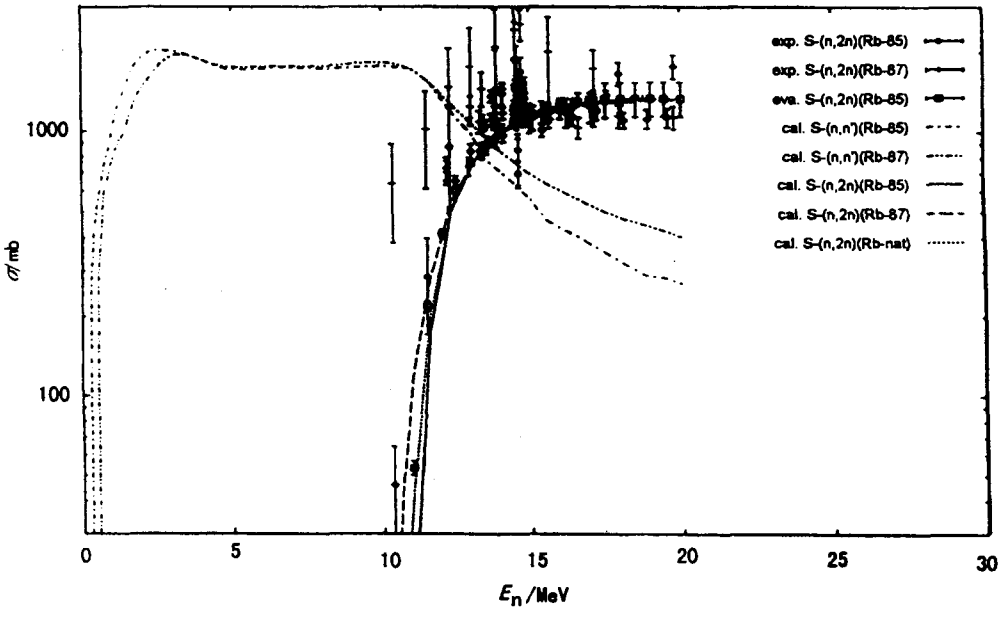

Fig. 5 Rb (n,n'') and (n,2n)cross sections

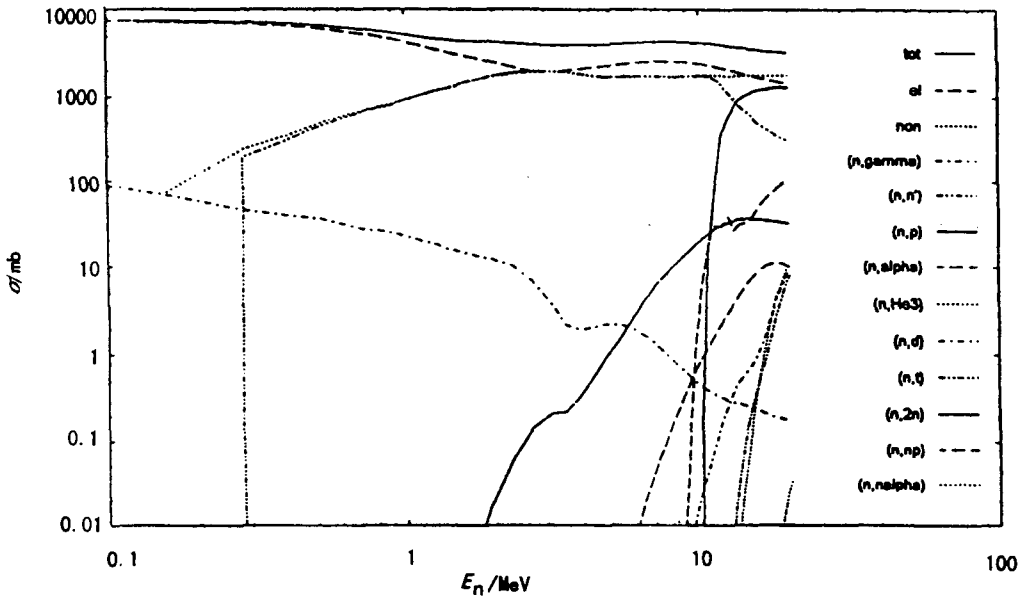

Fig. 6 All calculated cross sections of ^{Nat}Rb

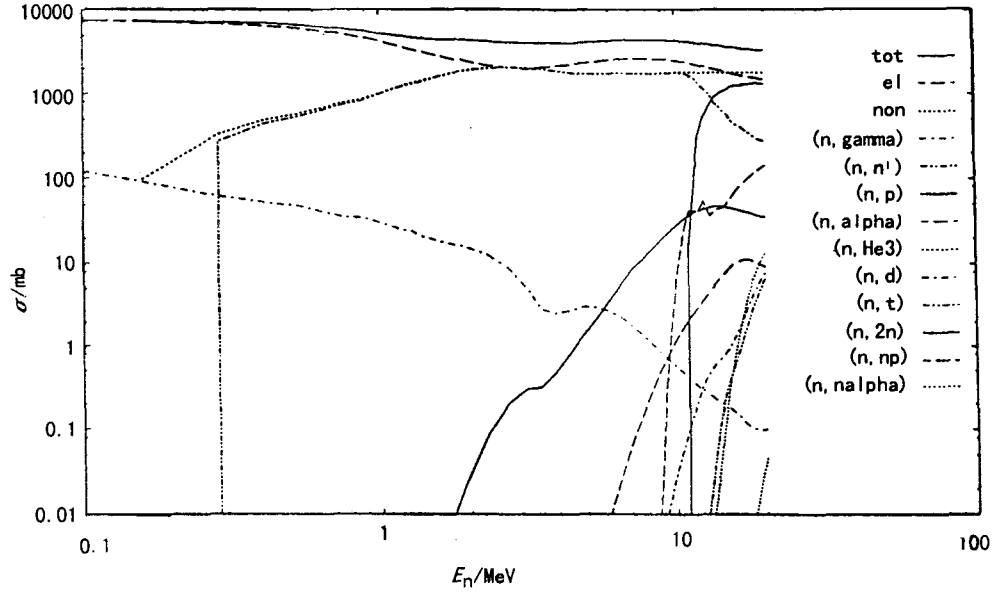

Fig. 7 All calculated cross sections of ^{85}Rb

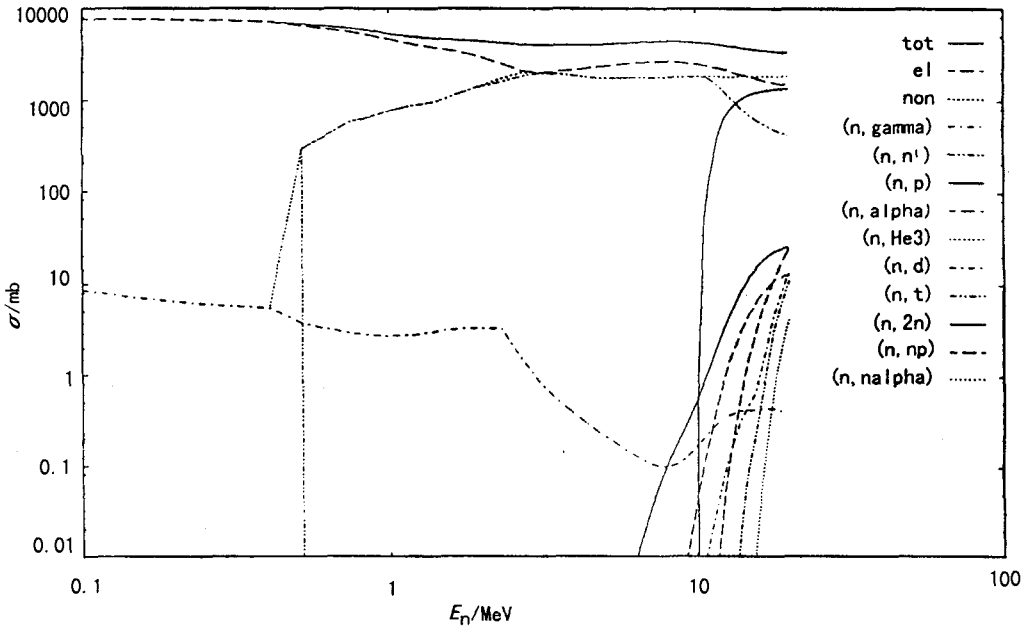

Fig. 8 All calculated cross sections of ^{87}Rb

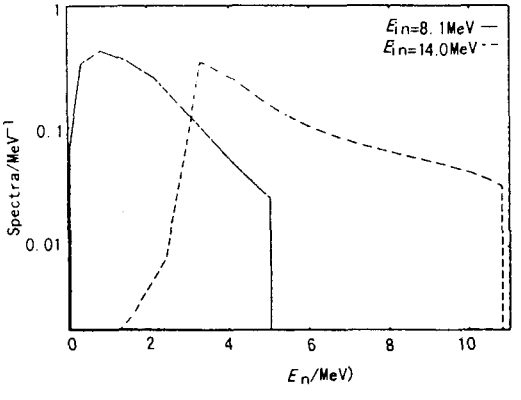

Fig. 9 ^{85}Rb secondary neutron spectra of (n,n') (MT=91)

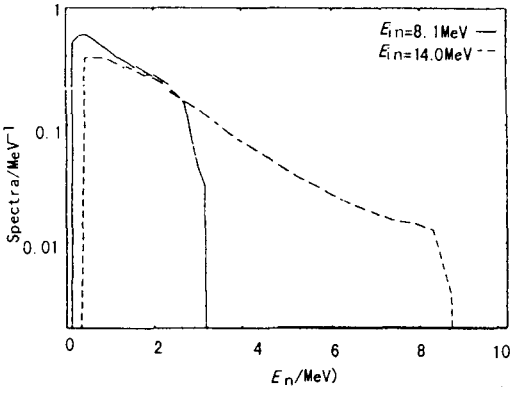

Fig. 10 ^{85}Rb secondary neutron spectra of (n,2n) (MT=16)

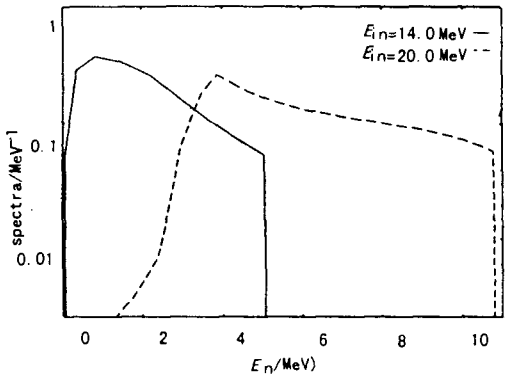

Fig. 11 ^{87}Rb secondary neutron spectra of (n,n') (MT=91)

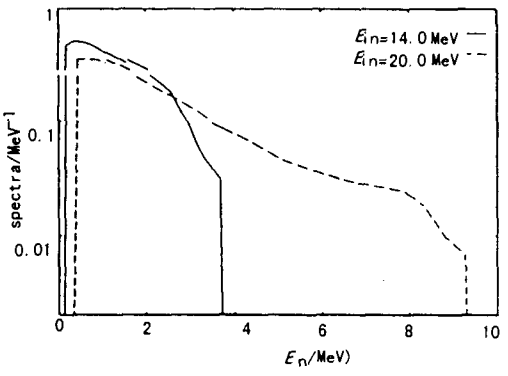

Fig. 12 ^{87}Rb secondary neutron spectra of (n,2n) (MT=16)

References

[1] Cai Chonghai and Shen Qingbiao, Comprehensive Calculations of All Reactions for n+^{89}Y in E_n=0.001 ~ 20 MeV, CNDP No. 20

[2] Shen Qingbiao, APMN, a code for automatically searching for a set of optimal optical potential parameters of many medium and heavy nucleus (unpublished)

[3] P. D. Kunz, DWBA code DWUCK4, University of Colorado, USA (unpublished)

[4] Zhang Jingshang, SUNF, a code for comprehensive calculations of fission product nucleus based on unified model, CNDC, CIAE (unpublished)

CN9901211

Calculation of Neutron Induced Reaction on ^{113}Cd in Energy Region from 0.01 to 20 MeV

Sun Xiuquan Zhang Zhengjun Zhang Jianshu Zhou Jinfeng Cao Ligang
(Department of Physics, Northwest University, Shaanxi)
Han Yinlu Shen Qingbiao
(China Nuclear Data Center, CIAE)

Abstract

A set of neutron optical potential parameters in energy region from 0.01 to 20 MeV is obtained on the basis of available experimental data. Based on this set of optical potential parameters, the elastic scattering angular distribution and all cross sections of neutron induced reaction on ^{113}Cd are calculated. Various calculated nuclear data are in good agreement with available experimental data.

Introduction

The cross sections $^{113}Cd(n,\gamma)^{114}Cd$, $^{113}Cd(n,2n)^{112}Cd$ are of considerable significance for nuclear science and technology. Because the experimental data are scarce, it is necessary to calculate the cross sections according to some theoretical models. This paper presents the calculated results of ^{113}Cd in energy region from 0.01 to 20 MeV.

1 Theories and Parameters

The code APOM94[1], DWUCK4[2] and SUNF[3] were used in the calculations. The experimental data were taken from EXFOR library. The nuclear discrete levels were taken from Ref. [4]. The parameters of nuclear level densities and giant dipole resonance were taken from Ref. [5].

With the aid of code APOM94 the best neutron optical potential parameters can be adjusted automatically to fit the total cross sections, nonelastic scattering cross sections and elastic scattering angular distributions. For the experimental data of neutron induced reactions on ^{113}Cd are scarce, the experimental data of ^{Nat}Cd and experiment data of neighbor nuclei were referenced in the calculation. A set of optimum neutron optical potential parameters of ^{113}Cd were obtained as follows:

$$V = 55.2769 - 0.41505E - 0.0018309E^2 - 24.0(N-Z),$$
$$W_s = \max\{0.0,\ 9.23119 + 0.222508E - 12.0(N-Z)/A\},$$
$$W_v = \max\{0.0,\ -1.56148 + 0.21883E - 0.074714E^2\},$$
$$U_{SO} = 6.2,$$
$$r_r = 1.17375,\quad r_s = 1.36780,\quad r_v = 1.26103,\quad r_{SO} = 1.17345,$$
$$a_r = 0.74542,\quad a_s = 0.40658,\quad a_v = 0.58002,\quad a_{SO} = 0.74542.$$

The exciton model parameter K is taken as 900 MeV.

The direct inelastic scattering cross sections are calculated by code DWUCK4 on the basis of this set of neutron optical potential parameters. Through adjusting the optical potential parameters of proton, alpha, ^3He, deuteron and triton particles, level densities and giant dipole resonance parameters, all reaction cross sections are calculated by using the code SUNF.

2 Calculation Results and Analyses

Fig. 1 shows a comparison of neutron total cross sections between the calculated results of ^{113}Cd and the experimental data of natural nucleus in the energy range from 0.01 to 20 MeV; the theoretical values reproduce the experimental data very well. The elastic scattering angular distributions are shown in Figs. 2a, 2b and 2c; the theoretical values are in good agreement with the experimental data. Fig. 3

shows the cross sections of $^{113}Cd(n,\gamma)^{114}Cd$. The calculated results reproduce the experimental data quite well. Fig. 4 shows the theoretical values of cross section for $^{113}Cd(n,2n)^{112}Cd$. Lack of the experimental data, the experimental values of $^{116}Cd(n,2n)^{115}Cd$ were referenced. Fig. 5 shows that the theoretical values cross two experimental points at 14 MeV for $^{113}Cd(n,p)^{113}Ag$ reaction. Fig. 6 shows comparison between the theoretical values and the experimental data of the neutron energy spectrum at E_n=14.5 MeV. The theoretical values are in agreement with the experimental data. Various calculated cross sections are shown in Fig. 7. They are all reasonable.

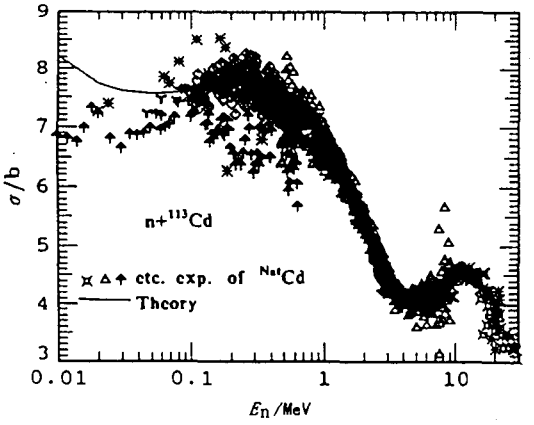

Fig. 1 Comparison of neutron total cross sections of ^{Nat}Cd between the calculated values and the experimental data of ^{Nat}Cd

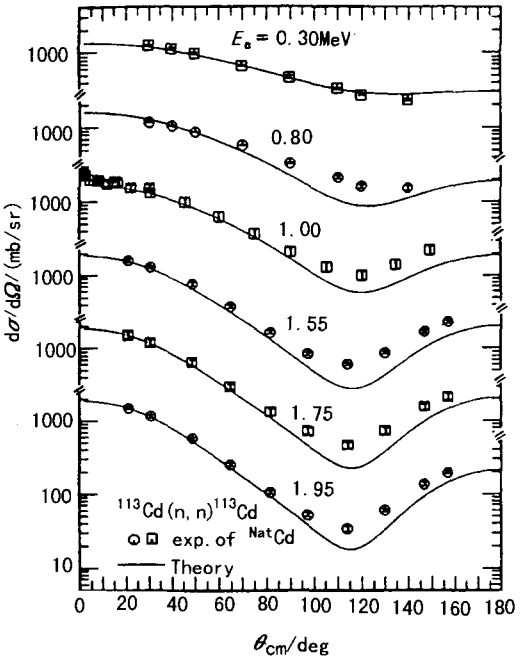

Fig. 2a Comparison of neutron elastic scattering angular distribution between the calculated values and the experimental data of ^{Nat}Cd

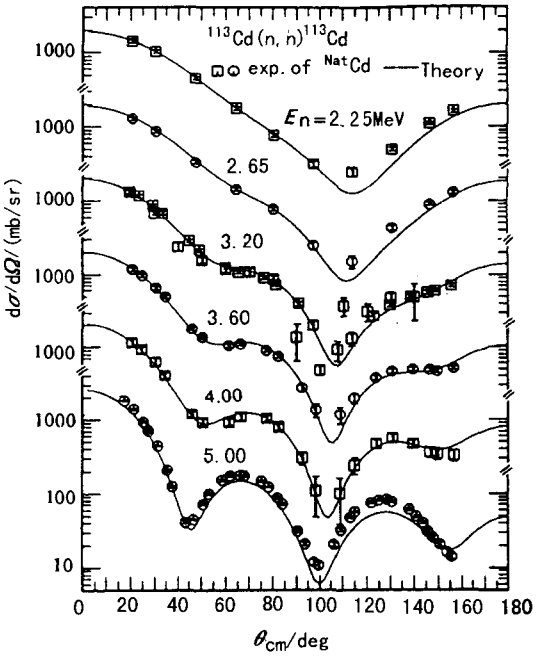

Fig. 2b Comparison of neutron elastic scattering angular distribution between the calculated values and the experimental data of ^{Nat}Cd

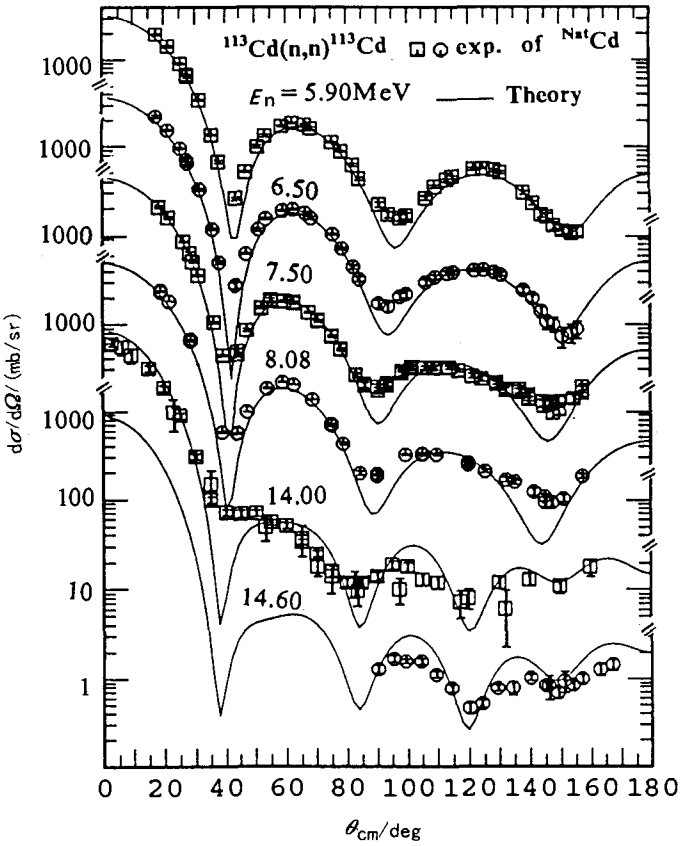

Fig. 2c Comparison of neutron elastic scattering angular distribution between the calculated values and the experimental data of ^{113}Cd

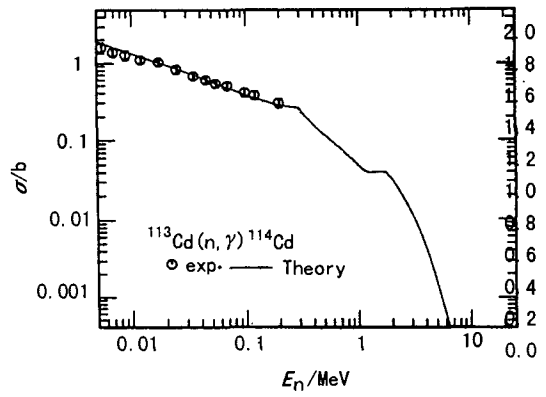

Fig. 3 The cross sections of (n,γ)

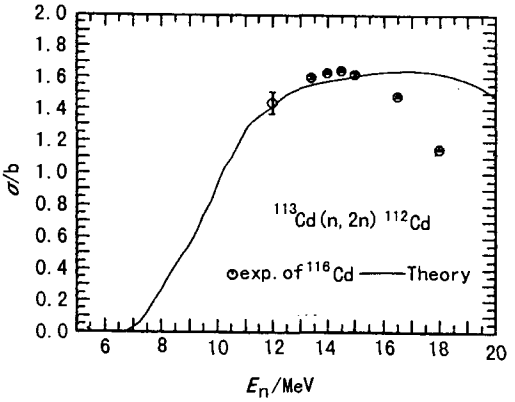

Fig. 4 The cross sections of (n,2n)

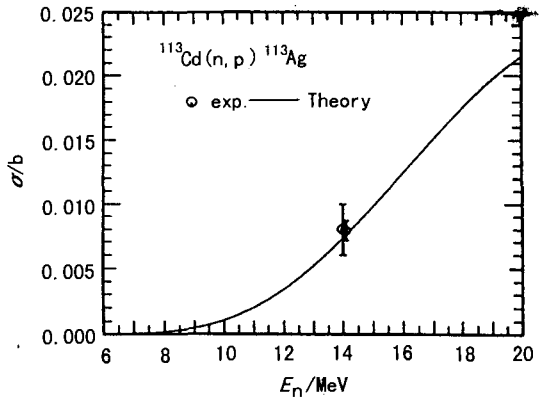

Fig. 5 The cross sections of (n,p)

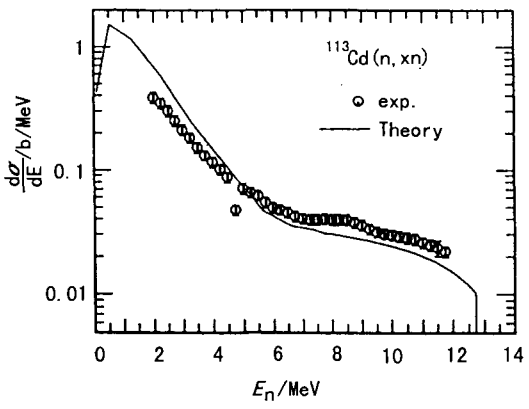

Fig. 6 The energy spectrum of neutron at E_n=14.5 MeV

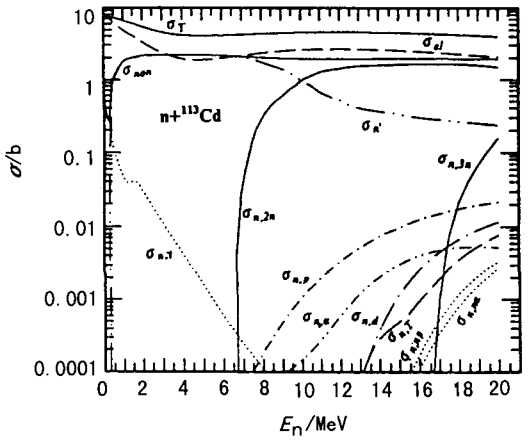

Fig. 7 The cross sections of n+^{113}Cd reaction

3 Summary

Based on the experimental data of ^{113}Cd and using the code APOM94, DWUCK4 and SUNF, a set of optimum neutron optical potential parameters were obtained for ^{113}Cd in the energy range from 0.01 to 20 MeV. Above-mentioned results show that calculated values are in basically agreement with the experimental data.

References

[1] Shen Qingbiao, Commun. Nucl. Data Progress, 7, 43 (1992)
[2] P. D. Kunz, "Distorted Wave Code DWUCK4", University of Colorado
[3] Zhang Jingshang, CNDP, No.17 and 18, (1997)
[4] Su Zongdi et al., Commun. Nucl. Data Progress, 12,83 (1994)
[5] Su Zongdi et al., Chin. J. Nucl. Phys., 8, 149 (1986); INC (CPR)-2, 1986

CN9901212

Calculation of Neutron Induced Reaction on $^{121,123}Sb$

Zhang Zhengjun Sun Xiuquan Zhou Jinfeng
(Depart. of Phyics, Northwest University, Shaanxi)
Han Yinlu Shen Qingbiao
(China Nuclear Data Center, CIAE)

Abstract

A set of neutron optical potential parameters for energy from 0.01 to 20 MeV is obtained on the basis of available experimental data of $^{121,123,Nat}Sb$ and neighbored nucleus. Based on this set of optical potential parameters, all cross sections of neutron induced reactions for $^{121,123}Sb$ are calculated. The calculated results reproduce the available experimental data well.

1 Theories and Parameters

The cross sections of neutron induced reactions on $^{121,123}Sb$ is useful for nuclear science and technology. The purpose of this paper is to present the caculated results. In our calculations, the code APOM94[1], DWUCK4[2] and SUNF[3] are used.

The experimental data were taken from EXFOR library. The nuclear discrete levels and the parameters of nuclear levels densities as well as giant dipole resonance were taken from Ref. [4] and Ref. [5], respectively.

There are a few experimental data for $^{121,123}Sb$ (n,2n) and (n,γ) of neutron induced reactions, while there are more total cross sections, elastic scattering angular distributions on ^{Nat}Sb. The abundaces of ^{121}Sb and ^{123}Sb are 57.21 and 42.79 %, respectively.

With code APOM94, the best neutron optical potential parameters for ^{121}Sb were obtained by fitting experimental total cross sections, nonelastic cross sections and elastic scattering angular distributions of ^{Nat}Sb and this set of neutron optical potential parameters were used in $n+^{123}Sb$ reaction without adjustment[6]. This set of optimum neutron optical potential parameters for ^{121}Sb and ^{123}Sb are as follows:

$V = 55.15506 - 0.358E - 0.01645E^2 - 24.0(N-Z)/A$,
$W_s = \max\{0.0, 4.91473 + 0.91999E - 12.0(N-Z)/A\}$,
$W_v = \max\{0.0, -1.56148 + 0.21883E - 0.074714E^2\}$,
$r_r = 1.19786$, $r_s = 1.34581$, $r_v = 1.31036$, $r_{SO} = 1.19786$,
$a_r = 0.64562$, $a_s = 0.49202$, $a_v = 0.58002$, $a_{SO} = 0.64562$,

U_{SO}=6.2.

The direct inelastic scattering cross sections were calculated by code DWUCK4 on the basis of this set of neutron optical potential parameters. All cross sections of n+^{121}Sb and n+^{123}Sb were calculated by SUNF code. In the calculation, the optical potential parameters of proton, alpha, ^{3}He, deuteron and triton paticales, level densities, giant dipole resonance, especially, the pair correction values were adjusted. The exciton model parameter K is taken as 900 MeV^{3}.

2 Calculation Results and Analyses

Fig. 1 shows a comparison of neutron total cross section between the calculated results of ^{121,123}Sb and experimental data of natural nucleus in the energy range from 0.01 to 20 MeV. It indicates that the theoretical values of ^{121}Sb and ^{123}Sb reproduce the experimental data rather well.

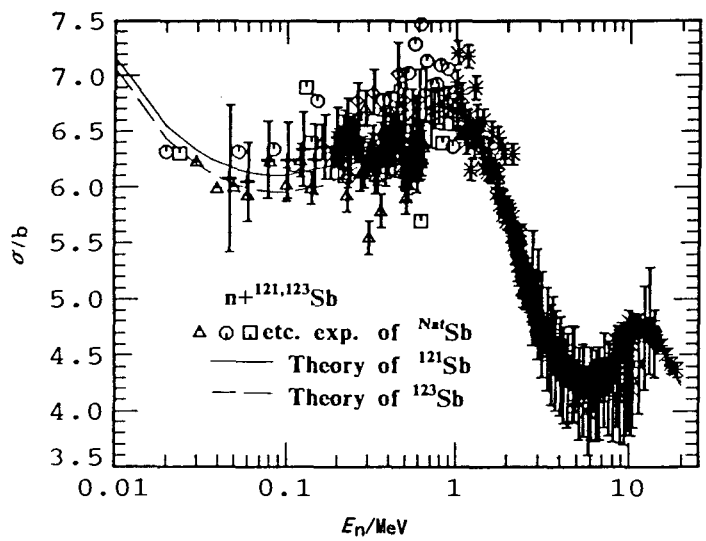

Fig. 1 Comparison of neutron total cross sections between the calculated values of ^{121,123}Sb and the experimental data of ^{Nat}Sb

The comparison between calculated values and experimental data of the elastic scattering angular distributions are shown in Fig. 2a and Fig. 2b. The theoretical values are also in good agreement with the experimental data of ^{Nat}Sb.

Fig. 3a and Fig. 3b the show comparison of ^{121,123}Sb(n,γ) cross section between calculated results and experimental data. The calculated values are in agreement with experimental data well in E_n<1.2 MeV. The shape both of theoretical curves of ^{121}Sb(n,γ) and ^{123}Sb(n,γ) is reansonable except in energy range from 1.2 to 3.0 MeV.

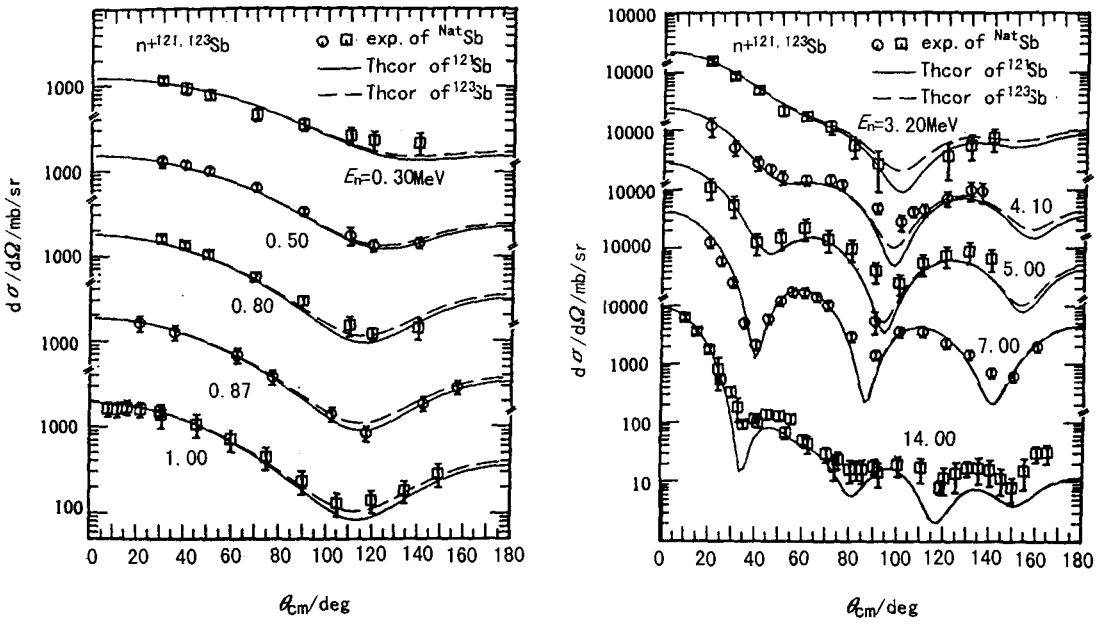

Fig. 2 Comparison of neutron elastic scattering angular distribution between the calculated values and the experimental data of ^{Nat}Sb

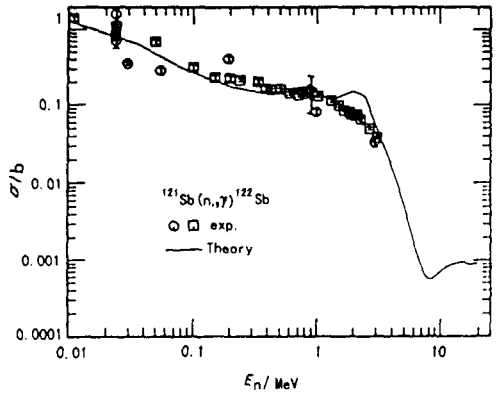

Fig. 3a The cross section of $^{121}Sb(n,\gamma)$

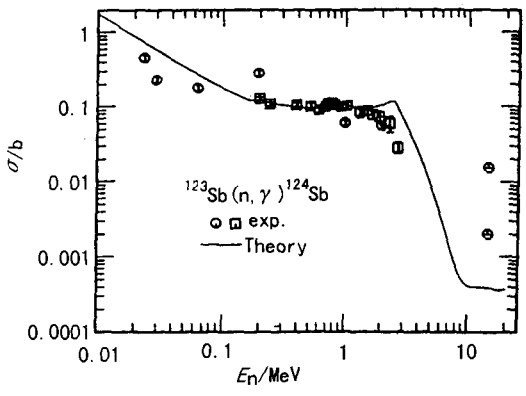

Fig. 3b The cross section of $^{123}Sb(n,\gamma)$

The calculated cross sections of $^{121,123}Sb(n,2n)$ reactions and available experimental data are shown in Fig. 4a and Fig.4b respectively. We can see from Fig. 4a theoretical values and the experimental data are in good agreement each other. In Fig. 4b the theoretical curve pass the experimental data[7] and are higher than the experimental data[8] obviously. It indicates that the calculated results and experimental data[7] are reasonable based on the evaluation and analysis of experimental data[7,8].

Fig. 5 gives out the energy spectrum of neutron at E_n=14.625 MeV. Beacause the calculated curve we given is without the contribution of discrete levels, so it becomes low rapidly when energy E_n>10.0 MeV.

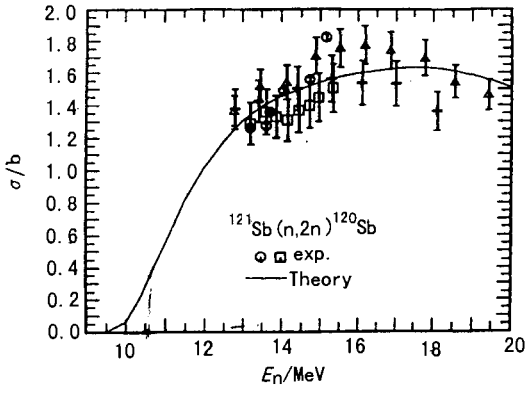

Fig. 4a The cross section of ^{121}Sb(n,2n)

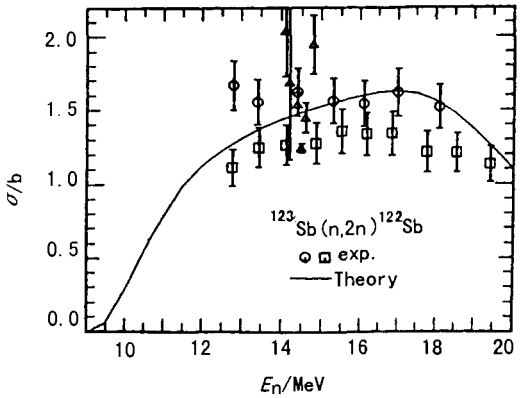

Fig. 4b The cross section of ^{123}Sb(n,2n)

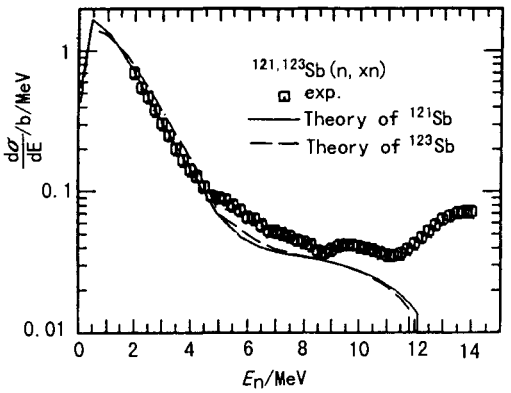

Fig. 5 The energy spectrum of neutron at E_n=14.625 MeV

All calculated cross section curves of n+^{121}Sb and n+^{123}Sb are shown in Fig. 6a and Fig. 6b, respectively.

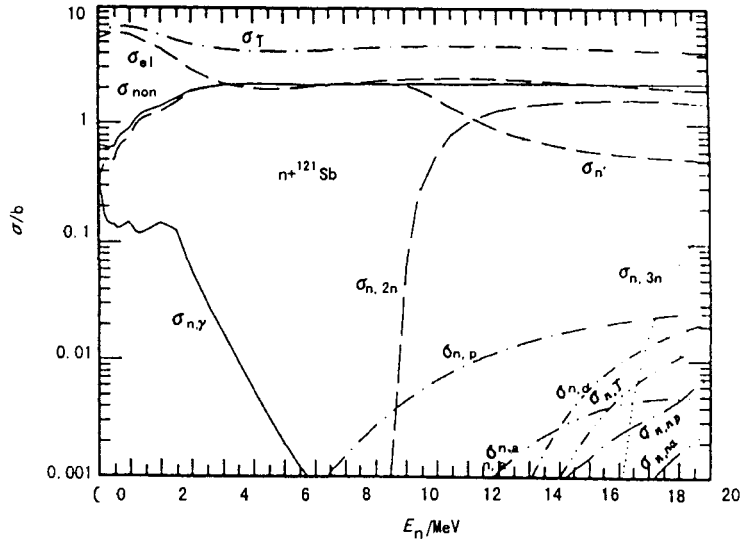

Fig. 6a The calculated cross section of n+^{121}Sb reaction

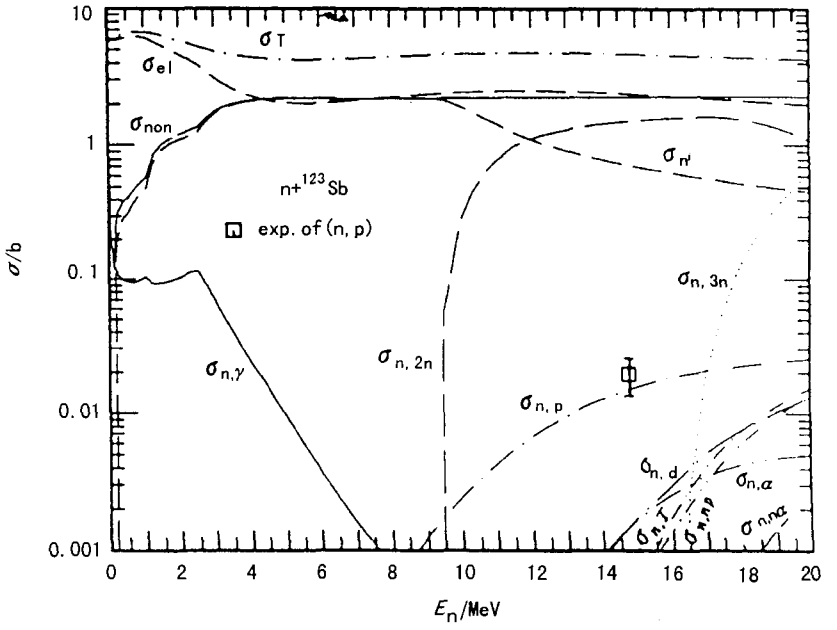

Fig. 6b The calculated cross section of $n+^{123}Sb$ reaction

References

[1] Shen Qingbiao, Commun. Nucl. Data Progress, 7, 43 (1992)

[2] P. D. Kunz, "Distorted Wave Code DWUCK4", University of Colorado

[3] Zhang Jingshang, Commun. Nucl. Data Progress, 17, 18 (1997)

[4] Su Zongdi et al., Commun. Nucl. Data Progress, 12, 83 (1994)

[5] Su Zongdi et al., Chin. J. Nucl. Phys., 8, 149(1986); INC(CPR)-2, 1986

[6] Zhang Zhengjun et al., Commun. Nucl. Data Progress, 19, 58 (1998)

[7] S. K. Ghorai et al., Nucl. Phys. A, 6, 393 (1980)

[8] M. Bormann et al., J. of Phys. Pt. G, Nucl. Phys. 115, 309 (1968)

CN9901213

Calculation of Photonuclear Data for $^{180,182,183,184,186}W$

Han Yinlu Yu Baosheng Zhang Jingshang
(China Nuclear Data Center, CIAE)

Abstract

Based on available experimental data of neutron and photonuclear reaction, a set of neutron optical potential parameter and giant resonance parameters of γ for W were obtained. The photonuclear reaction data for $^{180,182,183,184,186}W$ were calculated and compared with experimental data.

Introduction

The photonuclear reaction data have been widely used in basic scientific researches on neutron binding energy, nuclear level and deformation, as well as nuclear reaction mechanism, also used in engineering and technology such as medicine, electronic, activation analysis, radiation damage and shielding.

W is an important structral materials. It is necessary and useful to calculate its photonuclear data according to some theoretical models. The calculations of $^{180,182,183,184,186}W$ photonuclear data and comparisons of theoretical results with experimental data for photon energies in the range 4 ~ 30 MeV are given in this paper.

1 Theoretical Model and Parameters

There are no nuclear force and charge interaction between photo and nucleus, thus the photonuclear reaction is induced by electromagnetic interaction. The nuclear photon scattering process shows a higher order coherent phenomena[1], the total absorption and coherent scattering cross section can be obtained on basis of the optical theorem and the dispersion relation, associated with the absorption process. And the spherical optical model, the semi-classical theory of multi-step nuclear reaction processes was used in our calculation.

The code APOM[2], by which the best neutron optical potential parameters can be searched automatically with fitting experimental total, nonelastic scattering cross sections and elastic scattering angular distributions of $n+^{182,184,186,Nat}W$ reactions, were used to obtain a set of optimum neutron optical potential parameters for W. The optical potential parameters for particles p, α, ^3He, d and t were taken from the Ref.

[3]. A set of optimum neutron optical potential parameters of W is as follows:

$V = 54.5971+0.1085E-0.0219E^2-24(N-Z)/A$
$W_s = \max\{0.0, 7.8227-0.3482E-12(N-Z)/A\}$
$W_v = \max\{0.0, -0.0152+0.1508E-0.0007E^2\}$
$U_{SO} = 6.2$
$r_r = 1.1584, \quad r_s = 1.3877, \quad r_v = 1.6462, \quad r_{SO} = 1.1584$
$a_r = 0.5001, \quad a_s = 0.5609, \quad a_v = 0.8661, \quad a_{SO} = 0.5001$

The giant resonance parameters of gamma were adjusted automatically with the code GUNF[4] by fitting the experimental data of absorption cross sections of $\gamma+^{182,184,186}W$ reactions. The parameters are given in Table 1.

Table 1 The giant resonance parameters of gamma for W

σ_1^{E1} (b)	0.0098	σ_2^{E1} (b)	0.0068	σ^{E2} (b)	0.02552
Γ_1^{E1} (MeV)	3.9	Γ_2^{E1} (MeV)	4.36	Γ^{E2} (MeV)	2.2505
E_1^{E1} (MeV)	13.16	E_2^{E1} (MeV)	15.68	E^{E2} (MeV)	13.945

The exciton model parameter K was taken as 1200 MeV^3. The discrete level, the pair correction parameter and level density parameters were taken from Chinese Evaluated Nuclear Parameter Library (CENPL).

2 Calculated Results and Analyses

The code GUNF for structural materials with incident photon energies up to 30 MeV was used to calculate all cross section of $\gamma+^{180,182,183,184,186}W$ reactions.

The comparison of calculated results with the experimental data for $^{182}W(\gamma, abs)^{182}W$, $^{184}W(\gamma,abs)^{184}W$ and $^{186}W(\gamma,abs)^{186}W$ reactions were given in Ref. [5], respectively. The experimental data were taken from Ref. [6 ~ 8], respectively. Since the absorption cross section are mainly from the (γ,n) reaction for energy E_γ<14 MeV, the experimental data[9] of (γ,n) reaction are considered in analyses of absorption cross section. The calculated results of $^{182}W(\gamma,abs)^{182}W$, $^{184}W(\gamma,abs)^{184}W$ and $^{186}W(\gamma, abs)^{186}W$ reactions are in agreement with the experimental data taken from Ref. [6,7,9]. The comparison of calculated results with experimental data[9,10] for $^{186}W(\gamma,n+np)$ and $^{182,184,186}W(\gamma,n+np+2n)$ reactions shown the calculated results fit the experimental data quite well. The calculated results of $^{186}W(\gamma,3n)^{183}W$ reaction are in agreement with experimental data[9]. There are no experimental data reported up to now for ^{180}W and ^{183}W photonuclear reactions. All of photonuclear cross

sections for ^{180}W, ^{182}W, ^{183}W, ^{184}W and ^{186}W reactions were calculated. The calculated results are available for energy $E_\gamma \leq 30$ MeV.

3 Summary

Based on the experimental data of total, nonelastic scattering cross sections and elastic scattering angular distribution of $n+^{Nat}W$ reaction and absorption cross sections of $\gamma+^{182,184,186}W$ reaction, a set of neutron optical potential parameter and giant resonance parameters of gamma for W were obtained. Then photonuclear reaction data for $^{180,182,183,184,186}W$ were calculated by the code GUNF. Since the calculated results for many channels are in pretty agreement with existed experimental data, the predicted cross sections for which there are no experimental data are reasonable.

References

[1] E. Hayward, "Photonuclear Reactions" NBS MONGRAPH 118, Aug. 1970
[2] Shen Qingbiao, Commu. of Nucl. Data Prog., 7, 43 (1992)
[3] C. M. Perey, F.G. Perey, Atom. Data and Nucl. Data Tables, 17, 1 (1976)
[4] Zhang Jingshang, et al., Commu. of Nucl. Data Prog., 19, 33 (1998)
[5] Yu Baosheng, et al., Commu. of Nucl. Data Prog., 19, 143 (1998)
[6] G. M. Gurevich, et al., Zhur. Eksper. i Teoret. Fiz., Pis'ma v Redakiyu, 23, 411 (1976)
[7] G. M. Gurevich, et al., Nucl. Phys., A351, 257 (1981)
[8] G. M. Gurevich, et al., Zhur. Eksper. i Teoret. Fiz., Pis'ma v Redakiyu, 28, 168 (1978)
[9] B. L. Berman, et al., Phys. Rev., 185, 1576 (1969)
[10] A. M. Goryachev, G. N. Zalesny, EXFOR-M0025, 1978

CN9901214

III DATA EVALUATION

Evaluation of Activation Cross Sections for (n,α) and (n,n'α) Reactions on $^{63,65,Nat}Cu$

Ma Gonggui
(Institute of Nuclear Science and Technology, Sichuan University, Chengdu, 610064)

Introduction

Copper is a very important structure material in nuclear fusion engineering. The neutron activation cross section are very useful in fusion research and other applications such as radiation safety, environmental, material damage and neutron dosimetry. More efforts are required to identify and resolve the differences and discrepancies in the existing activation cross sections from different laboratories.

The natural copper consists of two stable isotopes, i.e. ^{63}Cu, ^{65}Cu. Their abundaces and threshold energies are given in Table 1.

Table 1 Isotopic abundaces and their reaction threshold energies of copper

isotope	(n,α) thresh. / MeV	(n,n'α) thresh. / MeV	abun. / %
^{63}Cu	1.715(Q-Value)	5.869	69.17
^{65}Cu	0.08423	6.876	30.83

The cross sections of (n,α) and (n,n'α) for $^{63,65,Nat}Cu$ are recommended based on the available experimental measured data and theoretically calculated results[1] from threshold up to 20 MeV. The evaluated cross sections are given in Figs. 1 ~ 6 with experimental data and compared with other evaluated data. The present work was done for CENDL-3.

1 $^{63}Cu(n,\alpha)^{60}Co$ Reaction

The experimental data were measured by Majdeddin(97), Lu Halin(91), Meadows(91), Csikai(91), Ikeda(91), Wang Yongchang(90), Greenwood(85), Winkler(80), Garuska(80), Artem(80), Paulsen(67), and Cserpak(94)[2~13] in the energy range from threshold up to 20.0 MeV, respectively. The evaluated data were

obtained by fitting experimental data from threshold energy to 20.0 MeV. The comparison of experimental data with evaluated ones is shown in Fig.1.

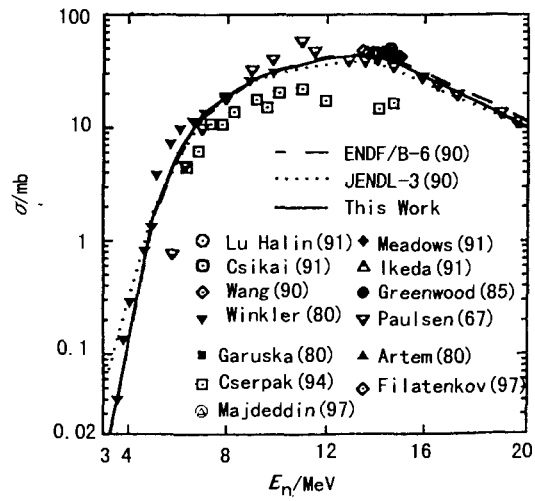

Fig. 1 (n,α) cross section for ^{63}Cu

2 $^{65}Cu(n,\alpha)^{62}Co$ Reaction

The experimental data were measured by Majdeddin(97), Molla(94), Cserpak(94), Gruzdevich(93), Mclane(88) and Clator(69)[14~17] from 6.32 to 16.7 MeV, respectively. The evaluated data were obtained by fitting experimental data from threshold energy to 14.0 MeV. Above 14.0MeV, the recommended data were taken from calculated result, and normalized to the fitting experimental datum of 11.6 mb at 14.0 MeV. The evaluated results are shown in Fig. 2.

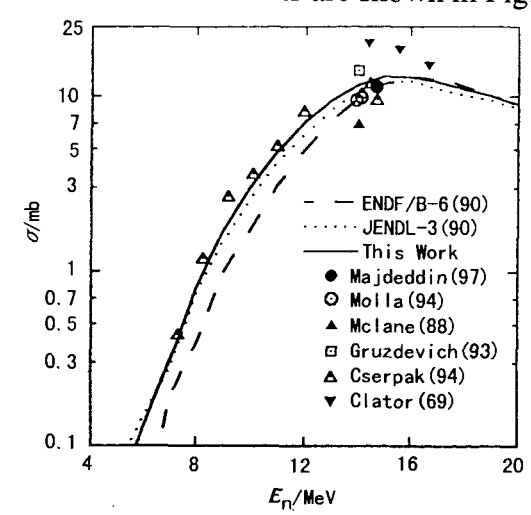

Fig. 2 (n,α) cross section for ^{65}Cu

3 $^{63}Cu(n,n'\alpha)^{59}Co$ Reaction

For (n,n'α) reaction, the recommended data were taken from calculated result due to lack of the experimental data(see Fig. 3).

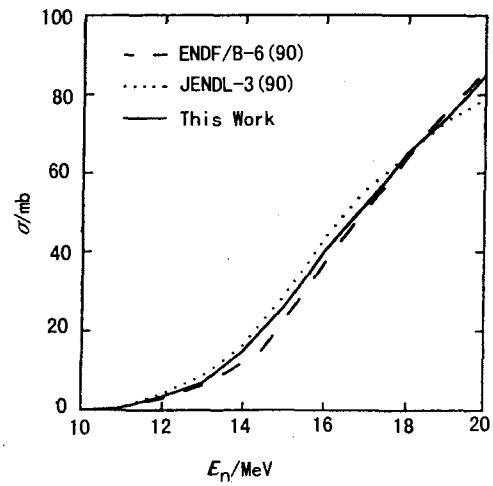

Fig. 3 (n,n'α) cross section for ^{63}Cu

4 $^{65}Cu(n,n'\alpha)^{61}Co$ Reaction

The experimental data were measured by Ryves(78), Qaim(74), Santry(65), Bramlitt(63) and Kantele(62)[18-22] from 13.58 to 19.8 MeV. The evaluated data were obtained by fitting experimental data from threshold energy to 20.0 MeV. The comparison of experimental data with evaluated ones is shown in Fig. 4.

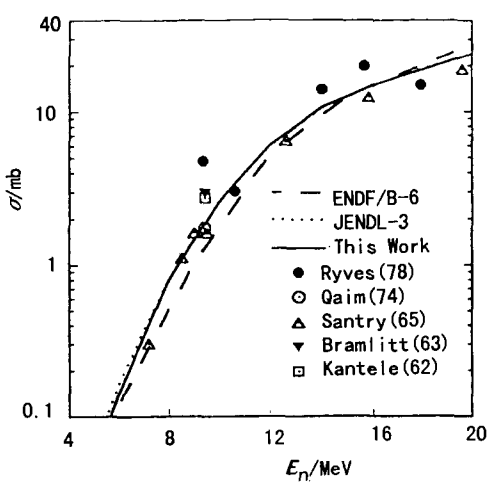

Fig. 4 (n,n'α) cross section for ^{65}Cu

5 The (n, α) and (n,n'α) Reaction for Natural Copper

For (n, α) reaction, there is only a datum measured by Majdeddin(97) at 14.7 MeV. For (n,n'α) reaction, there are no experimental data. The recommended data were obtained from summing the isotopic data weighted by the abundance. The comparison of other evaluated data with present evaluated data is shown in Figs. 5 ~ 6.

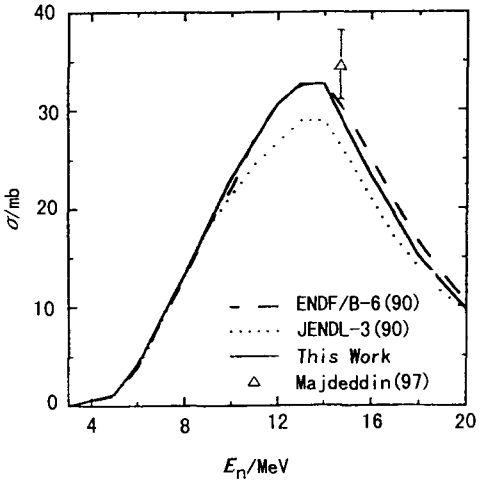

Fig. 5 (n,α) cross section for ^{Nat}Cu

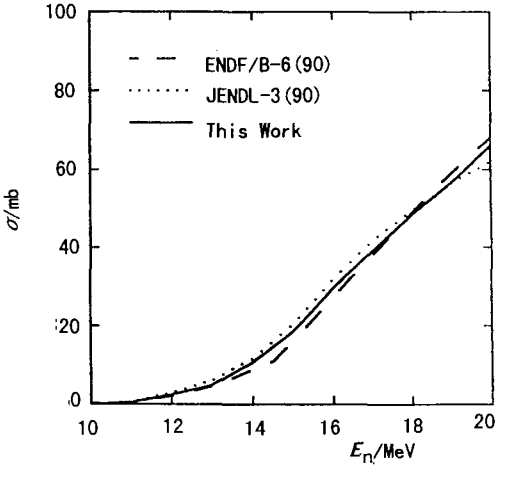

Fig. 6 (n,n'α) cross section for ^{Nat}Cu

6 Summary

The $^{63,65,Nat}Cu(n,\alpha)$ and $(n,n'\alpha)$ cross sections below 20.0 MeV were evaluated and compared with ENDF/B-6 and JEENDL-3. It was shown that our results have improved representation of experimental data.

Acknowledgement

The authors would like to thank Dr. Yu Baosheng for helpful discussion and suggestions.

References

[1] Zhang Jingshang. Nucl. Sci. Eng., 114, 55 (1993)
[2] A. D. Majdeddin et al., INDC(HUN)-031 (1997)
[3] Lu Hanlin et al., CNDP, No. 13, 80 (1995)
[4] J. W. Meadows et al., INDC(NDS)-286 (1993)
[5] J. Csikai et al., INDC-263-9 (1991)
[6] Y. Ikeda et al., INDC-263-9 (1991)
[7] Wang Yongchang et al., J. of Chinese High Ener. Phys. and Nucl. Phys., 14, 919 (1990)
[8] L. R. Greenwood et al., DOE-ER-006-21 (1985)
[9] G. Winkler et al., Nucl. Sci. Eng., 76, 30 (1980)
[10] U. Garuska et al., EXFOR Data No. 30553004 (1980)
[11] O. I. Artem et al., Atomic Energy, 49, 195 (1980)
[12] A. Paulsen et al., EXFOR Data No. 20388004 (1967)
[13] F. Cserpak et al., Phys. Rev., C49, 1525 (1994)
[14] N. I. Molla et al., Proc. of Conf. on Nucl. Data for Sci. And Tech., 2, 938 (1994) Gatlinburg, U. S. A.
[15] O. T. Gruzdevich et al., Ins. of Phys. and Power Eng., Obninsk, Russia (1993)
[16] V. Mclane et al., Neutron Cross Sections, Vol. 2, Boston (1988)
[17] Clator et al., Da/B 30, 2850; EXFOR Data No. 11536005 (1969)
[18] Ryves et al., NET 14 (3), 127 (1978)
[19] S. M. Qaim et al., EUR-5182E, 939(1974)
[20] D. C. Santry et al., Canadian Journal of Physics, 44, 1183 (1965)
[21] Bramlitt et al., Phys. Rev., 131, 2649 (1963)
[22] Kantele et al., Nucl. Phys., 35, 353 (1962)

CN9901215

Evaluation and Calculation of Photonuclear Reaction Data for ^{51}V below 30 MeV

Yu Baosheng Han Yinlu Zhang Jingshang
(China Nuclear Data Center, CIAE)

Introduction

Vanadium is a very important structure material in nuclear reactor engineering. The photonuclear cross sections of vanadium up to 30 MeV are concerned in radiation induced material damage, radiation safety, reactor dosimetry etc.

In this work, the experimental data of photonuclear reactions for ^{51}V were evaluated, and theoretical calculations were carried out. The recommended photonuclear data for ^{51}V were obtained on the basis of evaluated and calculated data, and compared with existing measured data.

1 Evaluation and Analysis of Experimental Data

The vanadium is an existing alone element in natural and its abundance of isotope ^{51}V is 100%. In the present work, evaluated photonuclear reactions cross sections are as follows: $^{51}V(\gamma,ABS)$, $^{51}V(\gamma,n)+(\gamma,n+p)$, $^{51}V(\gamma,2n)+(\gamma,2n+p)$, $^{51}V(\gamma.3n)$, $(\gamma,n+p)$, $(\gamma,n+\alpha)$,$(\gamma,2n)$, $(\gamma,3n)$, (γ,p), (γ,d), (γ,t), $(\gamma,^3He)$, (γ,α) and the double differential cross sections of $(\gamma,2n)$, $(\gamma,3n)$, $(\gamma,n+p)$, $(\gamma,n+\alpha)$ and $(\gamma,n'_{continue})$.

The experimental data of photonuclear reaction for vanadium sample up to 1998 from EXFOR master files were collected and analyzed. The available experimental data[1~3] for photonuclear reaction cross sections of ^{51}V are shown in Table 1. There are 3 groups of measured photonuclear reaction data from threshold to 28 MeV.

The photonuclear cross sections for $^{51}V(\gamma,n)+(\gamma,n+p)$, $(\gamma,2n)+(\gamma,2n+p)$ and $(\gamma,n)+(\gamma,n+p)+(\gamma,2n)+(\gamma,3n)$ reactions were firstly measured by S. C. Fultz[1] in gamma energy region of 10.3 ~ 27.8, 19.8 ~ 27.8 and 10.3 ~ 27.8 MeV, respectively in1962. In the measurement of S. C. Fultz[1], a xenon-filled transmission ionization chamber located between the photon collimator and sample was used and calibrated by a NaI(Tl) gamma-ray spectrometer, which was used to accurately monitor the photon flux. The photon beam energy collimated were determined by means of NaI γ-ray spectrometer which was located after neutron detector system. In the giant-resonance region, the photon energy resolution for ^{51}V is about 3% (10 to 27 MeV). The vanadium sample was used, the attenuation of photon flux in the sample was taken

into accounted and the necessary corrections were made. The neutron emitted by the sample were detected using 4π paraffin moderator neutron detector which consists of 24 BF_3 proportional counters. The obvious structure of photonuclear cross sections can be observed in measured data corresponding to (γ,n)+(γ,n+p), (γ,2n)+(γ,2n+p) reactions.

Table 1 Collected data of photonuclear reactions for ^{51}V

Year	Author	E_0/MeV	Sample	Detector	Reactions	Comment
1962	S. C. Fultz	10.3 to 27.8	^{51}V	PROPC*	(γ,n)+(γ,n+p)	
		19.8 to 27.8	^{51}V	PROPC	(γ,2n)+(γ,2n+p)	
		10.3 to 27.8	^{51}V	PROPC	(γ,n)+(γ,n+p)+ (γ,2n)+(γ,3n)	
1974	A. Veyssiere	13.2 to 27.8	^{51}V	STANK**	(γ,n)+(γ,n+p)	
		20.3 to 27.8	^{51}V	STANK	(γ,2n)	
		13.2 to 27.8	^{51}V	STANK	(γ,n)+(γ,n+p)+ 2(γ,2n)	
1976	A. S. Danagulyan	3.5	^{51}V	Ge(Li)	$^{51}V(\gamma,X)^{24}Na$	Activatin Method

* PROPC: Paraffin moderator with BF_3 counters

** STANK: Gd - loaded liquid scintillator tank

The second measurement of photonuclear cross sections for ^{51}V was performed by A. Veyssiere[2] using the improved Ga-loaded liquid scintillation tank with vanadium metal sample in gamma energy region between 13.2 ~ 27.8 MeV in1974. In order to improve the disadvantage of insufficient signal to noise ratio the STANK method was adopted. In the improved apparatus, two NaI crystal were used in coincidence for detecting annihilation radiation, together with some considerations on the optimal signal to noise ration, the neutron background were reduced. The measured data were corrected for pile up in the detector, the neutron detector efficiency, the photon beam attenuation in the sample, etc.. The experimental results were also improved compared with the previous work.

The results measured by A. Veyssiere[2] for the (γ,n)+(γ,n+p) reactions were compared with the ones of S. C. Fultz[1], seeing Fig.1. There are no great differences, the only exception is that the position of giant resonance peak measured by A. Veyssiere[2] is slightly higher than the one measured by S. C. Fultz[1] around 19 MeV. But the fact is that the errors of the measured data by A. Veyssiere[2] gave the statistical errors only, when the systematical errors were added, the data measured by A. Veyssiere[2] will be in a very good agreement with the data measured by S. C. Fultz[1] within errors. For ^{51}V(γ,2n)+(γ,2n+p) reactions, the data measured by A. Veyssiere[2] were lower than the ones given by S. C. Fultz[1], because the^{51}V(γ,2n+p)

reaction is not included in the data measured by A. Veyssiere[2]. The threshold energy for $^{51}V(\gamma,2n+p)$ reaction is 20.25 MeV. The comparison between both measured data[1,2] is shown Fig. 2.

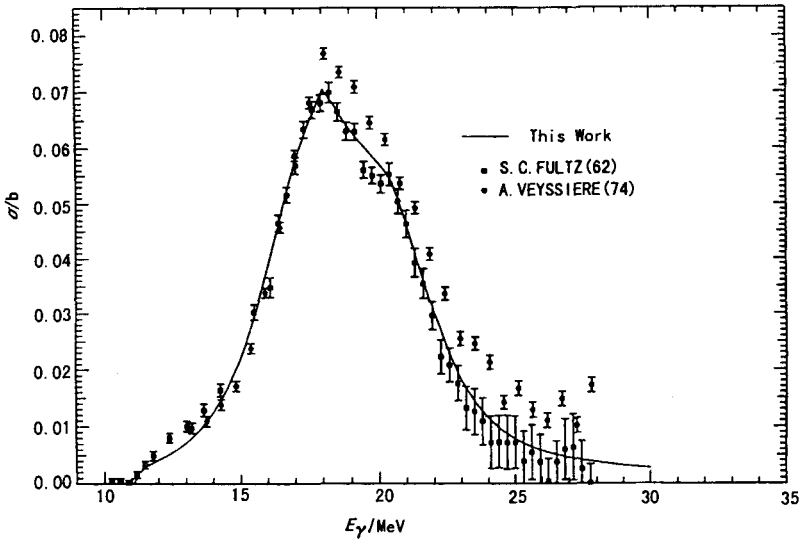

Fig. 1 The comparison of calculated results with experimental data for $^{51}V(\gamma,n+(n+p))$ reactions

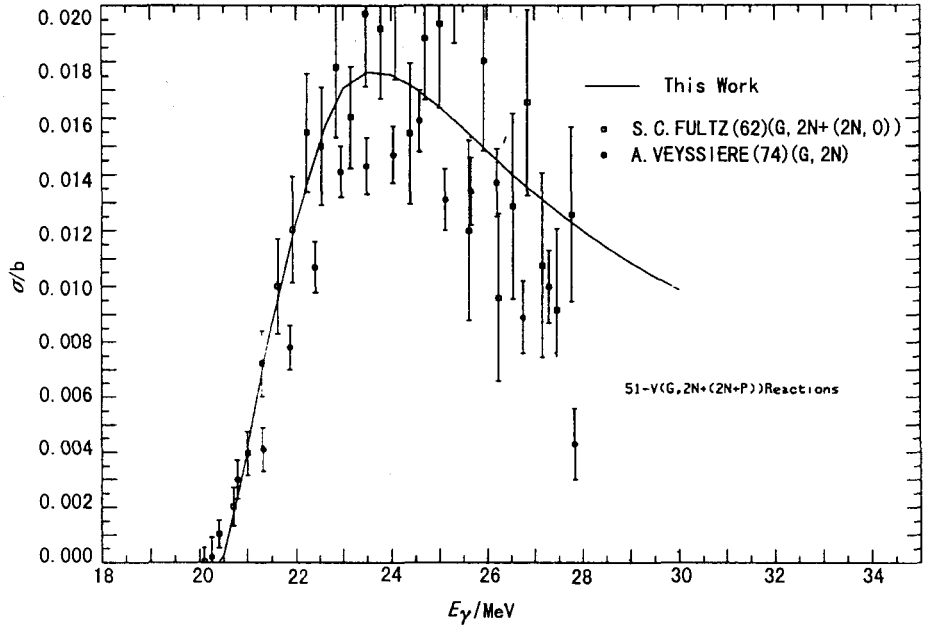

Fig. 2 The comparison of calculated results with experimental data for $^{51}V(\gamma,2n+(2n+p))$reactions

The photoabsorption cross section is the sum of $(\gamma,n)+(\gamma,n+p)+(\gamma,2n)+(\gamma,2n+p)+(\gamma,3n)$. The threshold energy for $^{51}V(\gamma,3n)$ is 31.9 MeV. Meanwhile the $(\gamma,2n+p)$ reaction is much lower than the $(\gamma,2n)$, photoabsorption cross section are

mainly from the contributions of (γ,n)+(γ,n+p)+(γ,2n). Therefore, the data measured by S. C. Fultz[1] were accepted as the photoabsorption cross section below 28 MeV, and are shown in Fig. 3.

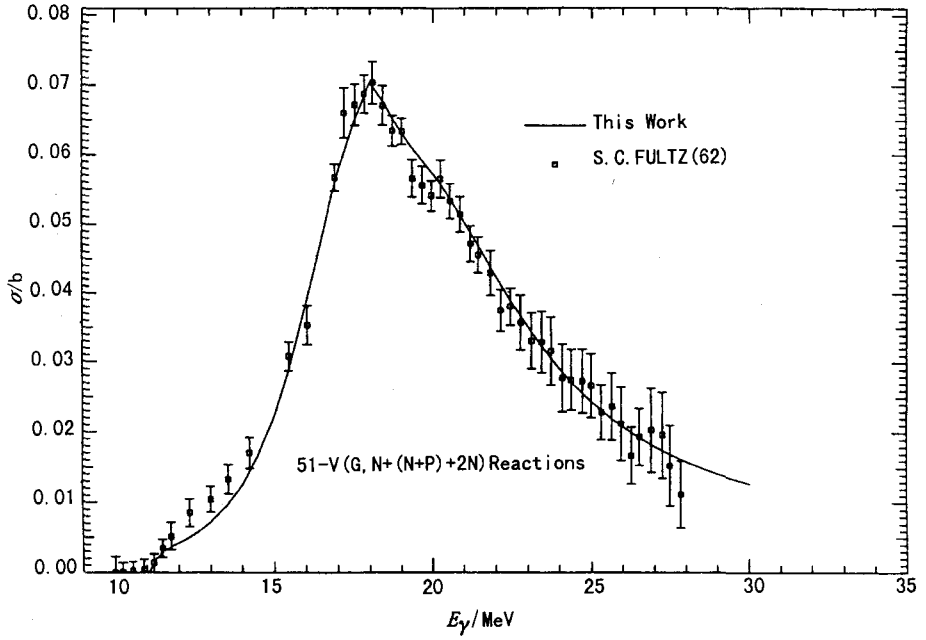

Fig. 3 The comparison of calculated results with experimental data for ^{51}V(γ,n+(n+p)+2n) reactions

The sum of photonuclear (γ,n)+(γ,n+p)+2(γ,2n) cross sections measured by S. C. Fultz[1] and A. Veyssiere[2] are in agreement with each other within errors. They are shown in Fig. 4.

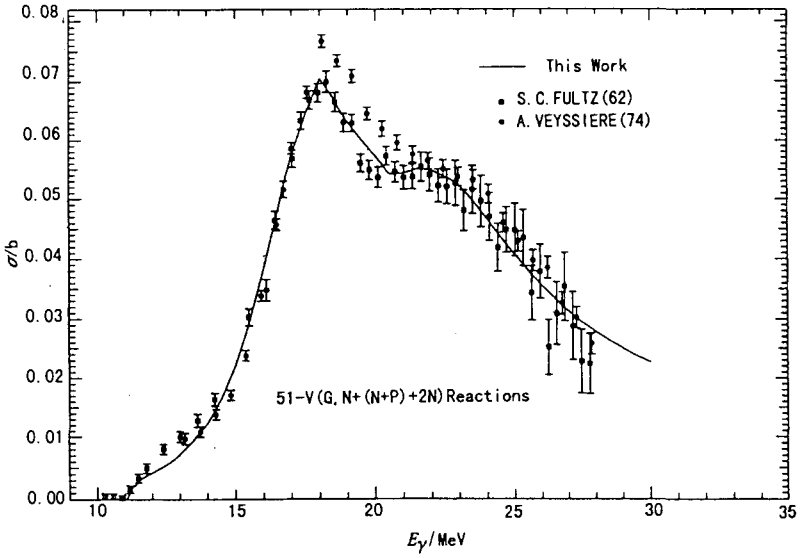

Fig. 4 The comparison of calculated results with experimental data for ^{51}V(γ,n+(n+p)+2(2n)) reactions

2 Theoretical Calculation and Recommendation

Based on the evaluation mentioned above, the theoretical calculation was used to fit the adopted experimental data[1,2]. In order to calculate the photonuclear reactions for vanadium, the spherical optical model, the semi-classical theory of multi-step nuclear reaction processes were used.

The code APOM[4] by which the best neutron optical potential parameters can be searched automatically with fitting experimental total and nonelastic scattering cross sections and elastic scattering angular distributions of n+^{51}V reaction, was used to obtain a set of optimum neutron optical potential parameters for *V*. They are as follows:

$V = 54.8195 - 0.2451E + 0.003577E^2 - 24(N-Z)/A$

$W_s = \max\{0.0,\ 9.2514 - 0.3141E - 12(N-Z)/A\}$

$W_v = \max\{0.0,\ -1.6464 + 0.1645E - 0.0005580E^2\}$

$U_{SO} = 6.2$

$r_r = 1.1439,\quad r_s = 1.1457,\quad r_v = 1.3879,\quad r_{SO} = 1.1439$

$a_r = 0.7367,\quad a_s = 0.5488,\quad a_v = 0.6450,\quad a_{SO} = 0.7367$

The optical potential parameters for particles p, α, He^3, d and t were taken from the Ref. [5]. The giant resonance parameters of gamma were adjusted automatically with the code GUNF[6] by fitting the experimental data of cross sections of ^{51}V(γ,n+np),^{51}V(γ,2n) and ^{51}V(γ,n+np+2(2n)) reaction. The parameters are given in Table 2.

Table 2 The giant resonance parameters of gamma for ^{51}V

σ_1^{E1} / b	0.0465	σ_2^{E1} / b	0.027001	σ^{E2} / b	0.030917
$\Gamma_1^{E_1}$ / MeV	6.090617	$\Gamma_2^{E_1}$ / MeV	9.833399	Γ^{E_2} / MeV	0.867939
$\Gamma_1^{E_1}$ / MeV	18.041727	$\Gamma_2^{E_1}$ / MeV	21.492451	Γ^{E_2} /MeV	18.082096

The exciton model parameter *K* was taken as 1900 MeV. The discrete level, the pair correction parameter and level density parameters were taken from Chinese Evaluated Nuclear Parameter Library (CENPL).

The total photoneutron cross section was a sum of the photoneutron excitation state, which were from ground state to the highest state and continuum state. The level scheme used for theoretical calculation are taken from CENPL. The continuum levels were assumed above1.7002 MeV for ^{51}V.

The cross sections of photonuclear reactions were calculated from threshold to 30 MeV. The theoretical calculated values are almost overlapped with the experimental

data and are shown in Figs. 1 ~ 4. Because the calculated data for photonuclear reactions channels are in pretty agreement with existing experimental data, the predicted cross sections that there are no any experimental data are reasonable.

For $^{51}V(\gamma,x)$ reactions, there are no any experimental data with the exception of data[3] for $^{51}V(\gamma,x)^{24}Na$ reaction. Therefore, the changed particle emission cross sections for $^{51}V(\gamma,p)$, (γ,d), (γ,t), $(\gamma,^3He)$, (γ,α) need to be calculated theoretically.

The pertinent calculations have already performed using GUNF Code[6]. In the present work, the recommended cross sections for ^{51}V reactions from threshold to 30 MeV are given and shown in Fig. 5.

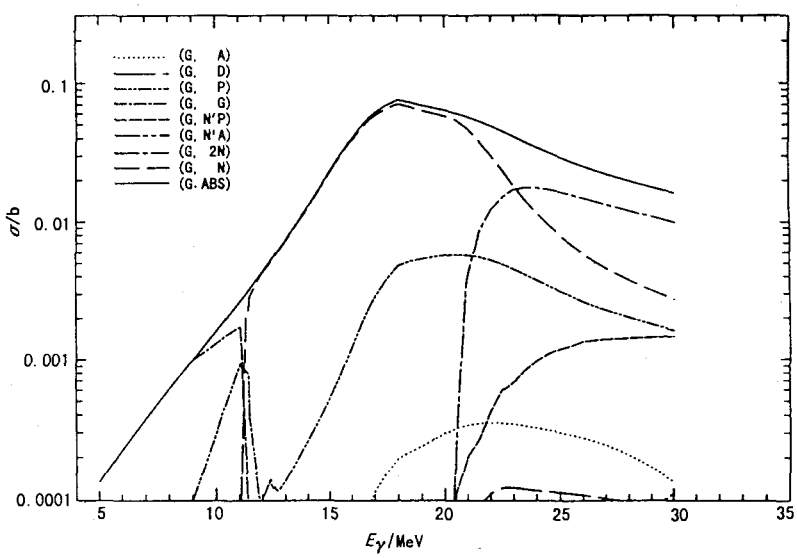

Fig. 5 The recommended photonuclear reactions data for ^{51}V

For the photonuclear double differential cross sections of V, the experimental data are very scarce. Therefore, the theoretical calculations are completely taken as the recommended data. The evaluation cross sections of photonuclear double differential cross sections for vanadium were obtained after testing other available experimental data, such as (γ,n), $(\gamma,2n)$, $(\gamma,2n+p)$, etc..

3 Summary

The cross sections of photonuclear reactions for ^{51}V have been evaluated and calculated. The recommended values were compared with experimental data below 30 MeV. It is shown that our results could reproduce experimental data very well. Therefore the predicted photonuclear reaction data for those are deficient in experimental ones are reasonable.

Acknowledgments

The authors are indebted to IAEA (International Atomic Energy Agency) for its supports. And many thanks to Drs. Oblozinsky, T. Benson and O. Schwerer for their kind helps and suggestions.

References

[1] S. C. Fultz et al., Phys. Rew., 128, 2345 (1962)
[2] A. Veyssiere et al., Nucl. Phy./A, 227, 513 (1974)
[3] A. S. Danagulyan et al., J. YF, 285, 482 (1977)
[4] Shen Qingbiao, CNDP, 7, 43 (1992)
[5] C. M. Perey, F. G. Perey, Atom. Data and Nucl. Data Tables, 17, 1 (1976)
[6] Zhang Jingshang et al., CNDP, 19, 33 (1998)

CN9901216

The Evaluation of Fission Product Yields for ^{238}U Fission

Liang Qichang Liu Tingjin
(China Nuclear Data Center, CIAE)

Introduction

In the basic research of fission process and application of nuclear industry, the fission product yields data have great significance, for example, in the reactor physics the fission yield data are widely used in the calculation of decay heat, burn-up determination, and dosimetry, transmutation studies, fuel handling, waste disposal, and safety prediction etc.

In this paper, the cumulative fission yields for 45 fission product nuclides of ^{238}U fission induced by neutron of fast reactor spectrum and high energy (around 14.0 MeV) neutron have been evaluated and compared with the main fission yield libraries in the world.

1 The Evaluation Method

1.1 Experimental Data Collection

All experimental data available up to now were collected, most of them were

obtained from the EXFOR master data library, some were taken from the China measured data, and some were also collected from the publications concerned.

1.2 Data Selection

The EXFOR BIB information and papers concerned were read carefully and analysed in physics, the data were adopted or abandoned according to the measured data, method, facility, detector, monitor, data error and discrepancy situation compared with others.

1.3 Error Adjusting

Experimentalists reported the errors in their papers in different ways, some experimental data even no errors were given, so the reported errors in the papers sometimes should be adjusted to a reasonable level, the different adjusting limits are set according to different measurement techniques.

1.4 Data Correction

The data were corrected if necessary by using new reference data including the standard fission yields, gamma intensity, fission cross section, and other standard cross sections used for neutron flux monitor such as Al(n,α) cross section, etc.

1.5 Data Processing

After making the selection, analysis and correction of the experimental data as mentioned above, then the data processing were made with two ways:

(1) Data Average

If there are only the absolute yields and several measurement data sets at the same incident neutron energy, for the same target and product nuclide, the weighted means yield was calculated by using the code AVERAG[1].

(2) Simultaneous Evaluation

If there are several absolute fission yields and their ratio measurements for some product nuclides at the same energy and target, in order to advoid the introduction of other 'standards', the simultaneous evaluation were made by using the code ZOTT[1], with this code, not only the optimum fission yields and ratios, but also their

covariance matrix can be calculated.

2 The results and comparison

The 68 cumulative fission yields (including fast reactor spectrum(F) and around 14 MeV energy(H)) for 45 product nuclides have been evaluated, the results are given in Table 1.

Table 1 The results of evaluation for some fission yields from ^{238}U fission

Nuclide	E_n	FY	Error	Data Sets*	Processed
^{66}Ni	F	3.9710E−06	1.6000E−06	1	
^{67}Cu	F	2.2980E−05	9.3000E−06	1	
	H	1.4838E−04	4.0000E−05	1	
^{72}Zn	F	6.4770E−05	2.5000E−05	1	
	H	3.1795E−03	4.0000E−04	1	
^{85}Kr	F	1.6600E−01	1.2000E−02	1	
	H	2.5290E−01	2.1000E−02	2	A
^{85m}Kr	F	7.4250E−01	2.8100E−02	2	A
	H	1.0820E+00	2.9000E−02	7	A
^{85}Br	F	7.4000E−01	1.0000E−02	1	
^{87}Kr	F	1.6030E+00	4.7400E−02	2	A
	H	1.7325E+00	6.4400E−02	4	A
^{87}Br	F	2.0200E+00	1.8000E−01	1	
^{87}Se	F	9.2788E−01	2.5053E−01	#	
^{88}Kr	F	2.0180E+00	9.6300E−02	3	A
	H	2.0253E+00	6.8000E−02	7	A
^{88}Br	H	1.9000E+00	3.7000E−01	1	
^{89}Br	H	1.1900E+00	2.0000E−01	1	
^{91}Y	F	3.9594E+00	7.8941E−02	2(2)	A S
	H	3.7723E+00	8.6100E−02	7	A
^{91}Sr	F	3.9231E+00	2.9650E−01	1	
^{91}Kr	F	3.3931E+00	1.6970E−01	1	
^{93}Y	F	5.0492E+00	2.1195E−01	1(1)	S
^{95}Zr	F	5.1438E+00	5.6800E−02	9	A
	H	4.9197E+00	6.7100E−02	13	A
^{99}Mo	F	6.1403E+00	1.9020E−01	4	A
	H	5.6423E+00	7.2800E−02	14	A
^{101}Mo	F	6.3298E+00	3.7430E−01	2	A
^{105}Rh	F	3.9059E+00	8.1867E−02	1(3)	A S
	H	3.2895E+00	5.4200E−02	8	A
^{109}Pd	F	1.5397E−01	2.5665E−02	2(1)	A S
^{111}Ag	F	6.9142E−02	3.0296E−03	3(1)	A S
	H	1.0477E+00	2.2800E−02	7	A
^{112}Pd	F	5.9151E−02	3.4672E−03	2(1)	A S
^{113}Ag	F	2.5000E−02	7.0000E−03	1	
^{115m}Cd	F	2.5790E−03	3.1000E−04	1	
	H	6.7700E−02	9.7000E−03	2	A

Table 1 Contin.

Nuclide	E_n	FY	Error	Data Sets*	Processed
^{121}Sn	F	2.5532E-02	5.2632E-03	1(1)	S
^{125}Sb	F	4.9220E-02	2.0310E-02	2	A
	H	1.2771E+00	7.1800E-02	2	A
^{126}Sb	H	2.5000E-01	1.0000E-02	1	
^{127}Sb	F	1.5761E-01	7.0481E-03	2(3)	A S
^{131m}Te	H	4.7724E-01	3.3671E-02	1(1)	S
^{131}I	F	3.2193E+00	3.4200E-02	12	A
	H	3.8538E+00	6.7381E-02	5(2)	A S
^{133}Xe	F	6.5664E+00	1.8590E-01	3	A
	H	6.0094E+00	1.1490E-01	6	A
^{134}Xe	F	7.5977E+00	3.2390E-01	3	A
	H	6.4616E+00	1.0870E-01	4	A
^{135m}Xe	F	1.0780E+00	2.1560E-01	#	
^{137}I	F	6.0000E+00	1.0000E+00	1	
	H	3.2800E+00	6.6000E-01	1	
^{140}Xe	H	2.8412E+00	5.6900E-02	3	A
^{141}Xe	F	3.0952E+00	1.1140E-01	1	
	H	1.2963E+00	3.9900E-02	3	A
^{143}Xe	F	3.9900E-01	4.9900E-02	1	
^{144}Xe	F	1.2734E-01	1.7800E-02	1	
^{144}Ce	F	4.5493E+00	8.4700E-02	7	A
	H	3.7165E+00	8.6800E-02	9	A
^{147}Nd	F	2.5867E+00	5.7200E-02	5	A
	H	2.0878E+00	3.3800E-02	12	A
^{148}Nd	F	2.1015E+00	1.8580E-02	3(1)	A S
	H	1.6000E+00	9.0000E-02	1	
^{156}Eu	F	6.7100E-02	2.1000E-03	3	A
	H	1.0900E-01	2.9000E-03	8	A
^{157}Eu	H	8.4144E-02	7.3410E-03	2	A
^{161}Tb	F	1.1436E-03	9.0000E-05	3	A
	H	8.2450E-03	5.0500E-04	2	A

Meaning of the symbol in the table:

* Number of data sets adopted in present evaluation, in the simultaneous evaluation case, it shows the number of absolutely measured data sets, and the number of measured ratio sets in parentheses ( ).

A Average with weight

S Simultaneous evaluation

F Fast reactor spectrum average

H High energy (around 14 MeV)

\# Model calculation

The present results were compared with the ENDF/B-6, JENDL-3/FY, CENDL-FY(86), and JEF-2/FY as shown in Table 2. It was found that in the total 68 evaluated values, 50(73.5% of total), 4(5.9%), 2(2.9%), and 4(5.9%) values of present evaluation are difference less than 7% with ENDF/B-6, JENDL-3/FY, CENDL-FY(87), and JEF-2/FY, respectively, that means the most of present results (88 percent in total) are in agreement with at least one of the main libraries within the quoted error limits. For the rest, i.e. ^{85}Kr(F), ^{87}Br(F), ^{88}Br(H), ^{89}Br(H), ^{109}Pd(F),

^{113}Ag(F), ^{121}Sn(F), and ^{131m}Te(H), present results are different more than at least 9% with other libraries, since these fission yields have only one or two experimental data as shown in Table 1. The results are less reliable, in this case, if present results are between the values of other libraries, they were recommended. ^{85}Kr(F), ^{109}Pd(F), and ^{131m}Te(H) are in the case, the others, i.e. ^{87}Br(F), ^{88}Br(H), ^{89}Br(H), ^{113}Ag(F), and ^{121}Sn(F) are obviously larger or smaller than those of all other libraries, so they are not recommended and only for reference. The differences (present value minus other library divided by present value) between present results and ENDF/B-6 are also given in Table 2.

Table 2 Comparison of present evaluated fission yields for ^{238}U with the main libraries

Nuclide	Libraries	F	H	D(F)	D(H)
^{66}Ni	This work	3.9710E−06		+6.57	
	ENDF/B-6	3.7100E−06			
	JENDL-3/FY	1.7495E−08			
	CENDL-FY(87)	3.9118E−06			
	JEF-2/FY	4.0088E−06			
^{67}Cu	This work	2.2980E−05	1.4838E−04	+6.44	+6.32
	ENDF/B-6	2.1500E−05	1.3900E−04		
	JENDL-3/FY	6.0617E−08	1.3992E−04		
	CENDL-FY(87)	2.2573E−05	1.3818E−04		
	JEF-2/FY	7.0495E−06	1.4015E−04		
^{72}Zn	This work	6.4770E−05	3.1795E−03	+6.59	+15.18
	ENDF/B-6	6.0500E−05	2.6970E−03		
	JENDL-3/FY	9.3144E−06	3.0202E−03		
	CENDL-FY(87)	6.3678E−05	2.9719E−03		
	JEF-2/FY	6.5347E−05	2.9965E−03		
^{85}Kr	This work	1.6600E−01	2.5290E−01	+10.48	+19.51
	ENDF/B-6	1.4861E−01	2.0357E−01		
	JENDL-3/FY	1.4011E−01	1.8720E−01		
	CENDL-FY(87)	1.4888E−01	2.5149E−01		
	JEF-2/FY	1.9599E−01	2.2915E−01		
^{85m}Kr	This work	7.4250E−01	1.0820E+00	−0.05	+7.33
	ENDF/B-6	7.4286E−01	1.0027E+00		
	JENDL-3/FY	6.5750E−01	8.7676E−01		
	CENDL-FY(87)	7.2019E−01	9.8375E−01		
	JEF-2/FY	9.1323E−01	1.0564E+00		
^{85}Br	This work	7.4000E−01		−0.38	
	ENDF/B-6	7.4282E−01			
	JENDL-3/FY	6.5864E−01			
	CENDL-FY(87)	7.1224E−01			
	JEF-2/FY	9.1553E−01			
^{87}Kr	This work	1.6030E+00	1.7325E+00	−1.40	+2.77
	ENDF/B-6	1.6254E+00	1.6845E+00		
	JENDL-3/FY	1.5879E+00	1.6630E+00		
	CENDL-FY(87)	1.4542E+00	1.6621E+00		

Table 2 Contin.

Nuclide	Libraries	F	H	D(F)	D(H)
	JEF-2/FY	1.5244E+00	1.8393E+00		
^{87}Br	This work	2.0200E+00		+23.90	
	ENDF/B-6	1.5372E+00			
	JENDL-3/FY	1.4766E+00			
	CENDL-FY(87)	1.3087E+00			
	JEF-2/FY	1.3836E+00			
^{87}Se	This work	*9.2788E–01		+5.60	
	ENDF/B-6	8.7596E–01			
	JENDL-3/FY	9.3769E–01			
	CENDL-FY(87)	1.0528E+00			
	JEF-2/FY	8.2763E–01			
^{88}Kr	This work	2.0180E+00	2.0253E+00	–0.40	–6.68
	ENDF/B-6	2.0260E+00	2.1605E+00		
	JENDL-3/FY	2.0838E+00	2.1978E+00		
	CENDL-FY(87)	2.2416E+00	2.2078E+00		
	JEF-2/FY	2.0820E+00	1.9896E+00		
^{88}Br	This work		1.9000E+00	+21.76	
	ENDF/B-6		1.4865E+00		
	JENDL-3/FY		1.5258E+00		
	CENDL-FY(87)		1.4169E+00		
	JEF-2/FY		1.3923E+00		
^{89}Br	This work		1.1900E+00	–26.00	
	ENDF/B-6		1.4994E+00		
	JENDL-3/FY		1.4669E+00		
	CENDL-FY(87)		1.4164E+00		
	JEF-2/FY		1.2975E+00		
^{91}Y	This work	3.9594E+00	3.7723E+00	–2.02	–2.53
	ENDF/B-6	4.0395E+00	3.8676E+00		
	JENDL-3/FY	4.0454E+00	3.7318E+00		
	CENDL-FY(87)	4.0577E+00	3.7190E+00		
	JEF-2/FY	4.1435E+00	3.7746E+00		
^{91}Sr	This work	3.9231E+00		–2.97	
	ENDF/B-6	4.0395E+00			
	JENDL-3/FY	4.0554E+00			
	CENDL-FY(87)	3.9577E+00			
	JEF-2/FY	4.1434E+00			
^{91}Kr	This work	3.3931E+00		+1.24	
	ENDF/B-6	3.3511E+00			
	JENDL-3/FY	3.7208E+00			
	CENDL-FY(87)	3.3184E+00			
	JEF-2/FY	3.2939E+00			
^{93}Y	This work	5.0492E+00		+2.69	
	ENDF/B-6	4.9133E+00			
	JENDL-3/FY	5.0009E+00			
	CENDL-FY(87)	4.7232E+00			
	JEF-2/FY	5.1687E+00			
^{95}Zr	This work	5.1438E+00	4.9197E+00	+0.06	+0.57

Table 2 Contin.

Nuclide	Libraries	F	H	D(F)	D(H)
	ENDF/B-6	5.1405E+00	4.8918E+00		
	JENDL-3/FY	5.1068E+00	4.9498E+00		
	CENDL-FY(87)	5.2337E+00	4.9230E+00		
	JEF-2/FY	5.1191E+00	4.6828E+00		
^{99}Mo	This work	6.1403E+00	5.6423E+00	−0.45	−1.12
	ENDF/B-6	6.1682E+00	5.7054E+00		
	JENDL-3/FY	6.1957E+00	5.5985E+00		
	CENDL-FY(87)	6.2295E+00	5.6231E+00		
	JEF-2/FY	6.2318E+00	5.7858E+00		
^{101}Mo	This work	6.3298E+00		+1.91	
	ENDF/B-6	6.2090E+00			
	JENDL-3/FY	6.0822E+00			
	CENDL-FY(87)	6.3691E+00			
	JEF-2/FY	6.5230E+00			
^{105}Rh	This work	3.9059E+00	3.2895E+00	−3.72	+2.24
	ENDF/B-6	4.0513E+00	3.2159E+00		
	JENDL-3/FY	3.9393E+00	3.2009E+00		
	CENDL-FY(87)	4.3175E+00	3.2965E+00		
	JEF-2/FY	3.7166E+00	3.1582E+00		
^{109}Pd	This work	1.5397E−01		−63.76	
	ENDF/B-6	2.5214E−01			
	JENDL-3/FY	2.6844E−01			
	CENDL-FY(87)	3.2655E−01			
	JEF-2/FY	1.1380E−01			
^{111}Ag	This work	6.9142E−02	1.0477E+00	−2.69	+5.57
	ENDF/B-6	7.1003E−02	9.8930E−01		
	JENDL-3/FY	7.9966E−02	1.1058E+00		
	CENDL-FY(87)	7.8050E−02	1.0189E+00		
	JEF-2/FY	6.3913E−02	1.0629E+00		
^{112}Pd	This work	5.9151E−02		+5.49	
	ENDF/B-6	5.5901E−02			
	JENDL-3/FY	6.5039E−02			
	CENDL-FY(87)	5.5798E−02			
	JEF-2/FY	5.3244E−02			
^{113}Ag	This work	2.5000E−02		−66.00	
	ENDF/B-6	4.1500E−02			
	JENDL-3/FY	5.2668E−02			
	CENDL-FY(87)	5.8481E−02			
	JEF-2/FY	2.8421E−02			
^{115m}Cd	This work	2.5790E−03	6.7700E−02	−20.59	−4.78
	ENDF/B-6	3.1100E−03	7.0933E−02		
	JENDL-3/FY	2.6874E−03	6.8003E−02		
	CENDL-FY(87)	2.6436E−03	7.0321E−02		
	JEF-2/FY	1.5665E−03	3.4807E−02		
^{121}Sn	This work	2.5532E−02		−43.73	
	ENDF/B-6	3.6696E−02			
	JENDL-3/FY	4.3056E−02			

Table 2 Contin.

Nuclide	Libraries	F	H	D(F)	D(H)
	CENDL-FY(87)	3.9273E−02			
	JEF-2/FY	2.8086E−02			
^{125}Sb	This work	4.9220E−02	1.2771E+00	+1.41	+6.33
	ENDF/B-6	4.8524E−02	1.1963E+00		
	JENDL-3/FY	5.2542E−02	1.2277E+00		
	CENDL-FY(87)	6.5760E−02	1.2172E+00		
	JEF-2/FY	9.6698E−02	1.2785E+00		
^{126}Sb	This work		2.5000E−01		+23.54
	ENDF/B-6		1.9115E−01		
	JENDL-3/FY		2.3244E−01		
	CENDL-FY(87)		1.9571E−01		
	JEF-2/FY		1.9161E−01		
^{127}Sb	This work	1.5761E−01		+13.55	
	ENDF/B-6	1.3625E−01			
	JENDL-3/FY	1.2606E−01			
	CENDL-FY(87)	1.4443E−01			
	JEF-2/FY	1.5850E−01			
^{131m}Te	This work		4.7724E−01		+11.92
	ENDF/B-6		4.2036E−01		
	JENDL-3/FY		6.7930E−01		
	CENDL-FY(87)		4.3177E−01		
	JEF-2/FY		2.6066E−01		
^{131}I	This work	3.2193E+00	3.8538E+00	−2.22	−3.60
	ENDF/B-6	3.2908E+00	3.9925E+00		
	JENDL-3/FY	3.2386E+00	4.0449E+00		
	CENDL-FY(87)	3.1668E+00	3.7999E+00		
	JEF-2/FY	3.3045E+00	3.8261E+00		
^{133}Xe	This work	6.5664E+00	6.0094E+00	−3.0	−0.13
	ENDF/B-6	6.7610E+00	6.0172E+00		
	JENDL-3/FY	6.6062E+00	6.1449E+00		
	CENDL-FY(87)	6.5778E+00	6.8114E+00		
	JEF-2/FY	6.7252E+00	5.7441E+00		
^{134}Xe	This work	7.5977E+00	6.4616E+00	−0.16	+0.13
	ENDF/B-6	7.6095E+00	6.4531E+00		
	JENDL-3/FY	7.7456E+00	6.5541E+00		
	CENDL-FY(87)	7.6589E+00	6.5986E+00		
	JEF-2/FY	7.5447E+00	6.1386E+00		
^{135m}Xe	This work	*1.0780E+00		+3.90	
	ENDF/B-6	1.0360E+00			
	JENDL-3/FY	1.1445E+00			
	CENDL-FY(87)	8.5812E−01			
	JEF-2/FY	1.0278E+00			
^{137}I	This work	6.0000E+00	3.2800E+00	+14.58	+4.84
	ENDF/B-6	5.1250E+00	3.1214E+00		
	JENDL-3/FY	5.3138E+00	3.3321E+00		
	CENDL-FY(87)	4.3613E+00	3.1512E+00		
	JEF-2/FY	5.5738E+00	4.8864E+00		

Table 2 Contin.

Nuclide	Libraries	F	H	D(F)	D(H)
^{140}Xe	This work		2.8412E+00		+3.67
	ENDF/B-6	2.7368E+00			
	JENDL-3/FY	2.8824E+00			
	CENDL-FY(87)	2.8490E+00			
	JEF-2/FY	3.6994E+00			
^{141}Xe	This work	3.0952E+00	1.2963E+00	−3.09	−4.84
	ENDF/B-6	3.1908E+00	1.3591E+00		
	JENDL-3/FY	3.2888E+00	1.4080E+00		
	CENDL-FY(87)	3.1518E+00	1.3322E+00		
	JEF-2/FY	4.0743E+00	2.0750E+00		
^{143}Xe	This work	3.9900E−01		+44.06	
	ENDF/B-6	2.2321E−01			
	JENDL-3/FY	1.0806E−01			
	CENDL-FY(87)	4.0221E−01			
	JEF-2/FY	8.1221E−01			
^{144}Xe	This work	1.2734E−01		+3.68	
	ENDF/B-6	1.2265E−01			
	JENDL-3/FY	1.2705E−01			
	CENDL-FY(87)	1.2477E−01			
	JEF-2/FY	1.8174E−01			
^{144}Ce	This work	4.5493E+00	3.7165E+00	+0.03	−0.17
	ENDF/B-6	4.5480E+00	3.7228E+00		
	JENDL-3/FY	4.5372E+00	3.6402E+00		
	CENDL-FY(87)	4.5835E+00	3.7167E+00		
	JEF-2/FY	4.3996E+00	3.6397E+00		
^{147}Nd	This work	2.5867E+00	2.0878E+00	−0.23	−0.16
	ENDF/B-6	2.5927E+00	2.0911E+00		
	JENDL-3/FY	2.5298E+00	2.0970E+00		
	CENDL-FY(87)	2.6027E+00	2.0835E+00		
	JEF-2/FY	2.6632E+00	2.1715E+00		
^{148}Nd	This work	2.1015E+00	1.6000E+00	−0.52	−8.16
	ENDF/B-6	2.1125E+00	1.7305E+00		
	JENDL-3/FY	2.0816E+00	1.7457E+00		
	CENDL-FY(87)	2.0944E+00	1.7628E+00		
	JEF-2/FY	2.2791E+00	1.6543E+00		
^{156}Eu	This work	6.7100E−02	1.0900E−01	−13.31	−4.93
	ENDF/B-6	7.6030E−02	1.1437E−01		
	JENDL-3/FY	6.7480E−02	1.0798E−01		
	CENDL-FY(87)	7.5270E−02	1.1259E−01		
	JEF-2/FY	6.3160E−02	1.1232E−01		
^{157}Eu	This work		8.4144E−02		+4.51
	ENDF/B-6		8.0347E−02		
	JENDL-3/FY		8.3791E−02		
	CENDL-FY(87)		8.3724E−02		
	JEF-2/FY		6.6064E−02		
^{161}Tb	This work	1.1436E−03	8.2450E−03	−6.24	−2.72
	ENDF/B-6	1.2150E−03	8.4690E−03		
	JENDL-3/FY	1.2798E−03	8.4900E−03		
	CENDL-FY(87)	1.1880E−03	8.7347E−03		
	JEF-2/FY	1.1560E−03	7.8741E−03		

$$*D=\frac{\text{This work}-\text{ENDF/B-6}}{\text{This work}}(\%)$$

Reference

[1] Liu Tingjin, CNDP, 19, 103 (1998)

CN9901217

IV DATA PROCESSING

A Method and Program CABEI for Adjusting Consistency between the Cross Section Data of Natural Element and Its Isotopes

Liu Tingjin Sun Zhengjun
(China Nuclear Data Center, CIAE)

Introduction

To meet the requirement of nuclear engineering, especially nuclear fusion research, now the dada in the major evaluated libraries, such as ENDF/B-6, JENDL-3.2, JEF-2.2, BROND-2.1 and CENDL-2.1, are given not only for natural elements, but also their isotopes. It is clear that these data must be consistent in physics. Unfortunately, it is not the case, the data in the libraries usually do not satisfy the consistent relationship. Inconsistency between element and its isotopes data is one major problems in present evaluated neutron libraries[1]. So far, the data in the libraries are given, in most cases, only for natural elements or isotopes, not for both, to avoid this problem.

As well known, the complete data must be consistent for each nuclide itself, such as total cross section equals the sum of elastic and noelastic cross section, nonelastic cross section equals the sum of all partial cross section except elastic cross section, and total inelastic cross section equals the sum of the cross sections of inelastic scattering to discrete and continuous states etc. The consistence between natural element and its isotopes makes the data must satisfy two kinds of consistent relationships at the same time, this is the key point and main difficulty for this kind adjustment.

1 Adjust Method and Formulas

Let σ_{ij} express the cross section of j-th reaction for i-th isotope, σ_{i0} express the 'total' cross sections for i-th isotope, σ_{0j} express the cross section of j-th reaction for natural element, and σ_{00} is the 'total' cross section of natural element. Suppose σ' is the cross section to be adjusted, and σ is one adjusted, so that

$$\sigma_{0j} = \sum_{i=1}^{I} A_i \sigma_{ij} \tag{1}$$

$$\sigma_{i0} = \sum_{j=1}^{J} \sigma_{ij} \tag{2}$$

$$\sigma_{00} = \sum_{j=1}^{J} \sigma_{0j} = \sum_{i=1}^{I} A_i \sigma_{i0} = \sum_{i=1}^{I} \sum_{j=1}^{J} A_i \sigma_{ij} \tag{3}$$

Define objective function

$$\begin{aligned} \chi^2 &= \sum_{i=0}^{I} \sum_{j=0}^{J} w_{ij} (\sigma_{ij} - \sigma'_{ij})^2 \\ &= w_{00} (\sigma_{00} - \sigma'_{00})^2 + \sum_{j=1}^{I} w_{0j} (\sigma_{0j} - \sigma'_{0j})^2 + \sum_{i=1}^{I} w_{i0} (\sigma_{i0} - \sigma'_{i0})^2 \\ &+ \sum_{i=1}^{I} \sum_{j=1}^{J} w_{ij} (\sigma_{ij} - \sigma'_{ij})^2 \end{aligned} \tag{4}$$

where $w_{ij} (i = 0, 1 \cdots, I;\ j = 0, 1, 2 \cdots, J)$ is the assigned weight of the corresponding cross section for adjusting.

Substitute equations (1) ~ (3) into equation (4), then

$$\begin{aligned} \chi^2 &= \sum_{i=1} \sum_{j=1} w_{ij} (\sigma_{ij} - \sigma'_{ij})^2 + \sum_{i=1} w_{i0} \left[\left(\sum_{j=1} \sigma_{ij} \right) - \sigma'_{i0} \right]^2 \\ &+ \sum_{j=1} w_{0j} \left[\left(\sum_{i=1} A_i \sigma_{ij} \right) - \sigma'_{0j} \right]^2 + w_{00} \left[\left(\sum_{i=1} \sum_{j=1} A_i \sigma_{ij} \right) - \sigma'_{00} \right]^2 \end{aligned} \tag{5}$$

Take the partial differential to variable σ_{kl} and let them equal zero

$$\frac{\partial \chi^2}{\partial \sigma_{kl}} = 0$$

under this conditions, the linear equation group is obtained

$$\begin{aligned} &w_{kl} \sigma_{kl} + w_{k0} \left(\sum_{j=1} \sigma_{kj} \right) + w_{0l} \left(\sum_{i=1} A_i A_k \sigma_{il} \right) + w_{00} \left(\sum_{i=1} \sum_{j=1} A_i A_k \sigma_{ij} \right) \\ &= w_{kl} \sigma'_{kl} + w_{k0} \sigma'_{k0} + w_{00} A_k \sigma'_{0l} + w_{00} A_k \sigma'_{00} \end{aligned} \tag{6}$$

where i=1, 2, ···, I and j=1, 2 ···, J, there are $I \times J$ equations, so the optimum values of $I \times J$ variables can be solved out. And the 'total' cross sections of each isotopes and natural element can be calculated from Eqs. (1) ~ (3).

2 Code and Test

According to the equation group (6), the program CABEI was developed, which

includes codes EPOIN, INTER, DIFFE, ADJUS and RECOV.

Code EPOIN is used for selecting and arranging energy in order. The adjusting is going on at same energy point one by one for all reactions of natural element and its isotopes, but the energy meshes of them are not the same. The energy points of each reaction are taken, and collect all of them together and then put them in order from small to large by the code.

Code INTER is for interpolation of the cross section data according to interpolation mode given in the data heading of corresponding section. As mentioned above, adjusting is going on at the energy points of all reactions, the cross section may not be given at some energy points for some reactions, in this case they are calculated by the code using the given interpolation mode.

Code DIFFE is used to calculate the difference between the data of natural element and sum of its isotopes taken their abundance as weight. This is a quantitative measurement of the inconsistency.

Code ADJUS is used for solving the linear equation group (6) and adjusting the data.

Code RECOV is used to select the energy points for outputting, in usual case, recover the original energy meshes, and output the data in ENDF/B-6 format.

Taken as an example, the data of Fe from CENDL-2.1 (the data are not consistent, the authors are different for $^{54,57,58,Nat.}$Fe and ^{56}Fe) were adjusted to test the program. The results are as follows.

(1) As desired, the difference between the data of natural element and the sum of its isotopes became zero, no matter how much the difference is before adjusted. It means that the data become consistent. Some examples are given in Figs. 1 and 2 for total and nonelastic cross sections.

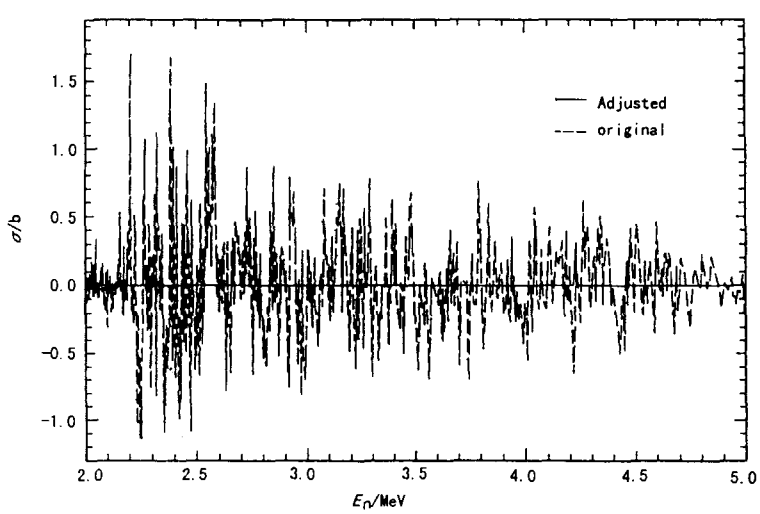

Fig. 1 The difference of total CS between ^{0}Fe and sum of its isotopes

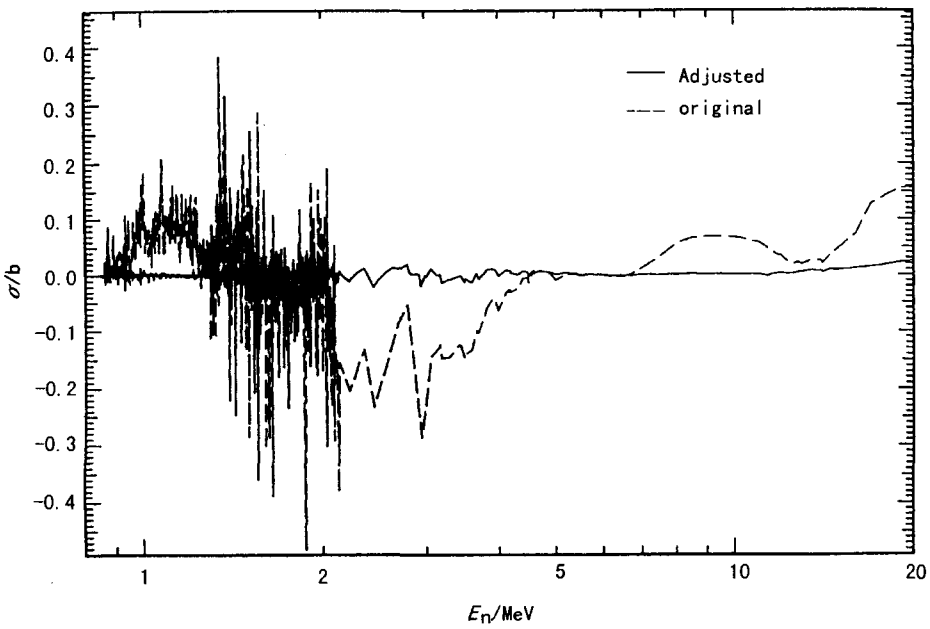

Fig. 2 The difference of nonelastic CS between ^{0}Fe and sum of its isotopes

(2) If the consistence is better before adjusted, the data keep unchanged basically; if it is worse, the data are changed larger; the worse, the larger. Some examples are given in Figs. 3 and 4 for the former and in Figs. 5 and 6 for the later. Also it can be seen from Figs. 5 and 6 that the changed directions are reasonable, it is clear that the original cross section curve of (n,α) is 'fat' for natural element, but thin for ^{56}Fe; after adjusted it becomes 'thinner' for natural element, and becomes 'fatter' for ^{56}Fe.

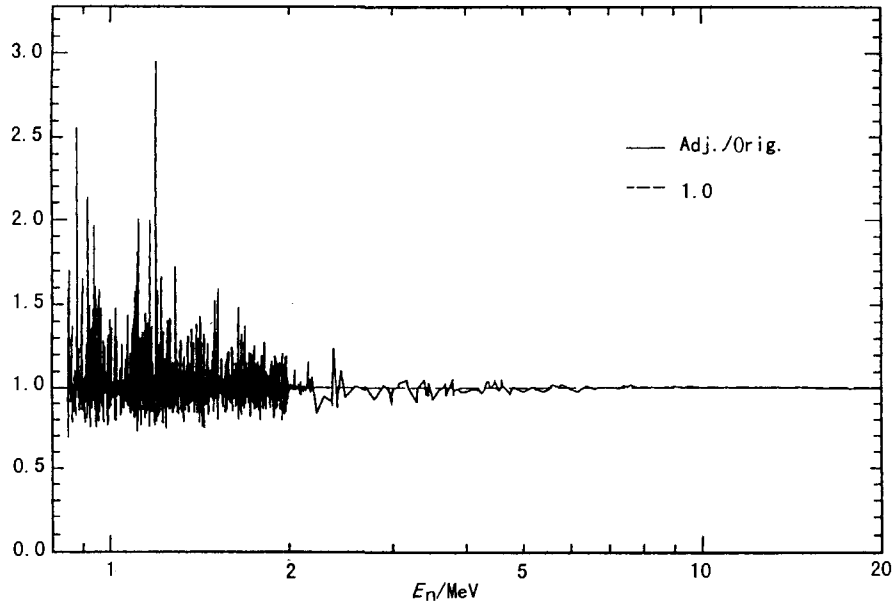

Fig. 3. 1 The ratios of adjusted to original for ^{56}Fe total cross section

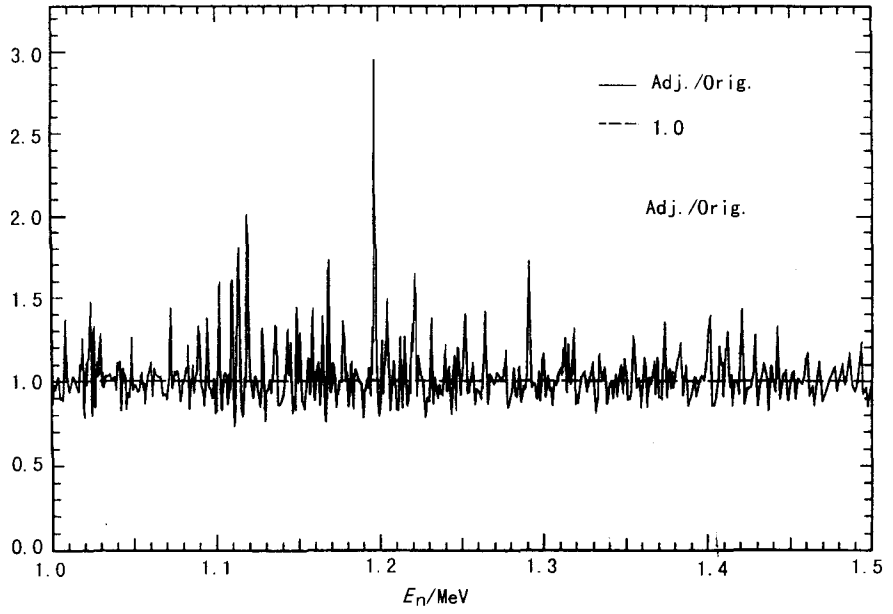

Fig. 3. 2 The ratios of adjusted to original for ^{56}Fe total cross section

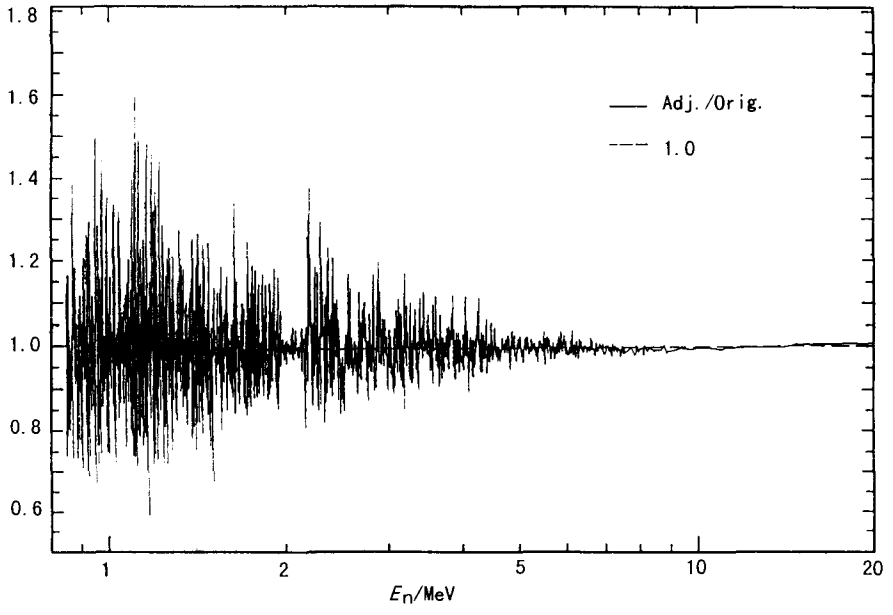

Fig. 4. 1 The ratios of adjusted to original for ^{0}Fe total cross section

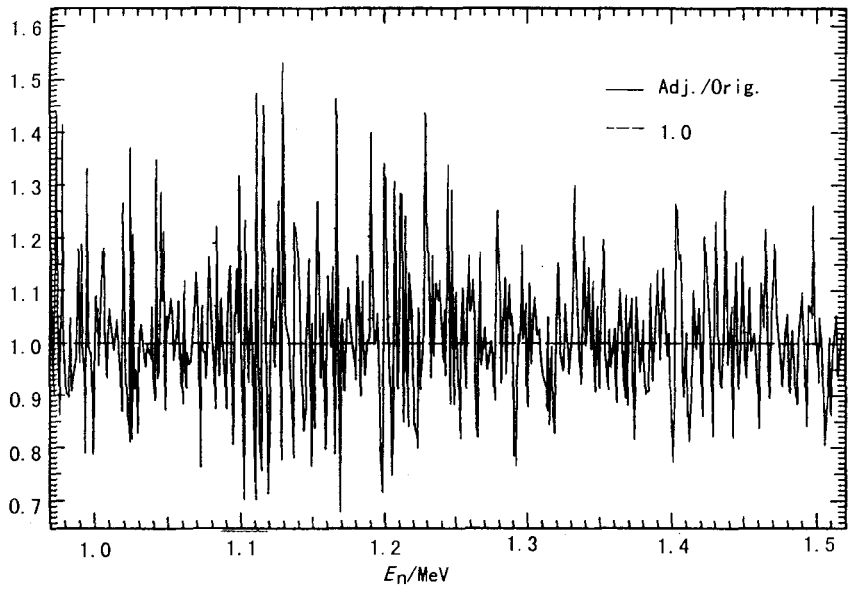

Fig. 4. 2 The ratios of adjusted to original for ^{0}Fe total cross section

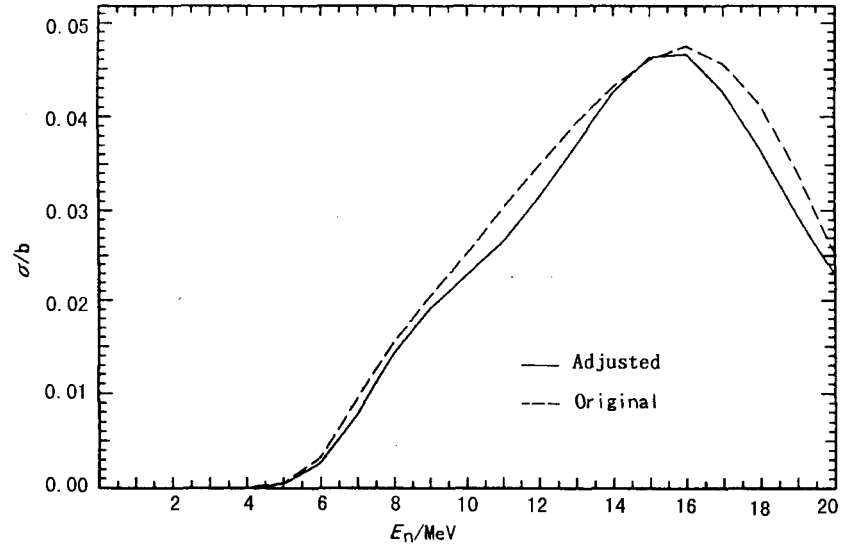

Fig. 5 Adjusting of ^{56}Fe(n,α) cross section

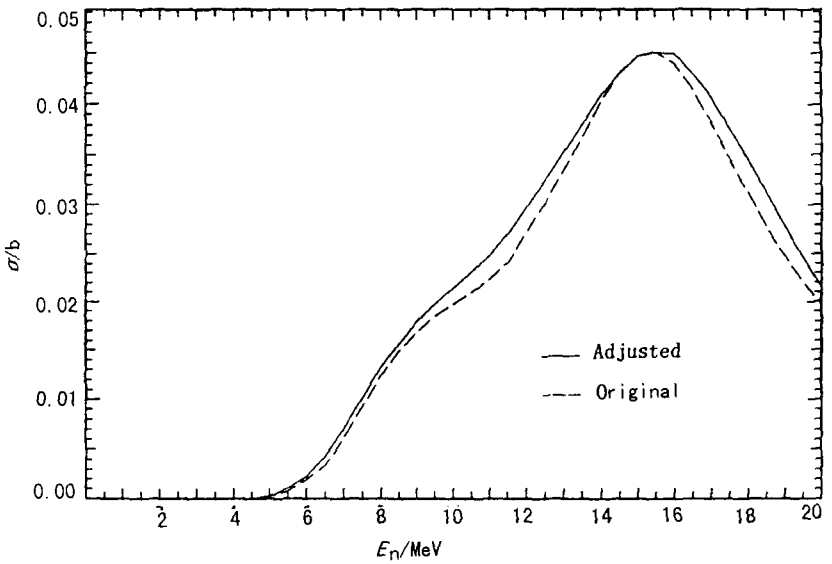

Fig. 6 Adjusting of ^{Nat}Fe(n,α) cross section

(3) If the original curve is smooth, it still keep smooth after adjusted. If there are some structures for original data, there remain small structures for adjusted data (Fig. 7).

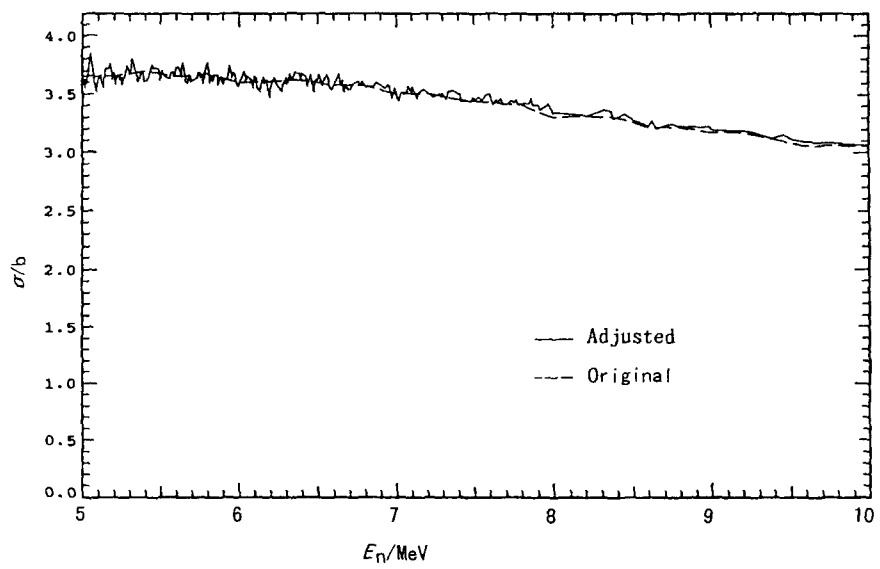

Fig. 7 Adjusting of ^{56}Fe total cross section

(4) In adjusting, the change is smaller for the isotopes having small abundance for they have small contribution to the cross section of natural element, and larger for isotopes having larger abundance for they have larger contribution. An example is given in Fig. 8.

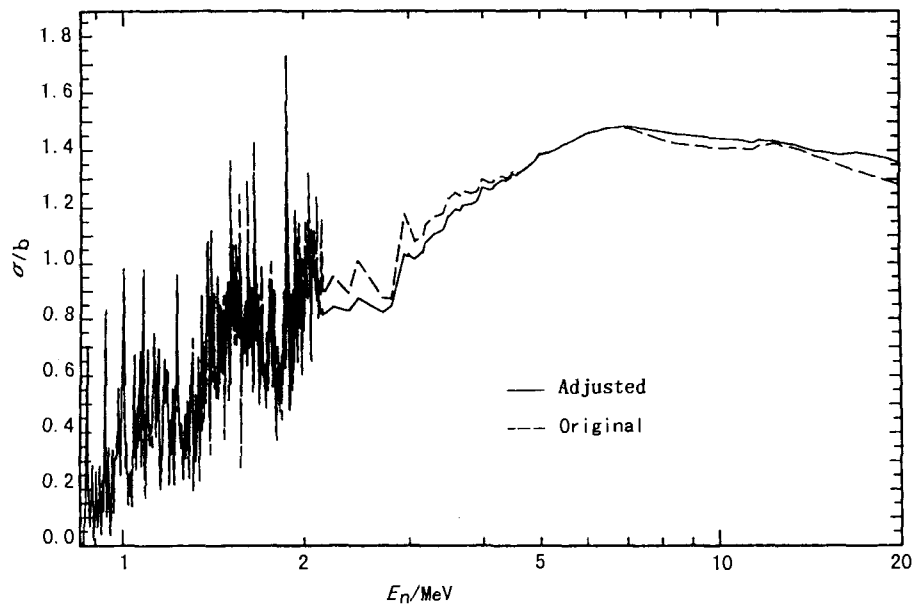

Fig. 8. 1 Adjusting of ^{56}Fe nonelastic cross section

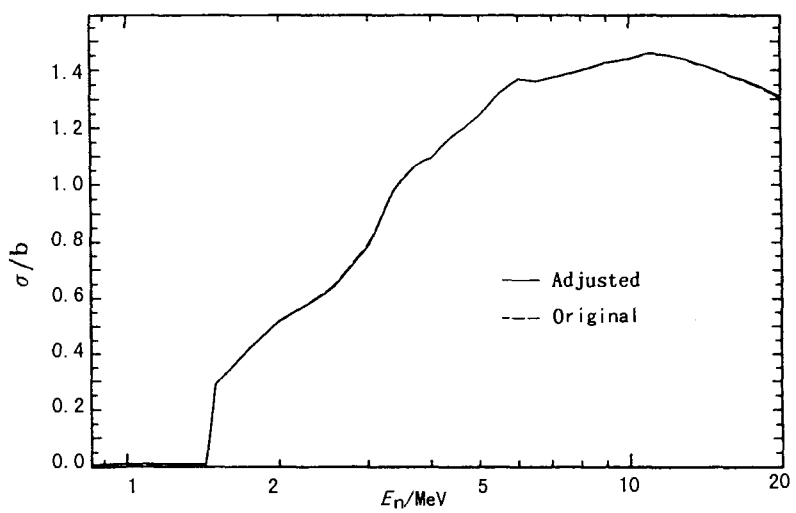

Fig. 8. 2 Adjusting of ^{54}Fe nonelastic cross section

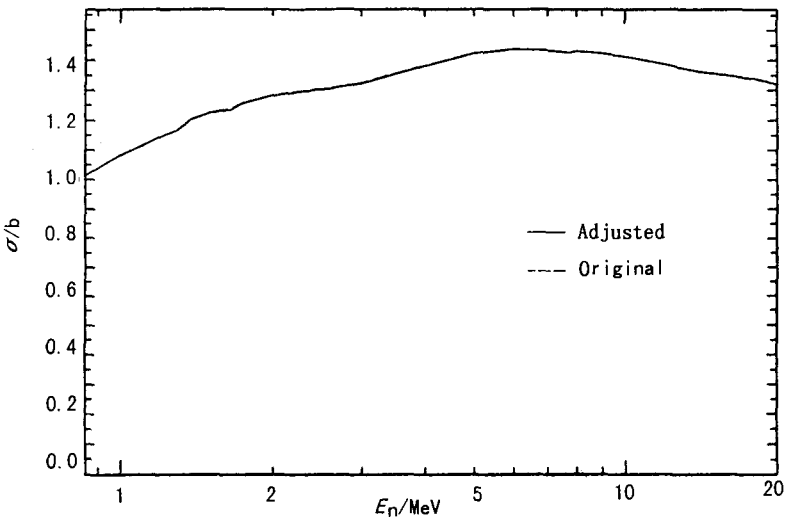

Fig. 8. 3 Adjusting of ^{57}Fe nonelastic cross section

It is concluded from above that the program works well as desired in physics; and in adjusting, the data change, including its direction and magnitude, is reasonable.

3 The Matter in Practical Adjusting

How to use the program, how to practically adjust a complete data, following is the matter in practical adjusting, to which should attention be paid.

3.1 Weight

In principle, the weight w_{ij} for adjusting can be taken arbitrarily. It can be taken as larger for some cross sections, for which there are more experimental measurements and the errors are smaller and you want them changed smaller, and otherwise, it should be taken as smaller. For example, if you want the total cross section remain unchanged basically in the adjusting, the weight w_{i0} should be taken very larger. Also if you want some cross sections, whose absolute values are very low, change smaller to avoid the relative value change too large, the corresponding w_{ij} can be taken larger, for example, as

$$w_{ij} = \frac{\sigma'_{i0}}{\sigma'_{ij}} w^0_{ij} \tag{7}$$

To treat conveniently, sometime the weight can be taken as

$$w_{ij} = w_i \times w_j \tag{8}$$

That is the partial weights are taken as the same for the cross sections of same isotope and same reaction. In this case, the number of input weight parameter is reduced to (I+J) from ($I \times J$).

If the error of the cross section itself should be taken into account, then the weight can be taken as

$$w_{ij} = w_i w_j \times 1/\Delta\sigma_{ij}'^2 \tag{9}$$

3.2 Adjustment of Complete Data

For a set complete data, except the consistence between the data of natural element and its isotopes, they also must be consistent between total, noelastic, inelastic cross section and their corresponding partial cross sections for each isotopes. In this case, the adjusting can be done via, for example, the following steps:

(1) Total CS= elastic CS + nonelastic CS (CS= Cross Section)

(MT 1 = 2 + 3)

(2) Nonelastic CS = sum of all corresponding partial CSs

(MT 3= 4 + 16 + 107)

Taken larger weight for nonelastic CS, to keep it unchanged during the adjusting.

(3) Inelastic CS = sum of CSs of inelastic scattering to continuous state and concrete levels

(MT 4 = 51 + 52 + 91)

Taken larger weight for inelastic CS, to keep it unchanged during the adjusting. Only do the adjusting for the consistence of each nuclide itself, not for natural element and its isotopes for there is no relationship between the CSs of inelastic scattering to concrete levels. In this case, the equation group (6) becomes

$$w_l\sigma_l + w_0(\sum_{j=1}\sigma_j) = w_l\sigma_l + w_0\sigma_0' \tag{10}$$

which is also included in the program.

The values of cross sections for different reactions and nuclides could be large different, which could lead difficulty for adjusting. To avoid this difficulty, let

$$\chi_{ij} = \frac{\sigma_{ij}}{\sigma'_{ij}} \tag{11}$$

as new variables in the equation group, the ratios of adjusted to original cross sections in physics, and then the adjusted cross sections

$$\sigma_{ij} = \chi_{ij}\sigma'_{ij} \tag{12}$$

If it is necessary, program CRECTJ5 can be used for each nuclide itself to make the energy meshes satisfy the rule requirement of ENDF/B-6 format.

3.3 The Treatment of Different Energy Region

The low energy bounds of different reactions and nuclides are different for smooth cross section (file 3), but the adjusting only can be done for file 3 and must be done in the same energy region. For this, they must be treated.

(1) If the low bounds are determined by the resonance upper bounds, the highest one is taken as low limit for all reactions of all nuclides, only in this region can be adjusted.

(2) For cross sections of continuous inelastic scattering, the highest threshold is taken as low limit for all nuclides, only in this region can be adjusted.

(3) For other threshold reactions, the lowest one is taken as low limit, the cross sections are taken as zero below the threshold for other reactions.

3.4 The Treatment of Different Reaction Channel

For some reactions, the cross sections may not be given for all nuclides, for there are no data for it for some nuclides. In this case, it can be treated according to the different situations.

(1) If the reaction is not open (the threshold is higher than 20 MeV) for a nuclide, or although it is open, the cross section is small enough to be neglected, this nuclide is not included in the adjusting (take the cross section of this nuclide as zero).

(2) If the cross section is not small enough to be neglected, but is not given in the file, this isotope is not included in the adjusting, but make the abundance of main isotope plus its abundance.

3.5 Energy Point for Output and Iteration

As mentioned above, the adjusting is going on at all energy points of all reactions of all nuclides, and the cross sections are interpolated for the energy points,

at which they are not given in the file. If all energy points are taken for outputting, there are too many points, and make the file too large, so the energy points must be selected for outputting, usually the original energy meshes are recovered. But in this case, the inconsistency of the new adjusted data may be appeared due to the interpolation.

To solve the problem, the iteration method is used, that is the new adjusted data can be as the input data for the next adjusting until the data is completely consistent at selected output energy meshes. To show the effecting of the iteration, some examples are given in Figs. 9 and 10 for the total and noelastic cross sections of ^{56}Fe respectively. It can be seen that the change is quite large in the first adjusting, only small but certainly existing corrections are made in following iterations.

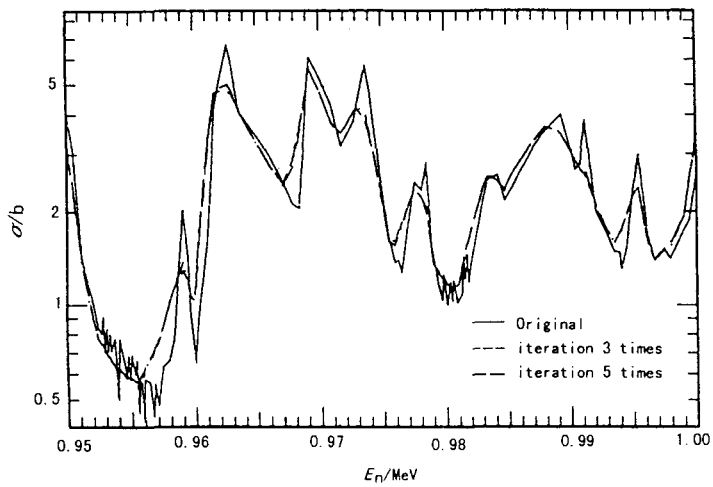

Fig. 9 An example of iteration effect on adjusted result: ^{56}Fe total cross section

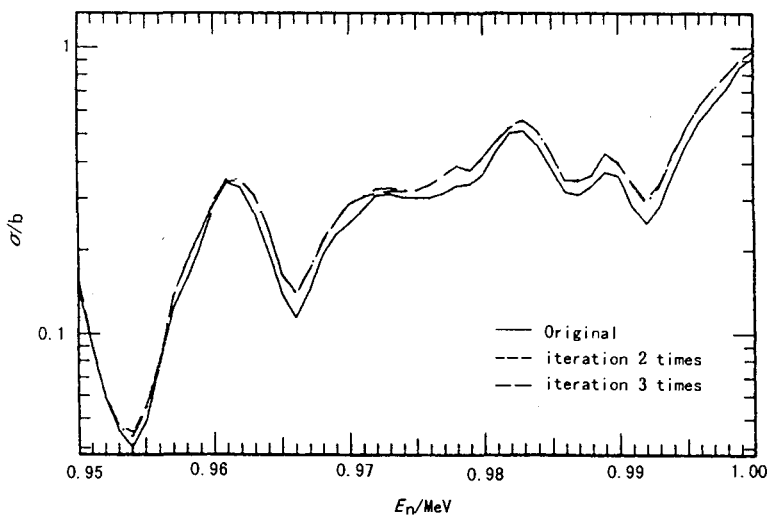

Fig. 10 An example of iteration effect on adjusted result: ^{56}Fe nonelastic cross section

4 Conclusion

The method and program CABEI have been developed to make the complete data of natural element and its isotopes satisfy at the same time the two kinds of consistent relationships, one is for each nuclides itself, and another is between the natural element and its isotopes. The method and program have been tested, and the matter in practical adjusting, including weight taking, complete data adjusting, treatment of different energy region and reaction channel, output energy point selection and iteration, have been studied.

As an example, the method and program were successfully used to adjust the data of ^{Nat}Fe and $^{54,56,57,58}Fe$ of CENDL-2.1. It works well. As a result, the adjusted data are consistent between ^{Nat}Fe and its isotopes $^{54,56,67,58}Fe$, and at the same time keep the consistence for each nuclide itself.

The method and program were also successfully used to adjust the data of ^{Nat}Ni and its isotopes $^{58,60,61,62}Ni$.

The method and program can be spread to used for making the data satisfy two kinds of consistent relationships in the evaluation and evaluated libraries in ENDF/B-6 format. It can become a powerful and convenient tool for making the consistence between the data of natural element and its isotopes. Of course, it is only a mathematical method hence, even to make it optimum in mathematics, could not replace the analysing and adjusting in physics, in other words, the analysing and adjusting in physics should be done at first before using the code.

Reference

[1] J. J. Schmidt, Proc. of International Symposium on Nuclear Data Evaluation Methodology, p. 1, BNL, USA (1992)

CN9901218

V INTEGRAL TEST

Testing of the Tritium Production for the ^{6}Li and ^{7}Li

Rong Jian
(China Nuclear Data Center, CIAE)

The tritium production cross section of the lithium, P_T^{Li} is a very important factor of the fusion system. Several experiments have been made to measure it. In 1954, the tritium production of ^{Nat}LiD was measured by M. E. Wyman for the first time in Los Alamos[1]. The P_T^6, the tritium production of ^{6}Li, was measured with a ^{6}LiD sphere by Hemmendinger et al.[2] in 1978, the radius of the sphere is 30 cm. A similar experiment was also done to measure the P_T^6 in China[3], the 14 MeV neutron source was used in the experiments.

Several calculations[4] for Chen's experiments have been done which based on the CENDL-2.1 and ENDF/B-6, respectively. The calculated results of the P_T^{Li} based on the CENDL-2.1 were lower than the experimental results in the Ref. [4]. So it was thought that the evaluated data of the ^{6}Li and ^{7}Li in the ENDF/B-6 are better than those data in the CENDL-2.1 in Ref. [4]. In order to make sure whether the evaluated data of the ^{6}Li and ^{7}Li in the CENDL-2.1 are good or not, the further calculation is necessary.

In our calculation the Monte Carlo method was applied and the data of the CENDl-2.1 and ENDF/B-6 were used. The comparison between the calculated and experimental results were also made. The experiment facilities are given in Table 1.

The formula to calculate the tritium production of the lithium is:

$$P_T^{Li} = N_T / A \tag{1}$$

where the N_T is the total number of the tritium production reaction in the experiment facility, and the A is the intensity of the neutron source.

In these experiments, the N_T can not be measured directly. Instead, the distribution of the tritium production reaction ratios $f(r)$ were measured, then N_T were calculated:

$$N_T = 2\pi\rho \int_0^{\pi} \int_0^{R} r^2 f(r) \sin\theta \, d\theta \, dr \tag{2}$$

where ρ is the density of the experiment material, R is the equivalent radius of the experiment facility.

The program NJOY was used to generate the ACE file from the ENDF file, which was used in the Monte Carlo code for our calculation. The calculated results are summarized in Table 2.

Table 1 The experiment facilities

experiment	radius / cm	compositions / %	density / g/cm^3
^{6}LiD sphere (China)	0~4	vacuum	0
	4~31	^{6}LiD	0.792
Hemmendinger	0~2.22	vacuum	0
	2.22~5.0	^{6}LiD (95.59) ^{7}LiD (4.41)	0.753
	5.0~5.1	vacuum	0
	5.1~7.615	^{6}LiD (95.59) ^{7}LiD (4.41)	0.753
	7.615~7.715	vacuum	0
	7.715~12.6	^{6}LiD (95.59) ^{7}LiD (4.41)	0.753
	12.6~12.7	vacuum	0
	12.7~20.0	^{6}LiD (95.68) ^{7}LiD (4.32)	0.751
	20.0~20.1	vacuum	0
	20.1~30.0	^{6}LiD (95.68) ^{7}LiD (4.32)	0.751
Wyman	0~4	vacuum	0
	4~30	^{Nat}LiD	0.8154

Table 2 The comparison between the calculations and the experiments

	reaction ratios	experiments	ENDF/B-6	CENDL-2.1
^{6}LiD sphere	P_T^6	0.79 ± 0.07(*) 0.75 ± 0.04(**)	0.7614	0.7708
Hemmendinger	P_T^6	0.853	0.7913(#) 0.8163(##)	0.7984(#) 0.8234(##)
Wyman	P_T^7	0.43 ± 0.004	0.4196	0.4200

where: * measured by the proportional counter; # not including P_T^7;
** measured by the scintillation detector; ## including P_T^7;

In Table 2 it can be found that the calculated results for the P_T^6 of the two libraries are very close. The results of the CNEDL-2.1 is slightly larger and more close to the experimental results than ENDF/B-6. The facility in the Hemmendinger experiment was composed of a series of sphere shells. The experimental condition is not as good as the ^{6}LiD sphere experiment used in China. So the results of the ^{6}LiD

sphere experiment of China are more reliable than the results of the Hemmendinger experiment. At the same time a little ^{7}Li was contained in the facility of the Hemmendinger experiment and its effect can not be neglected. It can be seen that the calculated results including P_T^7 are more close to the experimental results than those not including P_T^7 .

For P_T^7 , the calculated results of the two libraries are very similar and are all close to the experimental results. It means that the evaluated data of the tritium production cross section of the ^{7}Li in the two libraries are all reliable. There is a reaction type of the ^{7}Li, whose MT number is 205, in CENDL-2.1, the total tritium production. But there is no total tritium production of the ^{7}Li in the ENDF/B-6, so it has to sum all of the data from the MT=52 to the MT=82 in the file 3 to get it.

According to our calculation, it is believed that the conclusions in the Ref. [4] are not correct. The evaluated data of the ^{6}Li and ^{7}Li in CENDL-2.1 are all reliable.

References

[1] M. E. Wyman, LA-2234

[2] A. Hemmendinger et al, LA-7310

[3] Z. Y Chen et al , Nuclear Fussion (in Chinese) , Vol. 4, 225 (1980)

[4] Z. J. Na, W. L. Sun, private communication (1995)

CINDA INDEX

Nuclide	Quantity	Energy/ eV		Lab	Type	Documentation				Author, Comments
		Min	Max			Ref	Vol	Page	Date	
^{9}Be	Calculation	1.0+3	2.0+7	AEP	Theo	Jour CNDP	20	5	Dec 98	Zhang Jingshang+, MDL CALC, SIG, DA, DA/DE
^{12}C	Calculation	1.0+3	2.0+7	AEP	Theo	Jour CNDP	20	17	Dec 98	Zhang Jingshang+, MDL CALC, SIG, DA, DA/DE
^{51}V	(γ,x)	1.0+3	3.0+7	AEP	Eval	Jour CNDP	20	95	Dec 98	Yu Baosheng+, MDL CALC, SIG, DA, DE, EVAL
^{63}Cu	(n,α)	Thrsh	2.0+7	SIU	Eval	Jour CNDP	20	90	Dec 98	Ma Gonggui+, SIG
	(n,n'α)	Thrsh	2.0+7	SIU	Eval	Jour CNDP	20	90	Dec 98	Ma Gonggui+, SIG
^{65}Cu	(n,α)	Thrsh	2.0+7	SIU	Eval	Jour CNDP	20	90	Dec 98	Ma Gonggui+, SIG
	(n,n'α)	Thrsh	2.0+7	SIU	Eval	Jour CNDP	20	90	Dec 98	Ma Gonggui+, SIG
^{Nat}Cu	(n,α)	Thrsh	2.0+7	SIU	Eval	Jour CNDP	20	90	Dec 98	Ma Gonggui+, SIG
	(n,n'α)	Thrsh	2.0+7	SIU	Eval	Jour CNDP	20	90	Dec 98	Ma Gonggui+, SIG
^{85}Rb	Calculation	1.0+3	2.0+7	NKU	Theo	Jour CNDP	20	70	Dec 98	Cai Chonghai+, MDL CALC, SIG, DA, DE
^{87}Rb	Calculation	1.0+3	2.0+7	NKU	Theo	Jour CNDP	20	70	Dec 98	Cai Chonghai+, MDL CALC, SIG, DA, DE
^{88}Sr	Calculation	1.0+3	2.0+7	NKU	Theo	Jour CNDP	20	47	Dec 98	Cai Chonghai+, MDL CALC, SIG, DA, DE
^{89}Sr	Calculation	1.0+3	2.0+7	NKU	Theo	Jour CNDP	20	47	Dec 98	Cai Chonghai+, MDL CALC, SIG, DA, DE
^{90}Sr	Calculation	1.0+3	2.0+7	NKU	Theo	Jour CNDP	20	47	Dec 98	Cai Chonghai+, MDL CALC, SIG, DA, DE
^{89}Y	Calculation	1.0+3	2.0+7	NKU	Theo	Jour CNDP	20	39	Dec 98	Cai Chonghai+, MDL CALC, SIG, DA, DE
^{92}Mo	(n,p)	5.0+6	1.0+7	AEP	Expt	Jour CNDP	20	1	Dec 98	Zhao Wenrong+, ACTIV, Ge(Li), SIG
^{113}Cd	Calculation	1.0+3	2.0+7	UNW	Theo	Jour CNDP	20	77	Dec 98	Sun Xiuquan+, MDL CALC, SIG, DA, DE
^{115}In	Calculation	1.0+3	2.0+7	UNW	Theo	Jour CNDP	20	64	Dec 98	Zhang Zhengjun+, MDL CALC, SIG, DA, DE
^{121}Sb	Calculation	1.0+3	2.0+7	UNW	Theo	Jour CNDP	20	82	Dec 98	Zhang Zhengjun+, MDL CALC, SIG, DA, DE
^{123}Sb	Calculation	1.0+3	2.0+7	UNW	Theo	Jour CNDP	20	82	Dec 98	Zhang Zhengjun+, MDL CALC, SIG, DA, DE
^{180}W	(γ,x)	1.0+3	2.0+7	AEP	Theo	Jour CNDP	20	87	Dec 98	Han Yinlu+, MDL CALC, SIG, DA, DE
^{182}W	(γ,x)	1.0+3	2.0+7	AEP	Theo	Jour CNDP	20	87	Dec 98	Han Yinlu+, MDL CALC, SIG, DA, DE
^{183}W	(γ,x)	1.0+3	2.0+7	AEP	Theo	Jour CNDP	20	87	Dec 98	Han Yinlu+, MDL CALC, SIG, DA, DE
^{184}W	(γ,x)	1.0+3	2.0+7	AEP	Theo	Jour CNDP	20	87	Dec 98	Han Yinlu+, MDL CALC, SIG, DA, DE
^{186}W	(γ,x)	1.0+3	2.0+7	AEP	Theo	Jour CNDP	20	87	Dec 98	Han Yinlu+, MDL CALC, SIG, DA, DE
^{238}U	Fission Yield	Thrsh	1.5+7	AEP	Eval	Jour CNDP	20	101	Dec 98	Liang Qichang+, CUML YLDS, 45 PRODUCTS, TBL

* NKU — Nankai University, Tianjin, P.R.China

(京)新登字 077 号

图书在版编目(CIP)数据

中国核科技报告: CNIC-01300，CNDC-0023: 核数据进展通讯: 英文/刘廷进等著. -北京: 原子能出版社，1998.12
ISBN 7-5022-1916-1

Ⅰ. 中… Ⅱ. 刘… Ⅲ. 核技术-研究报告-中国-1998-英文 Ⅳ. TL-2

中国版本图书馆 CIP 数据核字（98）第 32270 号

©原子能出版社，1998

原子能出版社出版发行
责任编辑: 李曼莉
社址: 北京市海淀区阜成路 43 号 邮政编码: 100037
中国核科技报告编辑部排版
核科学技术情报研究所印刷
开本: 787 × 1092 1/ 16 . 印张 8 . 字数 140 千字
1998 年 12 月北京第一版 . 1998 年 12 月北京第一次印刷